VIBRATION AND NOISE RESPONSE OF ELECTRICAL MACHINE STATOR CORES EXCITED BY MAGNETIC FORCES

by

D. J. FINCH, B.Sc., M.Sc.

Submitted in fulfilment of the Degree of

Doctor of Philosophy

of

The University of Aston in Birmingham

Faculty of Engineering

Mechanical Engineering Department

APRIL 1976

Dedicated to my Father

and

Mr. M. Tarkanyi

ACKNOWLEDGEMENTS

Permission to conduct this research, given by Professor A.J. Ede, is gratefully acknowledged as is the supervision, encouragement and wealth of experience so readily given by Professor E. Downham.

The author also acknowledges with thanks the generous sponsorship of this research by G.E.C. Machines Co.Ltd., and the facilities made available for testing various production machines, and the manufacture of a special rotor and a large number of lamination samples. In particular, the author's indebtedness to Mr. Tarkanyi is readily acknowledged. It was under his supervision, and leaning heavily on his insight, that the author's work on noise was started at G.E.C. Machines Co.Ltd., and the present research was fostered.

Help and assistance given by the University laboratory staff and research colleagues in the Department of Mechanical Engineering is also acknowledged.

SUMMARY

A development project was undertaken by G.E.C. Machines Co.Ltd., to improve their existing methods for predicting no-load and full load noise levels of large induction motors. Improvements were being sought in the calculation of the machine electromagnetics which create the forces and the stator core dynamics which determines the response to these forces. The research work reported in this thesis concerns the latter aspect which applies to synchronous as well as induction machines.

Previous theories for calculating stator core resonant frequencies are reviewed and shown to be inadequate when applied to large machines. A large number of resonant frequencies were measured on sample laminations, mainly from large machines. From these tests it was found that the main inaccuracies in previous theories - as applied to large machines - centred on the treatment of the teeth. A series of tests on a production machine at various stages of manufacture is also given. These tests culminated in a live-machine test which maximises the amount of information obtainable about resonant frequencies without increasing the normal testing time.

A completely new theory for calculating stator core resonant frequencies is presented and compared with the measurements described above and also with a number of live-machine measurements made on production machines. Excellent agreement is obtained for large and small machines.

Finally, an example is given of the use of the theory and measurement techniques to help circumvent a noise problem that came to light mid-way through the manufacture of a very large machine.

CONTENTS

CHAPTER 1

INTRODUCTION AND OUTLINE OF THE RESEARCH AND MAIN CONCLUSIONS

1.1 NOISE IN ROTATING ELECTRICAL MACHINES

In the design of any piece of electrical equipment many parameters vie for pre-eminence in the designers considerations. These may be cost, efficiency, safety, reliability, speed, appearance or simply ease of manufacture but it seems that every designer is faced with ignoration or wholesale compromise as the only means of dealing with them all. A certain amount of engineering fashion determines which qualities are important; and genuine scientific advance also helps to drag more out of the dark of ignorance into the melee of compromise. Thus it is that noise (or lack of it) has become an important design parameter in all aspects of engineering and particularly in the manufacture of rotating electrical machines.

In rotating electrical machines there are three principal noise mechanisms giving rise to what are usually called bearing, windage and electromagnetic noise. It is the latter type of noise that is the least predictable and which gives rise to the differences between total noise levels with the machine loaded and unloaded. Moves within the manufacturing industry to reduce the material content of machines have increased the likelihood of machines giving rise to electromagnetic noise. Another fact has brought electromagnetically generated noise to the fore, from the manufacturers point of view. Of the three types of noise the electromagnetically produced is the most expensive and time consuming to remedy as it usually involves the redesign and production of a new rotor[2]

The customers who purchase rotating electrical machines have been requiring tighter noise 'performance' of their machines and so manufacturers have been obliged to develop design tools to predict and control noise levels[1]. As the mechanisms of noise production have been understood so customers have written more stringent specifications. There is considerable pressure now to have manufacturers measure noise levels on full-load in addition to the current practice of measuring noise levels uncoupled (no-load). Since meaningful load measurements are difficult, if not impossible, for most manufacturers to make, it is becoming important for manufacturers to be able to predict accurately the difference between no-load and full-load noise levels. It will then be possible to measure and guarantee no-load noise levels equal to the full load specification minus the predicted difference.

The work in this thesis is confined to noise of electromagnetic origin. The control of bearing and windage noise has been reported by Glew[3].

1.2 THE GENERATION OF NOISE OF ELECTROMAGNETIC ORIGIN

The logic and the steps involved in understanding the production and the calculation of magnitudes of electromagnetically produced noise in rotating electrical machines have been described by Erdelyi[4]. The steps described below are applicable to all rotating machines, although the greatest amount of work has been done on three phase synchronous and induction machines. The basis for the calculation of synchronous machine noise was founded by Carter[5] with Jordan[6] and Alger[7] simultaneously publishing work on the calculation of induction motor noise. The methods described by these authors still form the bases of modern methods

of calculating noise levels. A simplified approach based on equations given by Schwarz[2] has been in use for some time by various manufacturers but this does not give a quantitative noise analysis.

The first step is to obtain detailed information about all of the major flux harmonics in the airgap of the machine. The frequencies pole numbers, magnitudes and phases of between 25 and 35 harmonics are needed for a thorough analysis. A large number of these are likely to be the vectorial additions of components due to m.m.f effects and permeance effects.

From the flux waves the magnetic forces are calculated. It is usually the low order force waves that give rise to high noise levels. From Maxwells equation it can be shown that the radial force in an electrical machine is proportional to the square of the airgap flux wave.

The next step is to calculate radial core deflections for each of the component force waves and then to combine those of like frequency and mode. The usual procedure adopted for this calculation is to calculate 'static' deflections using beam theory and then to apply a factor to account for the dynamic response of the stator core and frame assembly. It is the dynamic response of the stator which is very difficult to calculate and which has been the subject of a number of papers in recent years. This particular aspect assumes even greater significance when it is realised that it is usually only machines with stators forces at or near resonance which vibrate with sufficient magnitude to produce unacceptable noise levels.

Having obtained vibration amplitudes the final step is to calculate sound pressure levels for each mode and frequency of vibration and then to relate these levels to a standard measurement so that designers have a ready assessment of any design. Four methods have been developed for calculating sound pressure levels from vibration amplitudes[4,5,7,8]. Each of these methods produce a noise radiation efficiency which is a function of the machine diameter and vibration frequency for each vibration mode. These methods are characterised by unity efficiency (compared with a plane radiator) at high frequencies and a sharp fall to very small efficiencies below a threshold frequency. The threshold frequency for any mode is a function of diameter, with small machines tending to be poor radiators and large machines good radiators.

1.3 DEFICIENCIES IN PRESENT METHODS WHEN USED TO CALCULATE LARGE MACHINE NOISE LEVELS

The following comments apply particularly to large induction motors although the mechanical aspects apply equally well to large synchronous machines.

The designers approach in the past to avoiding noise has been relatively simple. In the knowledge that low order force waves produce large vibration levels various rules have been formulated to avoid them. These rules have usually involved the choice of slotting and are often a severe limitation on the designer. As with most empirical rules the limits have been set by problem machines and frequently prevent the use of quite acceptable designs and occasionally fail to prevent the use of a machine design which obeys the rules but is nevertheless noisy.

The deficiencies in this approach lead to the present day quantitative approach which considers the mechanical and acoustic aspects of noise generation as well as the electromagnetics of any design. A comprehensive approach demands the use of a computer to execute all of the calculations. A computer program was written by the author for G.E.C. Machines Co.Ltd., using the logic outlined in Section 2 of this chapter. The theory for this program was laid down by Mr. M. Tarkanyi.

The G.E.C. Machines Co.Ltd., at Rugby is concerned with the manufacture of large rotating machines and the noise analysis program mentioned above has been applied to machines ranging from a few hundred kilowatts to some tens of megawatts of output power. The program field trials included a few machines which were noisy because of core resonance. The trials showed that improvements were necessary to give the required accuracy. This was not unexpected.

The errors in the calculation of the stator core resonant frequencies were sometimes quite large. The trials also showed the need for information about damping levels in large machines. In order to improve the selectivity of the program it was necessary to apply a tolerance to the calculated resonant frequencies. This automatically introduced a nominal noise level for each force wave and a band of levels obtained by varying the dynamic response in the frequency domain. Because of the tolerance on dynamic response the program can identify a machine as potentially noisy which may be acceptably quiet. The need to minimise such a tolerance is obvious.

The reason for the size of the tolerance was thought to be the fact that all of the available methods for calculating dynamic responses were

verified with measurements on small machines. The good agreement obtained by Erdeyli[4] and Ellison and Yang[9] and others for the first few modes in small machines was not translated to large machines where one is interested in many more modes. It was the desire to produce a better method for calculating the dynamic response of large electrical machine stators which gave rise to the research described in this thesis.

In developing the computer program electromagnetics use was made of measurements made at both no-load and full-load. The same components of force are present with the machine loaded and unloaded although the magnitudes are different. Since the frequencies of these forces do not change appreciably with load the differences in magnitudes of the various force waves appear directly as differences in SPL. This is another way of saying that the mechanical-plus-acoustic response is linear with force between no-load and full-load.

This statement is certainly not true if the machine is tested at differing speeds. Since there is a direct relationship between forces and SPL it is possible to use the no-load/full-load measurements as a check on the calculated forces, and thereby the calculated flux waves. If the fluxes are calculated correctly on no-load and full-load then the calculated differences in noise levels on no-load and full-load (expressed in logarithmic form) will be the same as the measured differences. This principle is used in Chapter 6 to demonstrate the accuracy of the electromagnetics calculations.

The step from vibration levels to radiated sound pressure levels has been treated by various authors. Very little exhaustive experimental work

has been reported in support of any of these treatments so there is no satisfactory basis for comparing them. In the noise analysis program referred to above the simplest of these (due to Carter[5]) has been used and not found to be deficient.

1.4 SUMMARY OF EXPERIMENTAL AND THEORETICAL WORK

A large number of resonant frequency measurements were carried out on short stacks of lamination from large machines. The various theoretical methods for calculating radial mode resonant frequencies were compared with these measurements. Each of the theories gave good or reasonable accuracy for small machines (a number of small machines were also tested) but poor results for large machines and especially for the higher modes in large machines. The experimental work showed that the teeth in large machines have a large coupling influence on the radial mode resonant frequencies. In large machines the teeth are sufficiently long (see Fig. 3.3.1) to resonate in the first transverse bending mode in the critical frequency range. Previous methods have assumed either that the teeth do not flex or that the teeth are parallel and the first tooth resonant frequency can be determined using elementary theory. In the authors theoretical work tapered teeth have been assumed and the first tooth resonant frequency has been determined accounting for secondary effects such as shear, rotary inertia and root flexibility.

In addition to the measurements on 'short cores' other measurements were made to gauge the influence of the machine windings and frame on resonant frequencies. Early in this part of the investigation it became apparent that the wedges that retain the windings could have an important

influence on resonant frequencies. Further experimental work on wedges showed that it was possible to move resonant frequencies quite considerably by bonding the wedges to the teeth. The theoretical work was expanded to enable the influence of bonded wedges to be accurately predicted. This aspect has not been considered before, although bonded wedges are increasingly being used. The theoretical work adduced to cover this phenomenon allows the designer an extra degree of freedom since he can decide to bond or not as late as the final erection-and-test stage of manufacture.

The effects of the winding were observed by making measurements on a complete machine with and without the winding. These measurements were also compared with those on the same laminations tested using the short core method. The main conclusion from these measurements is that the winding does not significantly effect the values of resonant vrequencies. This conclusion contradicts all previous work. Usually some fraction - often unspecified - of the winding mass is added to the equations of motion thereby reducing calculated resonant frequencies. The other main conclusion from these and other measurements on complete machines is that the frame increases resonant frequencies at low frequencies but becomes progressively uncoupled until its influence is negligible. The uncoupling frequencies have been measured for large machines and occur between 400 Hz and 700 Hz.

The measurements on short cores and complete machines built from the same laminations have validated the short core method. It is believed that this method has been used before but without experimental validation. Since only a small number of laminations are needed and since the frame is not required this method is practicable from the manufacturers point of view.

The short core method has already been used at G.E.C.Machines.Ltd., to help circumvent a noise problem in a large synchronous motor (see Chapter 6). Without the experimental validation the manufacturer would not have been in a position to rely on the results obtained.

As well as the static vibrator measurements on the complete machine, the live factory test was used (Chapter 6). This involves running the machine unloaded at varying supply frequency. Back of core accelerometer measurements are made and analysed using an instrument tape recorder and digital analysis. Since measurements are made direct onto a tape recorder and analysed subsequently, the test takes only approximately 90 minutes for twenty sets of measurements. Since accelerometer rather than noise measurements are made, it is possible to do this test while the bearings are being settled - this is usually done with the machine unloaded. Using this test on the experimental machine it was possible to excite nine different resonant frequencies, forced by the internal electromagnetics of the machine. Parallel noise and acceleration measurements showed clearly the improvement upon a similar technique based on sound pressure levels. Because of the ease with which this test can be made it is proposed that it is incorporated into the no-load test (during the time when the bearings are being settled). In this way it will be possible to collect resonant frequency information on a regular basis on complete, assembled and running machines.

A new theoretical approach to calculating resonant frequencies of stator cores has been developed. It recognises and takes account of the important factors that influence resonant frequencies in large machines.

These are: the use of tapered teeth; segmented cores; the effect of wedges and the skeleton frame into which the stator cores are built. The theory has also been extended to include things such as axial ventilation holes, back of core cooling fins and clamping plates. A worst-error margin has been obtained by comparing the theory with a large number of measurements. This is ± 6% for all modes where the frame is uncoupled. The theory developed to account for bonded wedges breaks new ground. When the theory is applied to small machines the accuracy obtained is better than previous theories. This is true of the present measurements on small machines and also those reported by the authors of other theories.

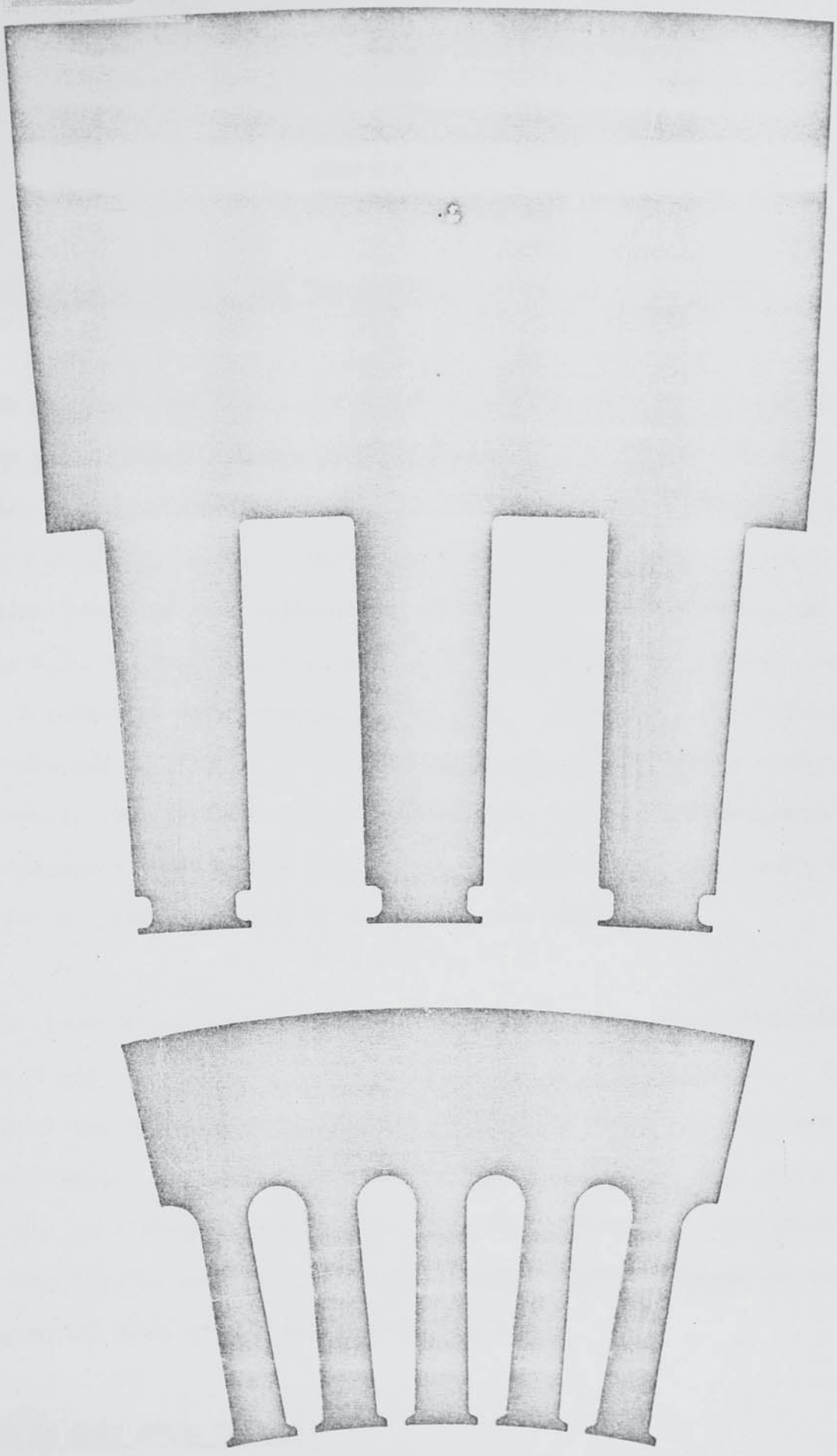

LARGE MACHINE AND SMALL MACHINE LAMINATIONS

Fig. 1.1.1

CHAPTER 2

THE CALCULATION OF THE TEST MACHINE FLUXES AND NOISE LEVELS

In Chapter 6 the results of comprehensive measurements on a production machine are reported. These include testsat various stages of manufacture. The most informative of these tests involved the running of the machine supplied with rated volts. The rotating flux waves produced in this situation gave rise to a multitude of force waves. The results given in Section 6.3.2 of Chapter 6 have been obtained by using these force waves to excite a number of core resonant frequencies. In order to determine the magnitudes and frequencies of the various forces present during these tests the computer program mentioned in Chapter 1 was used. This program predicts induction motor noise levels from geometric and electrical data and gives intermediate parameters such as forces and core deflections.

The production machine was tested with two rotors - the normal production rotor and one specially designed to produce high noise levels. The results of the noise analysis computer program for these two cases are discussed below. As with most machines only a few of the many force waves can excite core resonant frequencies. In the interests of confidentiality only those figures pertaining to measured core resonant frequencies are shown. The forces of interest are detailed in Fig. 6.3.5.

2.1 THE 58 SLOT ROTOR DESIGN

The production machine was designed with a 58 slot rotor. The mechanical details of the machine design are given in Fig. 2.1.1. In addition to the mechanical details this abbreviated data sheet contains three extra flux

densities. The program has been written to calculate the magnitudes etc. of a large number of flux density harmonics and also to accept additions to these at the designer's discretion. The three extras shown in Fig. 2.1.1 are saturation and rotating eccentricity harmonics. The saturation harmonics were obtained from another G.E.C. computer program and the eccentricity harmonic magnitude is an assumed value.

The first step in the sequence of calculating noise levels is to obtain the magnitudes, frequencies, phase and spatial distribution of the significant flux harmonics. This is done using the well used equivalent circuit technique. Butler[39] has given a comprehensive statement of the calculations involved in this approach. In the G.E.C. noise analysis program certain important modifications have been included in the equivalent circuit calculations in the light of comparisons with noise measurements. Reference to Fig. 2.1.2(2) shows that there are often a number of force waves of the same frequency and spatial distribution. These must be added vectorially to give a resultant force wave. This means that the phase relationships between all of the flux densities need to be known accurately. The noise analysis program gives special attention to the calculations of phase angles. In determining the various flux densities both m.m.f. and permeance effects are considered.

A table of flux densities is given in Fig. 2.1.2(1). Only those harmonics that feature in the excitation of core resonant frequencies (see Chapter 6) are included. The first three columns give the origins

and code numbers of the various flux densities. These are for identification purposes. The pole pairs (wave lengths) and frequencies take negative and positive values. This simply indicates the direction of rotation. The phases are given in relation to the stator current. Since the tests in Chapter 6 were made with the motor unloaded these calculations relate to no-load conditions.

From Maxwell's equation the radial force in a machine is directly proportional to the square of the airgap flux wave. Since this is a truncated sine series the resulting radial force is the summation of a very large number of sinusoidally distributed forces. The computer program orders the products and cross products that result from squaring the flux wave into ascending numbers of pole pairs. Further calculations are carried out in this order up to a maximum number of pole pairs as determined by the user on the data sheet; in this case 10. Fig. 2.1.2(2) is an abbreviated version of the computer print out and shows this ordering - Column 3.

The following sequence is followed for each component of vibration and noise caused by the force wave. The items in brackets refer to Fig. 2.1.2(2). From the force wavelength and magnitude and the core dimensions the static delfection (Column 5) is calculated. Knowing the force frequency and having calculated the corresponding core resonant frequency the amplification factor (Column 6) relating static and dynamic deflections can be obtained. From the dynamic deflections and the noise radiation efficiencies (Column 9) the noise

levels (Column 7) are calculated. The radiation efficiency is a function of the wave-length of the emitted noise, the diameter of the core and the particular vibration pattern. If a calculated resonant frequency is varied through the range specified (Fig.2.1.1) the amplification factor changes. The maximum value of amplification factor in this range is used to calculate the second noise figure - the maximum sound intensity (Column 8). It is this latter column which is used in judging whether a machine is likely to meet a noise specification. The sound intensities in Columns 7 and 8 apply to the machine core. The dynamic response calculations in the computer program did not include the results of this research when these figures were obtained.

Reference to the figures in Column 7 shows that the worst noise level produced by this machine on no-load is 76.9 dB. This was acceptable. This figure (row 8 of Fig. 2.1.2(2)) is one of three components, each with the same frequency and vibration pattern. The resultant noise is the vectorial addition of these components and is shown in row 11. It is noteworthy that the resultant noise level is smaller than the largest component noise. This serves to underline the importance of the correct calculation of the phase relationships between all of the forces.

The difference between the two columns of sound intensities is small unless there is a near resonance condition. A large value of amplification factor indicates this near resonance. A good example of this is given in the last row of Fig. 2.1.2(2) where the tolerance

on the resonant frequency is sufficient to make it co-incident with the forcing frequency. The difference between nominal and maximum sound intensities is approximately 30 dB. This was the only resonance/near resonance condition when the machine was run with a 50 Hz supply. By varing the supply over a wide range of frequencies the majority of these forces were brought into resonance. These measurements are reported in Chapter 6.

2.2 THE 60 SLOT ROTOR DESIGN

In order to produce a very noisy motor a second rotor was designed for the production machine described previously. By using two extra rotor slots the major force wave (produced by fluxes coded 1 and 7) was brought very close to the corresponding core resonance. Also the wavelength of this force is lengthened, thereby increasing the flexibility of the core. The rotor dimensions, including the slots, are the same as those of the production rotor.

A table of flux density harmonics is given in Fig. 2.2.1(1). Again, this is an abbreviated version of the computer print out. It can be seen from these and the corresponding figures in Fig. 2.1.2(1) that the magnitudes and frequencies of the fluxes for both rotors are very similar. The parameters G1, G2 etc., are the harmonics derived from an analysis of the permeance of the machine airgap and apply to both rotor designs. The computer program uses the results given by Freeman[10] for calculating these harmonics.

Although the flux density levels and frequencies are very similar the resulting noise levels with 60 slots - (Fig. 2.2.1(2)) are considerably greater than those with a 58 slot rotor. The reason for this lies in the fact that the force waves resulting from the fluxes, particularly numbers 1 and 7, have longer wavelengths. The response of the core is very much stronger since it is considerably more flexible and more nearly in resonance. When the machine was tested the mode 4 resonant frequency was found to be 830 Hz. Thus the mode 4 force at 849.2 Hz was able to produce a very high noise level. In the measurements with this rotor the supply frequency was over a wide range so that a number of core resonances were excited. Clearly this design would not be acceptable as a production machine.

INDUCTION MOTOR NOISE ANALYSIS

(ABBREVIATED MOTOR DATA)

6600	Volt	Line voltage
56.7	Amp	Line current
8		Poles of machine
50	Hz	Supply frequency
832	mm	Stator punching outside diameter
735	mm	Back of teeth diameter
597	mm	Air gap diameter
14	mm	Stator slop opening
72		Stator slots
332	kg	Stator winding weight, slot portion only
535	mm	Overall length of core
1.52	mm	Length of airgap
58/60		Rotor slots
.001	P.U.	Slip
10/8		Maximum force pole pairs to be considered
3		Number of extra fields
1/0		Are resonant frequencies to be calculated?
21000	kgf/mm^2	Young's modulus
1		Are intermediate parameters required?
-5	%	Error in resonances, lower limit
+5	%	Error in resonances, upper limit
500		Peak amplification factor

FIELDS EXTRA TO STANDARD SET

Pole pairs	Frequency Hz	Amplitude P.U.	Phase RAD
12	150	0.0463	-0.76578
20	250	0.0149	1.86529
3	50	0.05	0.0

INDUCTION MOTOR NOISE ANALYSIS

(FLUX DENSITIES INCLUDING EXTRAS IF ANY)

58 SLOT ROTOR

Code Number of Flux Harmonic	Stator Order	Rotor Order	B Max WB/m^2	Pole Pairs	Freq. Hz.	Phase Rad
1	1	0	.81546	4	50	-.15078
2	1	-13.5	.00919	-54	-674.6	-15.08033
3	1	15.5	.00800	62	774.6	27.33093
6	-17	0	.32376	-68	50	-3.21122
7	-17	-2.5	.04068	-10	774.6	-5.00311
9	19	4.5	.03396	18	674.6	-2.03910
13	37	-6.5	.00094	-26	-2123.9	1.02695
17	55	-3	.00286	-12	-2848.5	-1.73007
19	-71	1.5	.00039	6	3673.2	-7.86341
21	73	0.5	.00013	2	-3573.2	-4.74685
22	-5	0	.01147	-20	50	-.04888
25	13	0	.00928	52	50	3.14165
26	-	-	.03770	12	150	-.76578
27	-	-	.01215	20	250	1.86529
29	-	-	.04077	3	50	0

The above table of flux densities is an abbreviated version.

Only those harmonics that appear in the following table are given.

FIG. 2.1.2(1)

INDUCTION MOTOR NOISE ANALYSIS

(SOUND INTENSITIES)

58 SLOT ROTOR

Flux Number	Flux Number	Force Pole Pairs	Freq Hz.	Static Defl. mmx10^{-6}	Ampl. Factor	Nominal S.I. dB	Maximum S.I. dB	Rad Eff.
1	19	-2	-3623.2	83	.0020	34.6	35.4	1.0
2	25	-2	-624.6	22	.0721	39.2	40.1	1.07
9	22	-2	-624.6	101	.0721	52.4	53.3	1.07
VECT.	ADDN.	-2	-624.6	82	.0721	50.6	51.5	1.07
7	26	2	924.6	397	.0317	60.5	61.4	1.04
9	27	-2	-924.6	107	.0317	49.1	50.0	1.04
VECT.	ADDN.	2	924.6	473	.0317	62.0	62.9	1.04
1	7	-6	824.6	63	1.3316	76.9	77.2	1.28
3	6	-6	824.6	5	1.3316	54.7	55.0	1.28
9	26	6	-824.6	2	1.3316	48.6	48.9	1.28
VECT.	ADDN.	6	824.6	58	1.3316	76.1	76.4	1.28
1	21	6	-3523.2	0.2	.2820	25.4	26.5	1.03
13	27	-6	-1873.9	0.02	3.4959	22.6	27.3	1.11
7	29	-7	824.6	2	1.1786	40.4	40.6	0.52
1	17	-8	-2798.5	1	6.3669	67.1	77.4	1.09
17	29	-9	-2798.5	0.06	5.4330	35.7	41.3	1.11
1	19	10	3723.2	0.06	14.8148	51.8	82.3	1.07

FIG. 2.1.2(2)

INDUCTION MOTOR NOISE ANALYSIS

(FLUX DENSITIES INCLUDING EXTRAS IF ANY)

60 SLOT ROTOR

Code Number of Flux Harmonics	Stator Order	Rotor Order	B Max WB/m^2	Pole Pairs	Freq. Hz.	Phase Rad.
1	1	0	.81516	4	50.0	-.25526
2	1	-14	.01524	-56	-699.2	-15.97418
3	1	16	.01333	64	799.2	28.00807
6	-17	0	.32563	-68	50.0	-3.25917
7	-17	-2	.03484	-8	799.2	-5.00737
9	19	4	.03390	16	-699.2	-2.39062
11	-35	-5	.00476	-20	1548.5	-5.01211
17	55	-5	.00342	-20	-2947.0	-1.84156
22	-5	0	.01138	-20	50	-.05772
25	13	0	.00941	52	50	3.14179
26	-	-	.03770	12	150	-.76578
27	-	-	.01215	20	250	1.86529

PERMEANCE HARMONIC ANALYSIS USED IN THE ABOVE FIGURES

G1	G2	G3	G4	S/L	S/G
.6904	.0871	-.1267	-.0206	.537	8.9649

The above table of flux densities is an abbreviated version.

Only those harmonics that appear in the following table are given.

FIG. 2.2.1(1)

INDUCTION MOTOR NOISE ANALYSIS

(SOUND INTENSITIES)

60 SLOT ROTOR

Flux Number	Flux Number	Force Pole Pairs	Freq. Hz	Static Defl. mmx10^{-6}	Ampl. Factor	Nominal S.I. dB	Maximum S.I. dB	Rad. Eff.
11	22	0	1498.5	0.9	6.87	47.2	59.9	1.00
1	7	-4	849.2	458	1.66	96.2	98.8	1.24
3	6	-4	849.2	70	1.66	79.8	82.5	1.24
9	11	-4	849.2	3	1.66	51.2	53.9	1.24
9	26	4	-849.2	20	1.66	69.2	71.8	1.24
VECT.	ADDN.	-4	849.2	451	1.66	96.0	98.6	1.24
2	25	-4	-649.2	2	15.68	67.5	97.6	1.28
9	22	-4	-649.2	6	15.68	76.1	106.2	1.28
VECT.	ADDN.	-4	-649.2	5	15.68	74.6	104.7	1.28
7	26	4	949.2	21	1.00	65.8	67.7	1.20
9	27	-4	949.2	6.5	1.00	55.8	57.7	1.20
VECT.	ADDN.	-4	949.2	22	1.00	66.2	68.1	1.20

This table contains only those calculated levels which are above 40 dB.

FIG. 2.2.1(2)

CHAPTER 3

FACTORS INFLUENCING RESONANT FREQUENCIES AND PREVIOUS THEORETICAL METHODS

3.1 GENERAL CONSTRUCTION OF LARGE ELECTRICAL MACHINES

In the descriptions that follow comparisons are made with small machines since previous work was centred on these machines. Most large industrial machines are radially ventilated (cooled). This means that the body of the machine is made up of toroidal biscuits (packets) separated by ventilation ducts. A typical packet would be 50 mm long and contain 100 laminations. The laminations are made of electrical grade sheet steel, varnished on both sides. They are held together under pressure. In large diameter machines the laminations are segmental in form. Packets are built up with alternate layers of laminations displaced circumferentially by one half of a segment. Each packet is separated by radial spacers - usually along the centre line of each tooth. Small machines are constructed without these ducts and spacers.

The frames into which large machines are built are usually of a skeleton form; that is, the frame only provides the means for maintaining the pressure exerted by the two end clamping plates. There are a considerable number of ways of achieving this but each of them uses very little material between the two ends. Cover for the machine is provided either by thin plates attached to the frame or by an overall fibre-glass

cover. In small machines the frame is often cast and provides both strength and cover, and frequently the core of laminations is an interference fit down the whole length of the frame.

Large machines are normally for high voltage operation. This means that the windings are much more heavily insulated than those in small machines. In large machines the preformed consolidated windings are a clearance fit in the slots. The radial clearance is minimised by the wedge (Fig. 3.1.1). In small machines the lightly insulated wire is wound directly into the slots with the wedges packing the winding tight in the slot.

3.2 ASPECTS OF CONSTRUCTION THAT ARE SIGNIFICANT DYNAMICALLY

It is evident from Fig. 3.1.1 that the stiffness of the core to radial bending in large machines is provided by the depth of core behind the slot. In small machines with round bottomed slots the depth of core is not easily defined. The extent to which segmentation of the core reduces its stiffness has been an unknown quantity.

The teeth in electrical machines are invariably integral with the core and therefore share the motional behaviour of the core. This means that the teeth vibrate transversely, circumferentially and rotationally with respect to a diameter through the neutral axis of the core (Fig.3.2.1). The transverse motion of the teeth simply means that the teeth can be treated as added masses. The rotational and circumferential motion of the teeth can introduce large complications, especially if the teeth are able to resonate in their own right.

The windings and retaining wedges may be very significant dynamically. If they are loose in the slots it is easily imagined that they play no part in the dynamics of radial vibrations. However, if the windings and/or wedges are a perfect fit in the slots, it is apparent that they can add both mass and stiffness to the core system. The continuum of teeth-winding-teeth etc. is capable of taking strain and thereby adding to the stiffness of the core. The extent to which the windings and wedges add stiffness depends on the fit in the slot and the inherent stiffness of the windings.

With a packet construction the core is evidently flexible in the axial direction. The laminating and packeting of cores have not been studied previously. It must be assumed that these effects could make the use of a 3 dimensional dynamic model necessary.

Previous methods for dealing with the influence of a frame on a core have assumed a solid coupling between the two. With the skeleton frame which is so often used for large machines this assumption needs verification. There are no radial contacts at the back of the core as in small machines. The frame coupling is through the end surfaces - which are at right angles to the direction of motion.

In addition to these primary aspects of the machine features there are a number of secondary aspects which may be significant dynamically. Occasionally large machines are constructed with a number of rows of ventilation holes in the core. Large high speed machines have deep cores. With these cores second order bending effects become significant.

A few machines are manufactured using a large number of grooves at the back of the core for cooling purposes. All of these more unusual features may be important in determining resonant frequencies.

3.3 THE DEVELOPMENT OF PREVIOUS THEORIES FOR THE CALCULATION OF STATOR CORE RESONANT FREQUENCIES

The following critical analysis of previous methods is based on experimental results obtained from a moderately large induction motor. This approach has been chosen to give a measure of numerical reality to the implications of various assumptions. A machine with long teeth was chosen to emphasise the deficiencies/merits in various methods. In the next section an explanation of the measurements is given.

3.3.1 A Typical Set of Measured Resonant Frequencies

The essential features of the laminations used in this series of measurements are given in Fig. 3.3.1. It should be noted that the slots are parallel sided and very deep compared with the core depth. The slotting of this machine is such that the teeth have a taper ratio of 1.0/1.629 with fillet radii of 0.5 mm. The mass of the teeth is 2.33 times the mass of the core. The measurements were made without a winding.

The mode numbers given in Figs.3.3.1 and 3.3.2 are the number of wavelengths in the vibrating shape. Mode 2 has 4 nodes - this is the lowest radial bending mode. Curves have been drawn in Fig.3.3.2 to aid visual presentation. It is obvious that there are only a discrete number of modes. The curves numbered 1 and 4 are measured values. Curve 1 is a complete set of radial mode resonant frequencies below the first

tooth resonant frequency (transverse bending mode). The high radial bending modes have resonant frequencies which are asymptotic to this tooth resonant frequency. Curve 4 is the second complete set of resonant frequencies and occurs above the first tooth resonant frequency. This curve is not generally assymptotic to the tooth resonant frequency. In this example the lowest mode resonant frequency is still some 12% above the tooth frequency. At very high frequencies - above the second tooth resonant frequency - there are further sets of core resonant frequencies. These have been ignored. The shapes of curves 1 and 4 are typical of all machines. In the past the experimental evidence has been confined almost exclusively to the first modes in the first set. This 'break' in core resonant frequencies was first predicted by Holzmann[11].

3.3.2 The Various parameters which influence core resonant frequencies

In all the theories published for calculating resonant frequencies the core is considered to be a plain ring (or cylinder) with added teeth. Curve 3 of Fig.3.3.2 shows the calculated resonant frequencies obtained by taking one of the more accurate ring theories[12] and assuming that the teeth add only mass. Curve 2 gives the calculated resonant frequencies based on a derivation of the same theory, assuming that the teeth add both mass and rotary inertia to the ring but that the teeth do not flex. It is evident that tooth inertia becomes significant only at the higher mode resonant frequencies. In straight beam theory the inclusion of rotary inertia produces calculated resonant frequencies below the values obtained excluding it. The same is true for curved beams and rings. As the teeth begin to flex the inertia moment exerted

by the teeth on the core, and the apparent mass of the teeth in circumferential motion, increase above the values produced for rigid teeth. Thus the resonant frequencies are reduced below curve 2 when the teeth begin to flex. As the core resonant frequencies approach the first tooth resonant frequency the teeth flex more and the asymptotic curve 1 is produced. Above the first tooth resonant frequency the tooth inertia moment and apparent tooth mass (in circumferential motion) reverse sign, thus producing a curve above curve 3 which eventually becomes asymptotic to it. As with curve 1 the flexibility effects predominate near the tooth resonant frequency and gradually diminish to secondary factors away from it. It is apparent that the assumption of tooth rigidity becomes inaccurate above approximately 50% of the first tooth resonant frequency. This figure has been confirmed in a large number of measurements on various sets of laminations but has not been reported previously. Also drawn in Fig.3.3.2 are the calculated resonant frequencies using the theory developed in Chapter 4. The separate influences of tooth flexure on the rotary inertia and circumferential mass factors, and thereby on core resonant frequencies, are shown in curves 6 and 5 (only the resonant frequencies above the tooth resonant frequency are shown). These curves show that the mass factor is dominant at low mode numbers and that the inertia factor eventually assumes a similar degree of importance at high mode numbers.

The influence of tooth flexibility is often negligible in medium and small machines where teeth tend to be short and the first tooth resonant frequency is well outside the usual frequency band of concern (100 Hz to 3000 Hz). In the example given, and in large machines in general, tooth flexure must be taken into account for accurate calculation of core

3.3.3 Basic Methods

The first method for calculating core resonant frequencies was based on the most elementary thin ring theory and assumes that the teeth effectively increase the density of the ring. The method is given by Alger[13]. It is still used since it can easily be evaluated using a calculator. The limitations of the elementary ring theory are severe, especially for the thick rings found in electrical machines. Even the relatively thin ring shown in Fig.3.3.1 does not lend itself very well to the use of this method - compare columns 2 and 3 in Fig.3.3.3. At mode 5 the error is already +18%. In the following methods the effect of tooth inertia has been taken into account, with the exception of that due to Erdelyi[4].

Jordan[6] seems to have been the first to try to account for the inertia moment exerted by teeth on a ring. His book has given rise to a number of papers on core resonant frequencies, usually with Jordan as a co-author[14,15,16,17]. His approach is well illustrated in the paper by Jordan and Frohne[14]. The same method for accounting for the teeth is used by Uner[15], and by the latest authors[9,18] on this subject. Since 1950 all of the methods published have used Jordan's approach for the teeth, each with a different treatment of the core to which the teeth are attached. The major assumption made is that the teeth are additions to the core and that the core resonant frequencies are obtained using previously determined equations with certain multiplying factors or boundary conditions added to account for the teeth. The teeth have not been considered as an integral part of the core. An example of such a factor is Frohne's Δ_m which is the ratio of moment of inertia of the core-plus-teeth and the core alone about the mid radius of the core.

Implicit in this factor is the assumption that the radius of the centre of gravity of an elementary portion of the ring is co-incident with the mid radius of the ring. This approximation is reasonable for plain thin rings. It is far from adequate for toothed cores or thick rings. In the example given in Fig.3.3.3 the mid radius 'a' is 0.40103 m and the radius of the C. of G. 'R' is 0.36964 m. The two are obviously not co-incident. Since the moment of inertia is obtained about a point other than the C. of G. the value is too high - leading to an excessive reduction in resonant frequencies.

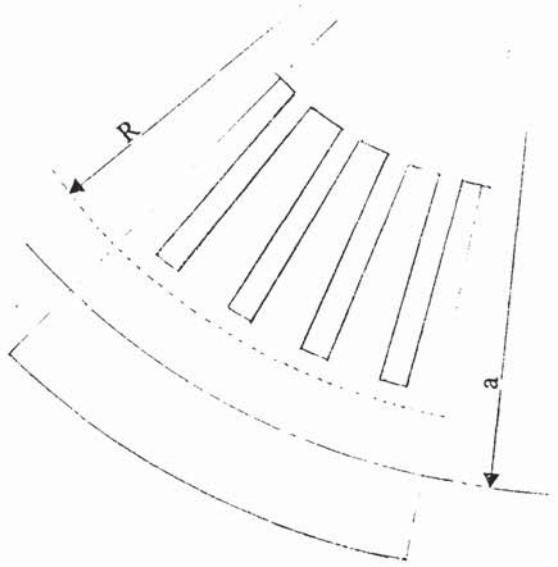

In all of the theories published the teeth have been assumed to be parallel. In small machines this is often true although slight tapers are not uncommon. The suggested technique for using the various methods with tapered teeth is to specify parallel teeth of width equal to the average tooth width. The errors involved in this approach can be seen by comparing columns 2 and 4 of Fig.3.3.3. Column 4 was obtained by evaluating Frohne's equation 29. It has been found that tooth flexure does not appreciably affect radial resonant frequencies below 50% of the tooth resonant frequency. . This means that for the example given modes 2-6 should be accurately calculable using theories, such as Frohne's, that ignore tooth flexure. In fact Frohne's calculated value for mode 6 is 14.4% low.

Frohne mentions tooth flexure at the end of his paper but does not give any method for including this effect. Shear, rotary inertia and extension of the neutral layer are taken into account using approximations that are strictly applicable to thin rings only. Uner[15] has introduced another class of vibrations and so refined Frohne's work although his own experimental evidence shows that the changes decrease the accuracy of the calculations. Both authors take account of the winding, saying that a part (unspecified) of the winding adds both mass and inertia to the system. No indication is given of the size of the winding mass to be used, although an example is given where the whole of the mass is added. It should be acknowledged that Frohne's and Uner's methods produce solutions which are easily evaluated since they involve only the roots of a quadratic or cubic equation.

Pavlovsky[19] defines and uses a Bessel function solution of the equations of motion of a plain ring. The teeth are accounted for by defining the boundary conditions at the inner surface of the ring in terms of the forces and moments exerted by the teeth. The teeth are assumed parallel and able to flex. The resulting characteristic equations are very complex, involving Bessel functions of the first and second kind. He uses an unspecified numerical method to solve these equations. No indication is given of the number of iterations needed for obtaining a solution for each mode of vibration. Pavlovsky is the only author to attempt to take account of the way the machine winding is fitted into the slots. This he does by assuming that the winding mass loads the teeth through a system of springs (see over).

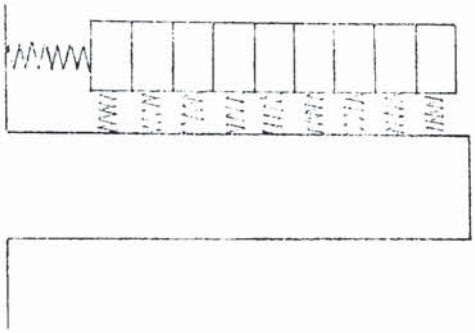

In physical terms the mass can be regarded as being produced by the copper conductors and the springs by the flexibility of the winding insulation. Slightly modified equations of motion are deduced for the teeth which are then reflected back into the equations of motion of the ring through the changed boundary conditions. Empirical values of spring constants are used in the numerical calculations of four small machines. According to Pavlovsky's measurements and theory windings reduce radial resonant frequencies but do not significantly modify the principal tooth resonant frequency. A clear verification of Pavlovsky's approach would have been the measurement of the two winding resonant frequencies that are introduced as a result of the model adopted. Calculations are given for these frequencies but no corresponding measurements are shown. The conclusions drawn regarding the influence of the windings in Pavlovsky's machines are quite different from those given in Section 6.2 which apply to large machines. For large machines, where one may need to calculate resonant frequencies as high as mode 30, Pavlovsky's method is very complex and no indication is given of its superiority over other methods. When the method developed in Chapter 4 is applied to Pavlovsky's examples the figures given in Fig.3.3.4 result. These suggest that his method is unnecessarily complex.

Holzmann[11] has considered the core and teeth as a coupled system and was the first author to predict clearly the break in the resonant

frequencies shown in Fig.3.3.2. He has also shown that further breaks occur at the second and higher tooth resonant frequencies (transverse bending modes and longitudinal modes). These higher breaks have not been confirmed experimentally by Holzmann but Poon[20] has shown them to exist for toothed straight beams. By using an energy method Holzmann reduces the coupled system equations of motion to an eigenvalue problem of degree eight which is evaluated for each mode of vibration. By using a number of simplifications an extremely compact solution of the problem is produced which does not involve iteration. The limitations of these simplifications are not at all clear since Holzmann's one set of measurements is given only graphically. He does not compare his calculations with previously reported measurements. The most important simplifications are given below. It is those relating to the shape of the teeth that are the most restrictive in applying this method to large machines.

Holzmann has assumed that the radii of the neutral axis, the centre of gravity and the mean radius of a ring are co-incident. This is a reasonable approximation for thin rings but not for thick toothed rings as found in electrical machines. It is also assumed that the teeth are parallel and that second order tooth effects such as root flexibility, rotational inertia and shear can be neglected when considering the energies of the teeth. An approximate modal shape is assumed for the encastre teeth vibrations. The need to assume parallel teeth is centred round the difficulty of calculating the potential and kinetic energies of an element of varying cross section. Holzmann uses the average tooth width in applying his method of analysis to machines with

tapered teeth. Some measurements made early in the course of this study were compared with Holzmann's calculation method. Dr. Holzmann was kind enough to supply these calculations which are compared with the author's values in Fig.3.3.5.

It should be underlined that in the above methods, and those that follow, no attempt has been made to take account of tapered teeth or of 'secondary' tooth effects or to include the effects of wedges or segmentation. In the example in Fig.3.3.5 the secondary effects alone account for a reduction of 25% in the tooth resonant frequency. In making comparisons between different theories and measurements the total error band for a 95% confidence limit has been taken as 3.92 times the standard deviation (or r.m.s. error).

3.3.4 Methods Including the Frame

Most of the methods below have been developed for small machines and the assumed models of the core plus frame do not begin to approximate to the configuration found in large machines. The essential details of a medium machine frame are shown in Fig.3.3.6. Dynamically the two endplates are the most important - there being only a skeleton frame connecting them.

The first method published for taking into account the frame of the machine is due to Erdelyi[4]. He assumes that the frame is represented by a thin continuous ring connected solidly to the core by ribs. Using a two rib example Erdelyi shows that the discontinuity of the contact between the core and the frame leads to a number of resonant frequencies having the same mode number but with nodes in different circumferential

positions. If these frequencies are reasonably separate it is possible for a rotating force wave - the norm in electrical machines - to excite a sensibly standing wave vibration. Such a vibration has been observed in practice and is described in Section 6.1. Erdelyi uses an energy method to arrive at an eigenvalue problem which is solved to obtain the various resonant frequencies. He assumes that the core is thin, thereby ignoring the shear and rotational inertia of the core and the teeth. An example is given of the second and third modes only of a small induction motor.

Ellison and Yang[9] have extended Erdelyi's method using the same form of equations and solution. They have included the effects of shear and rotary inertia - assuming parallel teeth which do not flex. Good agreement is obtained between the measurements and calculations of a very small machine for modes 2 to 5.

In their example Ellison and Yang use four ribs connecting the core to the outer frame. Verma and Girgis[21] start by assuming that the connection between the frame and the core is solid and continuous. This type of construction is found in small flameproof motors. These authors have generalised their treatment of this type of construction by assuming a three dimensional model. In all other published work two dimensional models have been assumed. The authors specify the differential equations of the core and frame separately and equate boundary conditions at the frame inner surface. The solutions of the differential equations of motion are n^{th} order Bessel functions. The influence of the teeth and winding is taken into account in the same

manner as Pavlovsky, i.e. by using the motion of the teeth and winding to specify the forces at the inner boundary of the core. No expressions are given for these forces - they are simply stated in a generalised form.

In their second paper[22] Verma and Girgis have used Frohne's work[23] to obtain the forces and moments exerted by the teeth. Calculated resonant frequencies are compared with measurements. The main body of comparative measurements is of machines without frames. In solving their equations to obtain resonant frequencies, Verma and Girgis have used a search method - presumably by choosing a frequency and then evaluating displacements. It is significant that for two of the machines quoted certain modes were not traceable. The authors give no indication of what influence the laminations have on the material strength in the axial direction. No measurement is given where there is any axial variation in the vibration mode. The theory developed in Chapter 4 is compared with the theory of Verma and Girgis (applied to machines without a frame) in Fig.3.3.7. Dr. Verma was kind enough to supply calculations of the configuration shown in Fig.3.3.1. These calculations are compared with measurements and various other theories in Fig.3.3.3. It is evident that the use of Frohne's work to account for the teeth leaves room for improvement. The need for a three dimensional theory has still to be established experimentally. The measurements in Chapter 5 do not support the use of a 3D theory.

A number of papers[24-26] have been concerned with the effect of the frame/housing of large machines on noise levels. It is evident that the extent of the influence of the frame is very variable because of the

multiplicity of frame types and the variability of coupling between the cores and frames of large machines, which are individually designed and built up by hand. In all of these papers the endplates of the frames have been disregarded. It is shown experimentally in Chapters 5 and 6 that this is the most important member of the frame.

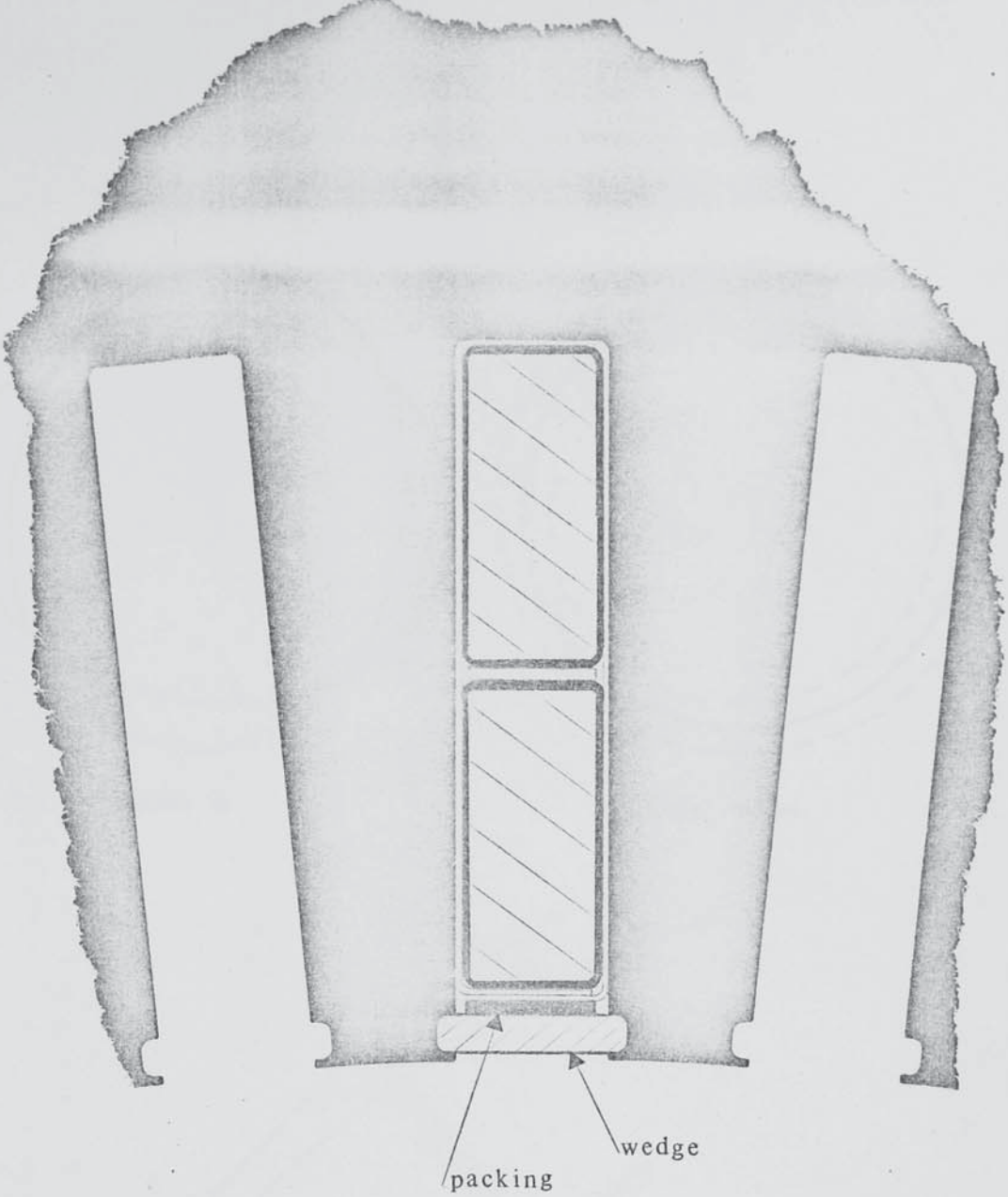

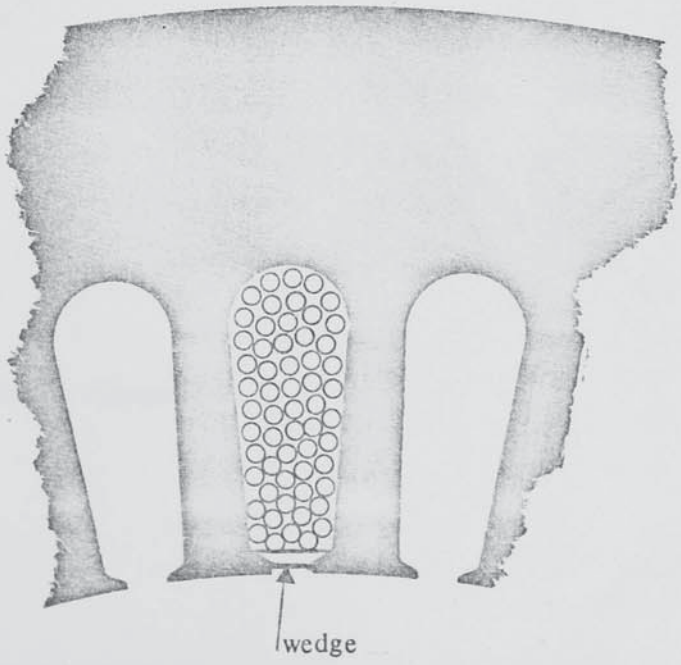

WINDINGS AND WEDGES IN LARGE AND SMALL MACHINES

Fig. 3.1.1

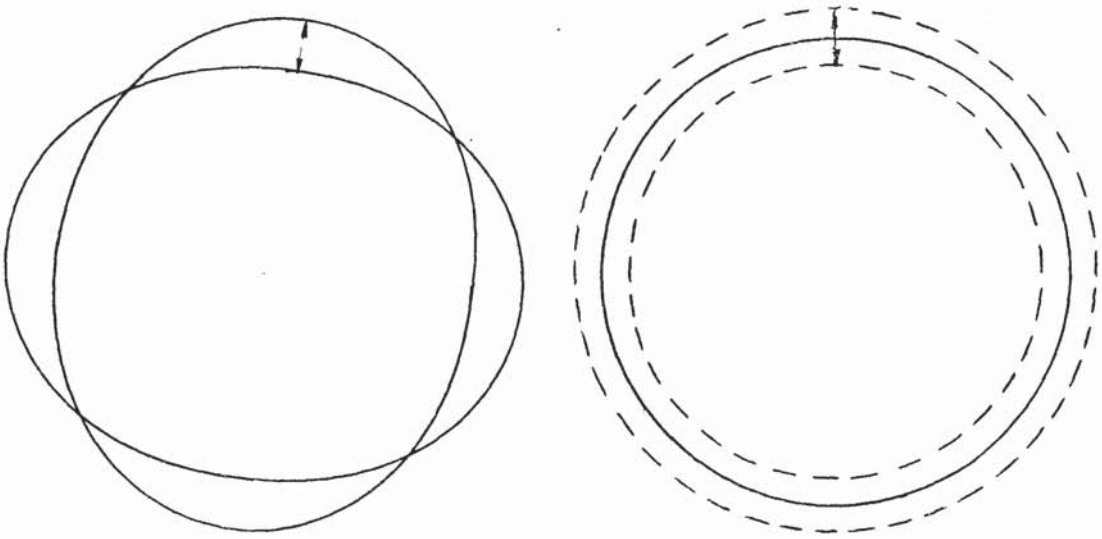

mode 2

zero mode

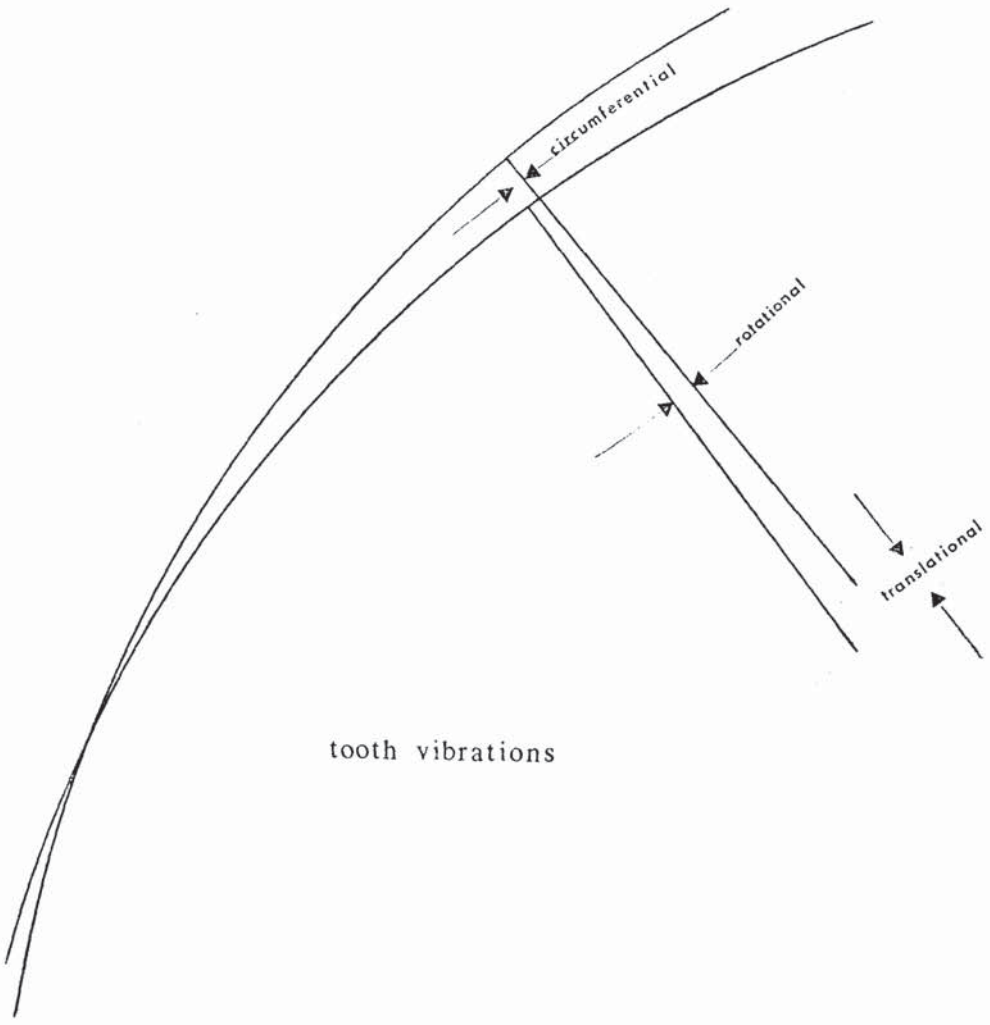

tooth vibrations

VIBRATION MODES OF CORES

Fig. 3.2.1

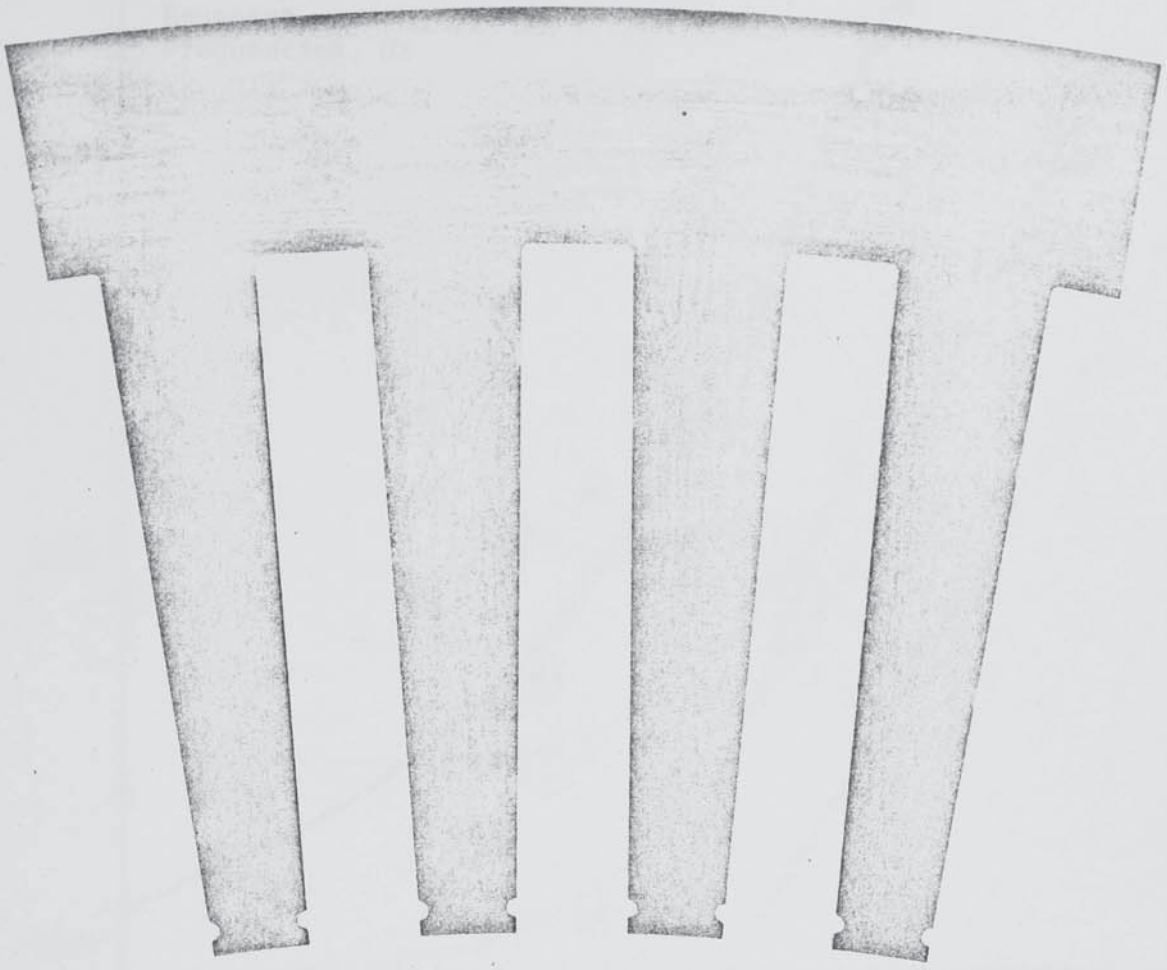

OD = 831.85mm, ID = 772.25mm, GD = 597.63mm, slots 72 x 13.97mm.

Refer to Fig.3.3.2

Curves / Mode	1	2	3	4	5	5	6	6	7	7
2	74.7	74.5	76.7	2095	74.5	-	74.5	1883	74.4	2384
3	200.8	205.2	216	2184	205	2468	205.2	1900	204.6	2563
4	382.4	832.3	411.8	2272	380.5	2468	382	1922	380	2691
5	571.9	598	661.3	2383	591.5	2468	596	1948	589.6	2788
6	800.8	845	962	2522	826	2468	835	1976	818.8	2858
7	1008	1117	1311	2709	1068	2480	1085	2038	1047	2965
8	1200	1407	1705	2946	1294	2548	1318	2144	1249	3149
9	1349	1712	2141	3227	1479	2677	1501	2320	1409	3398
10	1463	2028	2617	3607	1612	2869	1619	2581	1525	3697
11	1547	2350	3129	4033	1699	3109	1689	2904	1609	4028
12	1619	2676	3673	4483	1756	3380	1732	3266	1666	4376
13	1668	3007	4248	4996	1788	3669	1763	3652	1707	4735
14	1706	3336	4849	5458	1796	3965	1779	4052	1739	5099
15	1738	3672	5473	-	1802	4265	1791	4462	1763	5468

FACTORS INFLUENCING RESONANT FREQUENCIES

Fig. 3.3.1 (Dimensions and numerical values)

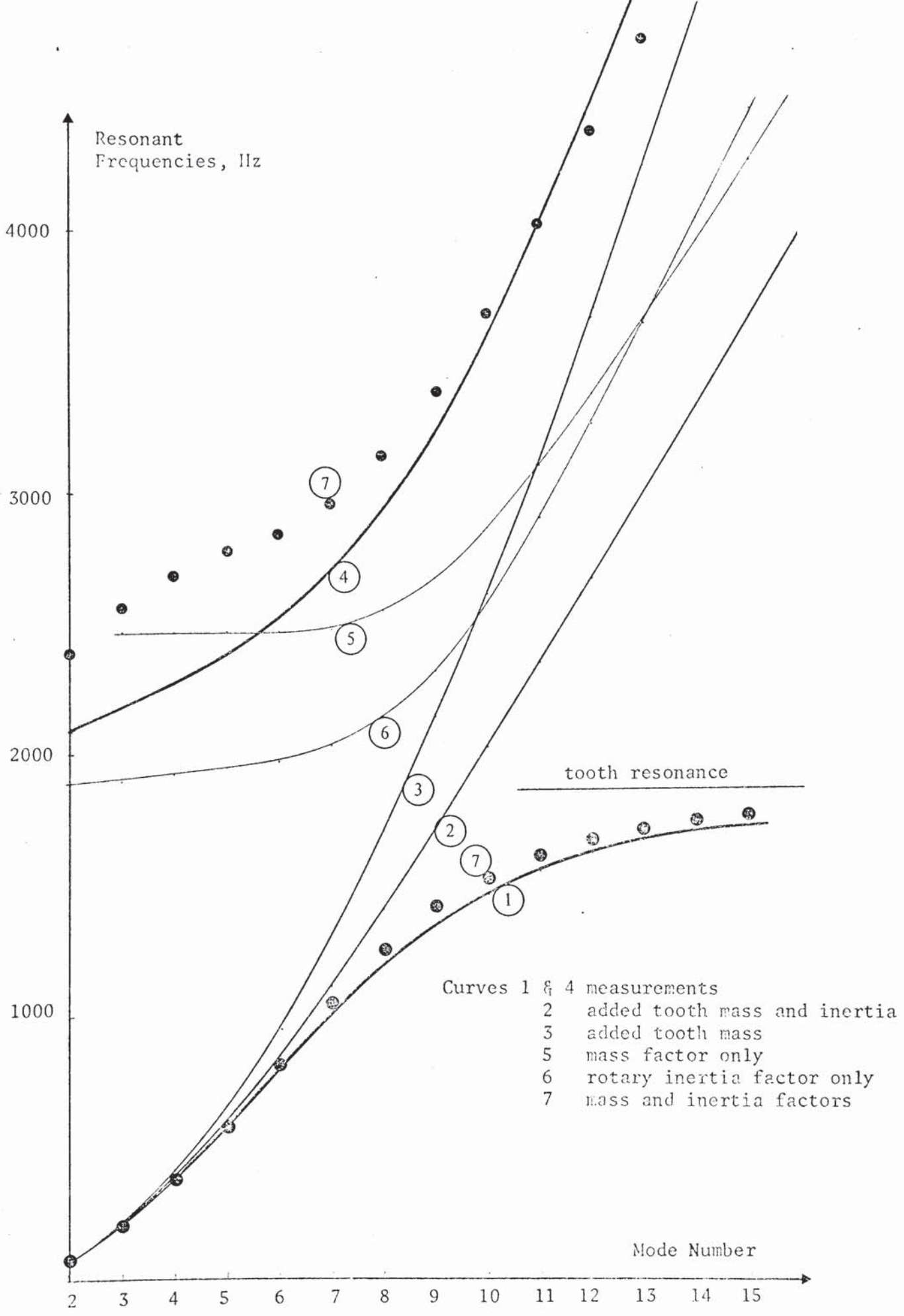

FACTORS INFLUENCING CORE RESONANT FREQUENCIES

Fig. 3.3.2

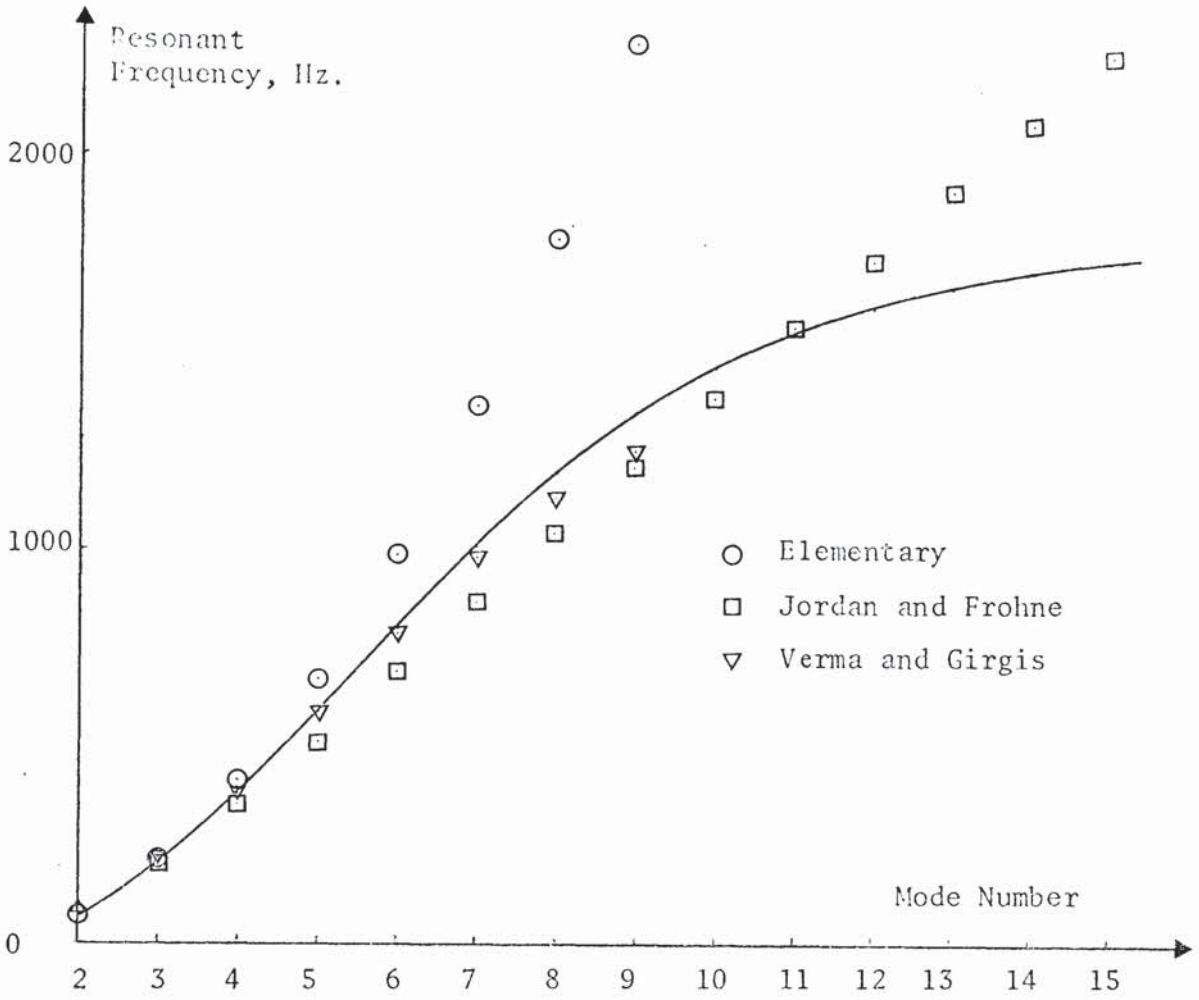

Mode	Meas.	Classical	Frohne Jordan	Verma Girgis	Present Theory
2	74.7	76.9	74.1	85	74.4
3	200.8	217.4	196.2	221	204.6
4	382.4	416.9	346.3	385	380
5	571.9	674.2	512	586	589.6
6	800.8	989	685	792	818.8
7	1008	1361	861.3	980	1047
8	1200	1791	1038.2	1138	1249
9	1349	2278	1214.6	1258	1409
10	1463	2822	1390	-	1525
11	1547	3424	1564	-	1609
12	1619	4082	1737	-	1666
13	1668	4799	1908	-	1707
14	1706	5572	2079	-	1739
15	1738	6403	2249	-	1763

Dimensions as per Fig. 3.3.1

COMPARISON OF BASIC METHODS OF CALCULATION

Fig. 3.3.3

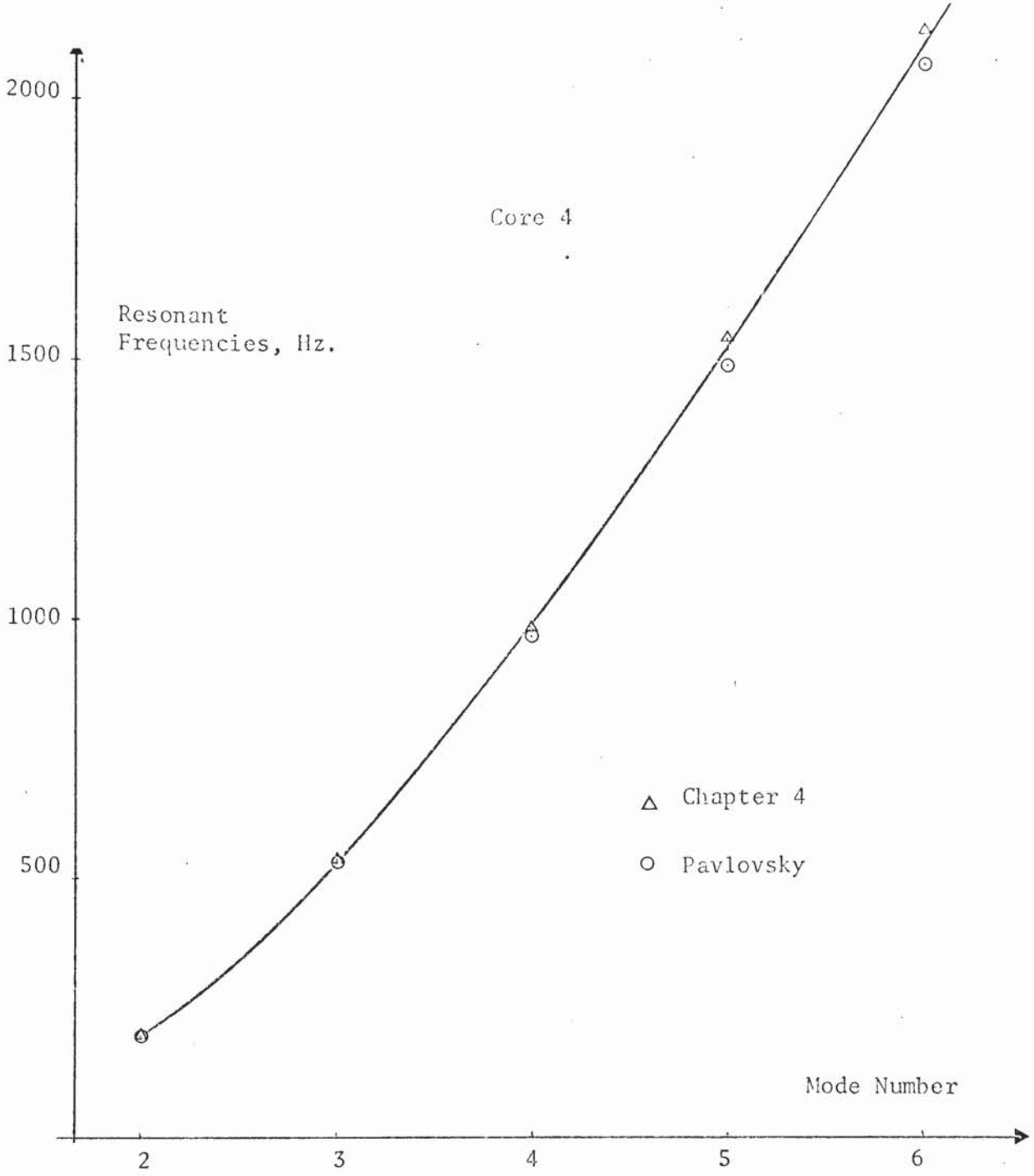

Mode	0	2	3	4	5	6	
Meas.	3244	527	1441	2642	3901	4926)	
Pavlov.	3198	547	1470	2632	3909	5133)	Packet 1
Ch.4	3240	544	1464	2624	3861	4845)	
Meas.	2840	276	750	1394	2138	2989)	
Pavlov.	2856	269	735	1357	2095	2900)	Packet 2
Ch.4.	2847	270	745	1382	2138	2954)	
Meas.	2842	479	1255	2266	3334	4190)	
Pavlov.	2891	469	1256	2248	3336	4375)	Packet 3
Ch.4.	2885	471	1268	2274	3343	4190)	
Meas.	2398	195	531	988	1524	2106)	
Pavlov.	2388	191	575	968	1493	2065)	Packet 4
Ch.4.	2382	194	535	993	1540	2131)	

Total Error band (95% confidence): Pavlovsky = 8.71%,
Chapter 4 = 4.57%

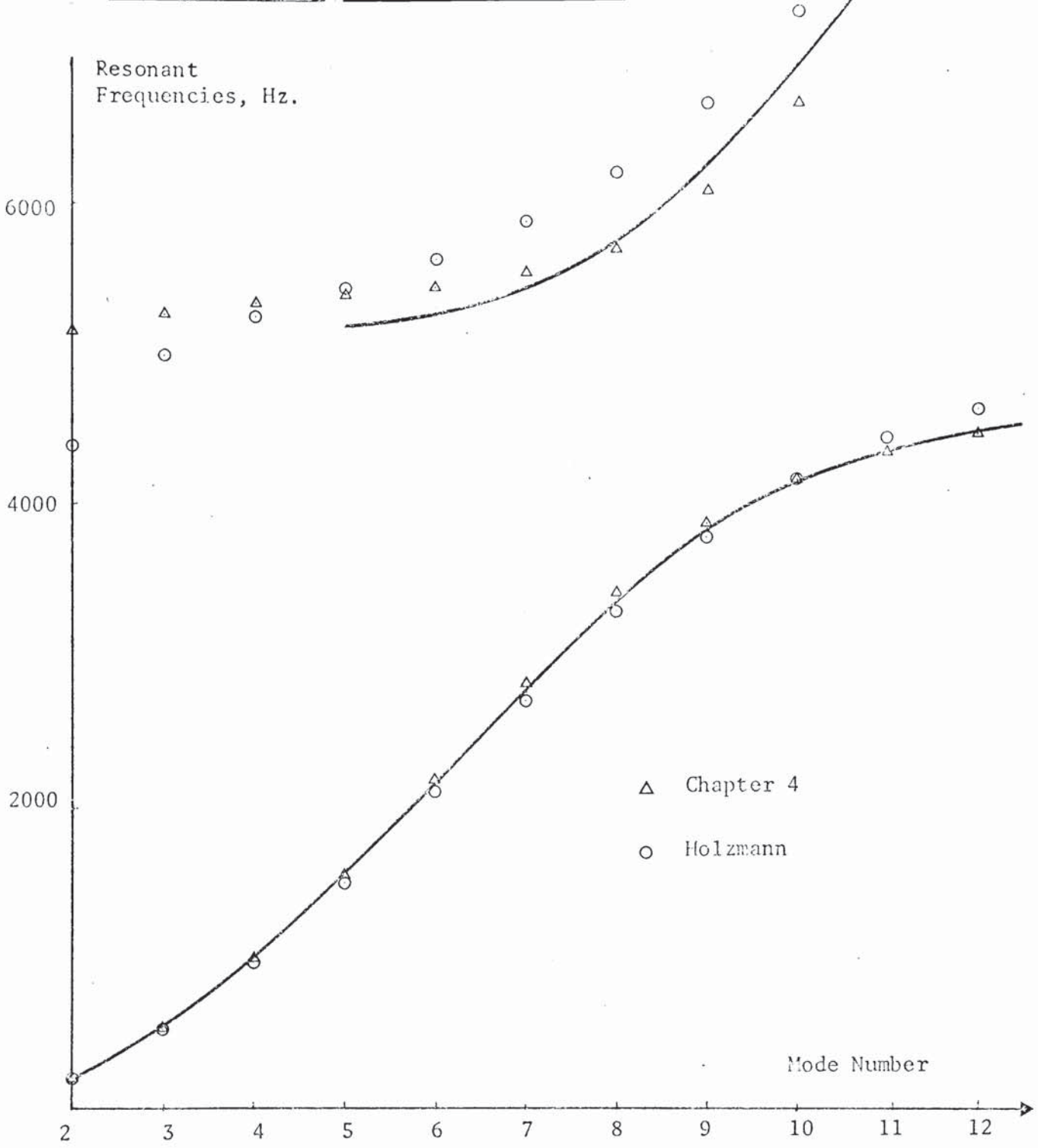

OD = 831.6mm, ID = 721.5mm, GD = 634.6mm, slots 84 x 12.97 mm.

Mode	Measurements		Holzmanns Calculations		Calculations from Ch.4.	
2	191.5	-	191.7	4135	196	5148
3	539	-	525.2	4988	541.4	5273
4	1002	-	972.2	5263	1006	5356
5	1541	5203	1507.7	5450	1566	5410
6	2160	5317	2102	5647	2190	5441
7	2777	5444	2717	5891	2837	5511
8	3370	5794	3302	6219	3439	5703
9	3863	6283	3805	6672	3903	6088
10	4183	6924	4190	7267	4209	6672
11	4385	7672	4466	7988	4379	7399
12	4508	8568	4698	8793	4484	8201

Total error band (95% confidence) is

Holzmann = 16.1%, Chapter 4 = 9.0%

HOLZMANNS CALCULATIONS

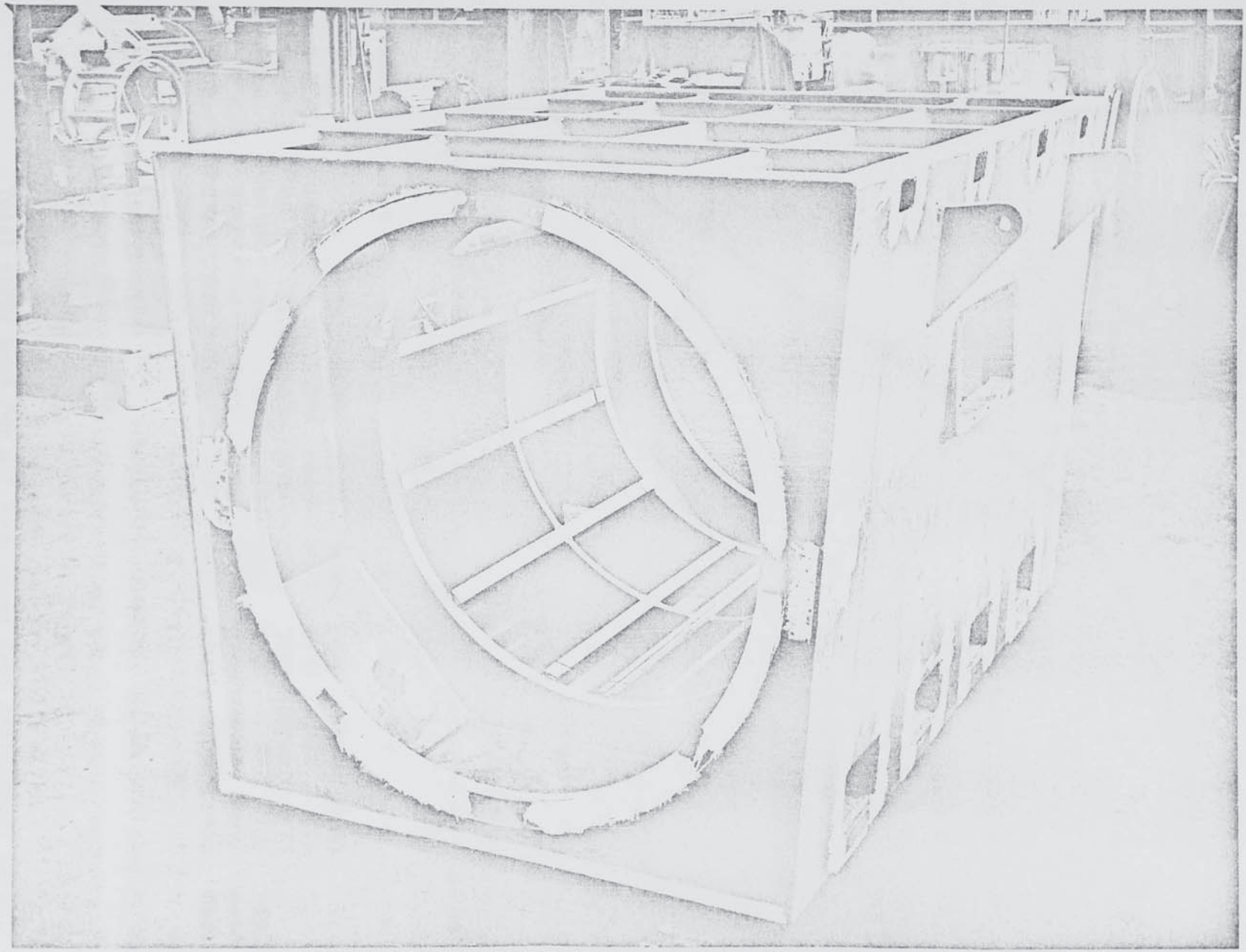

A MEDIUM MACHINE FRAME (Larger machine frames are much less solid)

Fig. 3.3.6

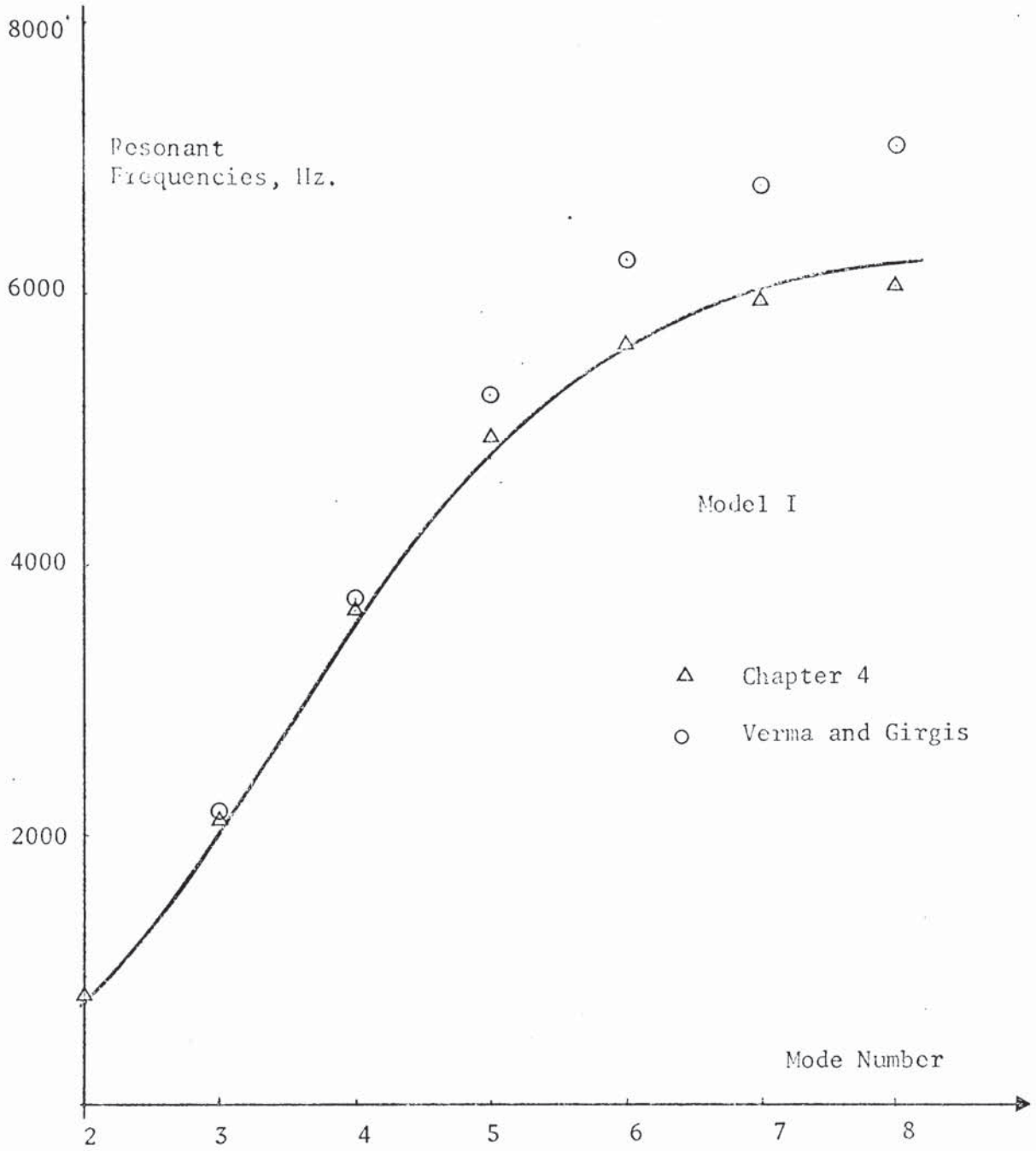

Mode	0	2	3	4	5	6	7	8	9
Meas.	6620	770	2025	3550	4800	5630	6050	6250	-
V & G.	6870	-	2156	3766	5275	6283	6820	7111	-
Ch.4.	6823	794.3	2118	3684	4953	5642	5967	6073	
Meas.	6170	530	1400	2410	3450	4450	5180	5590	5850
V & G.	6350	-	1369	2469	3628	4703	5524	6087	6496
Ch.4.	6381	510.8	1379	2481	3639	4604	5236	5615	5835
Meas.	2009	943							
V & G.	2012.6	935.4							
Ch.4.	1988.3	932							
Meas.	-	465	1099						
V & G.	-	481	1092						
Ch.4.	-	462.9	1098						

Total error band for all four cores (95% confidence) is:-

V & G = 28.6% (19 calcs.), Chapter 4 = 10.7% (21 calcs.)

VERMA AND GIRGIS EXAMPLES

Fig. 3.3.7

CHAPTER 4

THE THEORY OF STATOR CORE RESONANT FREQUENCIES

4.1 RING THEORY

In the methods described in Chapter 3 the majority of authors have taken thick or thin ring theories and modified them to account for teeth etc. The most recent theories[11,19,21] have departed from the modified ring approach and are thereby restricted to the most elementary treatment of the teeth. The present theory is a modified ring theory. This approach was adopted so that tapered teeth and secondary tooth effects could be included in the analysis. In view of the importance of the underlying ring theory in any analysis of complete stator cores the various theories were compared with Kuhl's measurements[27]. These measurements are for steel rings with radial thickness to outside radius ratios (h/r_a) varying from 0.1 to 1.0 and include modes 2 to 8. This is the most comprehensive set of ring measurements published.

The assumptions used in developing various ring theories are given in Chapter 3. The limitations of these assumptions can be seen in the numbers of Fig. 4.1.1. The figures attributed to Erdelyi are based on a later work[28] in which he developes his original thin ring theory[4] to include secondary effects. The calculations based on Bucken's theory[12] are included for comparison purposes. This theory has not been used previously as a basis for a modified theory. Bucken suggests a Timoshenko shear coefficient which is a function of the shape of the

ring cross-section. For thin rectangular laminations as found in the stators of electrical machines the value of n is 1.5. A large number of different values of n have been suggested,[29,30] mainly without any experimental validification. In applying Bucken's theory an empirical value of n (equal to 1.0) has been used. This value has been derived specifically for steel with Poisson's ratio, ν, assumed equal to 0.29. It is apparent that Bucken's theory is sufficiently accurate at the modes considered for all ring thicknesses found in electrical machines and specifically for $h/a < 0.2 + 1/k$ (k is the mode number).

In calculating ring resonant frequencies a correction factor C_r may be used and defined as the 'accurate' resonant frequency divided by the value obtained using the elementary theory. A full table of correction factors is given in Appendix I. Such a table is most useful in the design office where the elementary theory can be easily evaluated but the complex theories cannot.

4.2 MODIFIED RING THEORY

4.2.1 Basic Equations

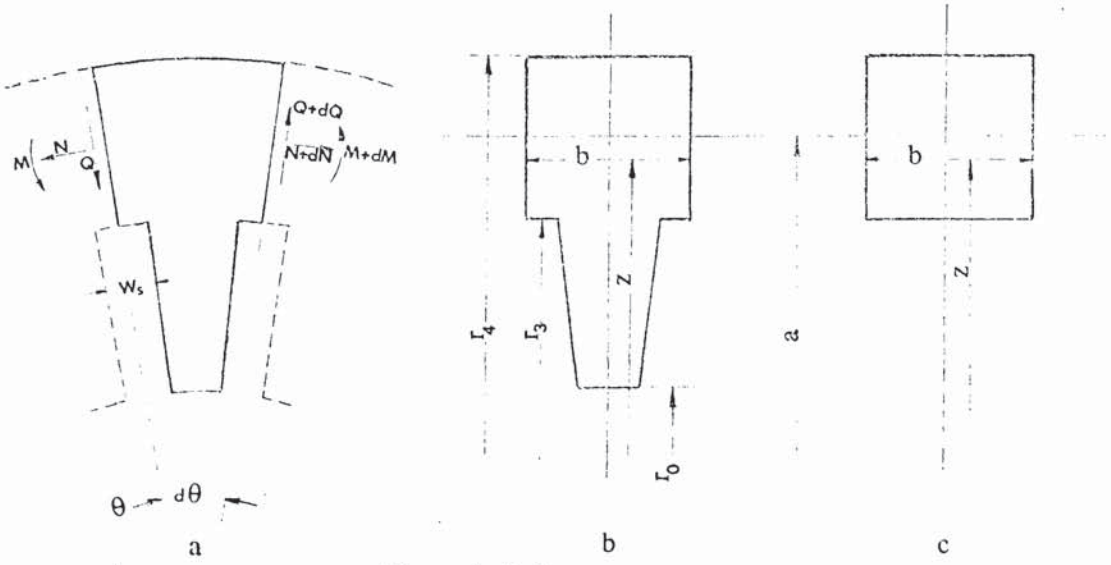

Fig. 4.2.1.

In developing the equations for plain rings the ring cross-section round the circle is assumed constant. It is evident from Fig.4.2.1(a) that the configuration found in electrical machines violates this assumption. An artifice is required that enables the assumption that the cross-section is continuous circumferentially. Two cross-sections are assumed for the ring with teeth. The first of these sections, Fig.4.2.1(b) is assumed to apply for mass and rotary inertia calculations. The second cross-section Fig.4.2.1(c), is assumed to apply for the calculation of the radius of the neutral layer, r, and thus the bending stiffness of the ring. Although the ring is strictly rectangular in cross-section the width b in Fig.4.2.1(b) is a function of the radius z between r_o and r_3. The presence of the slots means that the section between r_o and r_3 is able to flex freely, being constrained only by the root stiffness of the tooth. Strictly, the arrangement is that of a coupled system with two principal types of vibration. In the present analysis the additional flexure of the section r_o - r_3 is accommodated by mass and inertia multiplying factors.

Consider Fig.4.2.1(a) and let derivatives with respect to θ be denoted by a prime. The equations of motion for an elementary volume are:

$$N - Q' = -ma\partial^2 w/\partial t^2 \qquad (1)$$

$$Q + N' = m\psi a\partial^2 v/\partial t^2$$

where N and Q are the normal and shear stress resultants, m the mass per unit length along the circle of radius a (which runs through the centroids of each section - Fig.4.2.1(c)) and w and v the radial and tangential displacements defined on the neutral layer. The parameter ψ is the

tangential displacement mass factor. Taking into account the effect of shearing stresses the curvature is given by:

$$w'' + w = -Mr^2/EI_c + nQ'r/AG \qquad (3)$$

where M is the bending moment and I_c is the equivalent second moment of area for curved beams. The constant E is Young's modulus, G the shear modulus and n the Timoshenko shear coefficient which relates the average shear stress on a section to the shear stress measured at the neutral layer, which lies at a distance r from the ring centre. A is the area of the section - Fig.4.2.1(c).

By considering the moments of the elastic and inertia forces with respect to the ring's centre it is found that:

$$M' + N'a = maR\partial^2 v/\partial t^2 - J_r \xi \partial^2/\partial t^2 (w' - v)/R \qquad (4)$$

where R is the radius of the centre of gravity of the elementary portion of the ring (Fig.4.2.1(b)) and J_r the corresponding moment of inertia around the same point per unit angle θ. The inertia moment factor ξ and the tangential displacement mass factor ψ take values other than 1.0 when the teeth shown in Fig.4.2.1(a) begin to flex.

The above equations are completed by the extension of the ring which is given by

$$w + v' = Nr/AE \qquad (5)$$

The various parameters in the above equations are evaluated as below:

From Fig. 4.2.1(c)

section area $$A = \int_A bdz \qquad (6)$$

radius of centroids $$a = \int_A bzdz/A \qquad (7)$$

radius of neutral layer $r = A/\int_A (b/z)dz$ (8)

From Fig. 4.2.1(b)

radius of C. of G. $R = \int_A bz^2dz / \int_A bzdz$ (9)

moment of inertia $J_r = (m/A)\int_A bz(z-R)^2dz$ (10)

radius of C. of Percussion $R_p = \int_A bz^3dz / \int_A bz^2dz$ (11)

The coefficient of $ma\partial^2v/\partial t^2$ in equation (4) equals the radius of the centre of percussion by definition so that:

$$R + J_r/maR = R_p$$

From equations 1, 2 and 5

$$(w + v' + w'' + v''')\ EA/mar = \psi\ \partial^2v'/\partial t^2 - \partial^2w/\partial t^2 \quad (12)$$

and by eliminating M, N and Q from equations 1, 3, 4, and 5 it is found that

$$[(\delta s+1)(w'+v'')-\delta(w'''+w')]\ EA/mar = \partial^2/\partial t^2[(\sigma+1)v - \varepsilon\xi(w'-v)-s\delta w'\ ] \quad (13)$$

where $\delta = (a-r)/a, \quad \varepsilon = (R_p-R)/a, \quad \sigma = (R-a)/a, \quad s = nE/G$ (14)

From equations 12 and 13 it can be deduced that v and w are displaced in phase 90° with respect to θ. This gives a general solution of the following form:

$$v_k = V_k \cos(k\theta) \sin(\Omega_k t)$$
$$w_k = W_k \sin(k\theta) \sin(\Omega_k t) \quad (15)$$

Substituting equations 15 into 12 gives

$$W_k[1-k^2-z] + V_k[k^3-k-\psi kz] = 0 \text{ where } z = mar\Omega_k^2/AE \quad (16a)$$

and putting equations 15 into 13 gives

$$W_k[k(\delta s+1)-\delta k+\delta k^3-\varepsilon\xi kz-s\delta kz]+ V_k[-k^2(\delta s+1)+\varepsilon\xi z+(\sigma+1)z] = 0 \quad (16b)$$

from which W_k and V_k can be eliminated to produce the following quadratic in z:

$$z^2[(\sigma+1)+k^2\psi(\varepsilon\xi+s\delta)+\varepsilon\xi]$$
$$- z[k^2([k^2-1][\varepsilon\xi+s\delta+\psi\delta]+[1+\psi][\delta s+1])-(k^2-1)(\varepsilon\xi+\sigma+1)]$$
$$+ [\delta k^2(k^2-1)^2] = 0 \quad (17)$$

The general solution of this equation gives four roots. The two radial flexural modes of vibration are considered significant in the majority of cases. At this stage a simplification may be introduced. The resulting equation is somewhat simpler.
If the ring is assumed to be inextensible then equation 5 is replaced by the identity:

$$w + v' = 0 \quad (18)$$

The elimination of w, N, M and Q from equations 1, 2, 3, 4 and 18 is very tedious and eventually leads to the following expression:

$$EA\delta(v''''' + 2v'''' + v'')/r - (\xi\varepsilon ma+s\delta ma)\partial^2v''''/\partial t^2$$
$$-(2\xi\varepsilon ma+m\sigma a - \psi(s\delta+1)ma)\partial^2v''/\partial t^2$$
$$- (\xi\varepsilon ma+mR)\partial^2v/\partial t^2 = 0 \quad (19)$$

The general solution of equation 19 is assumed to be a Fourier series of the following form:

$$v_k = V_k\cos(k\theta)\sin(\Omega_k t)$$

which leads to the following expression for Ω_k^2

$$\Omega_k^2 = EA\delta k^2(k^2-1)/mar[k^4(\xi\varepsilon+s\delta)-k^2(2\xi\varepsilon+\sigma-\psi(s\delta+1))+(\xi\varepsilon+1+\sigma)] \quad (20)$$

It is useful to define a normalised response function. Such a function can be used to obtain dynamic deflections at non-resonant frequencies. From equations 16a and 16b it is straightforward to separate out the radial displacement W_k.

$$W_k[k(\delta s+1)-\delta k+\delta k^3 - \varepsilon\xi kz-s\delta kz]$$

$$+ W_k[1-k^2-z][-k^2(\delta s+1)+\varepsilon\xi z + (\sigma+1)z]/[k^3-k-\psi kz] = 0$$

The radial displacements $W_{k,o}$ and $W_{k,\Omega}$ are defined as the displacements at zero frequency and at frequency Ω for any order k. The normalised response function R_n is equal to $W_{k,\Omega}/W_{k,o}$ i.e.

$$R_n = \delta k(k^2-1)/[(k[\delta s+1] - \delta k+\delta k^3-\varepsilon\xi kz-s\delta kz)$$

$$- (1-k^2-z)(-k^2[\delta s+1]+ \varepsilon\xi z+[\sigma+1]z)/(k^3-k-\psi kz)] \qquad (22)$$

where z equals $mar\Omega^2/AE$. A typical response function is given in Fig.4.2.2 showing clearly the influence of the circumferential displacement mass factor and the inertia moment factor. The two resonant frequencies are of the same type (radial flexural modes) with one occurring below and one above the tooth resonant frequency.

In all of the calculations of resonant frequencies reported in this thesis equation 17 has been used. The solution of equation 17 is straightforward and presents no difficulties when using a computer so that recourse to the simplified equation 20 is not necessary. It should be noted that some computers lack the necessary precision in calculating the small quantities δ, ε and σ using single precision variables.

4.2.2 Applications to large machines

Implicit in the following derivations is the assumption that axial vibrations of the core are uncoupled. The following theory applies to oscillations in the plane of the ring only. Sections are assumed which take into account: the core with axial ventilation holes, teeth, endrings, solidly connected frame with cooling fins, and slot wedges. The endrings may be in practice either the core clamping ring or the frame endplates, as found in large machines. The frame and cooling fins may be the type found in small flameproof motors or they can be the core and teeth of an inverted stator. It has been found that in large machines the winding does not significantly influence the values of resonant frequencies. For this reason the winding is not treated separately. It may be included as an additional mass by increasing the effective mass per unit length m.

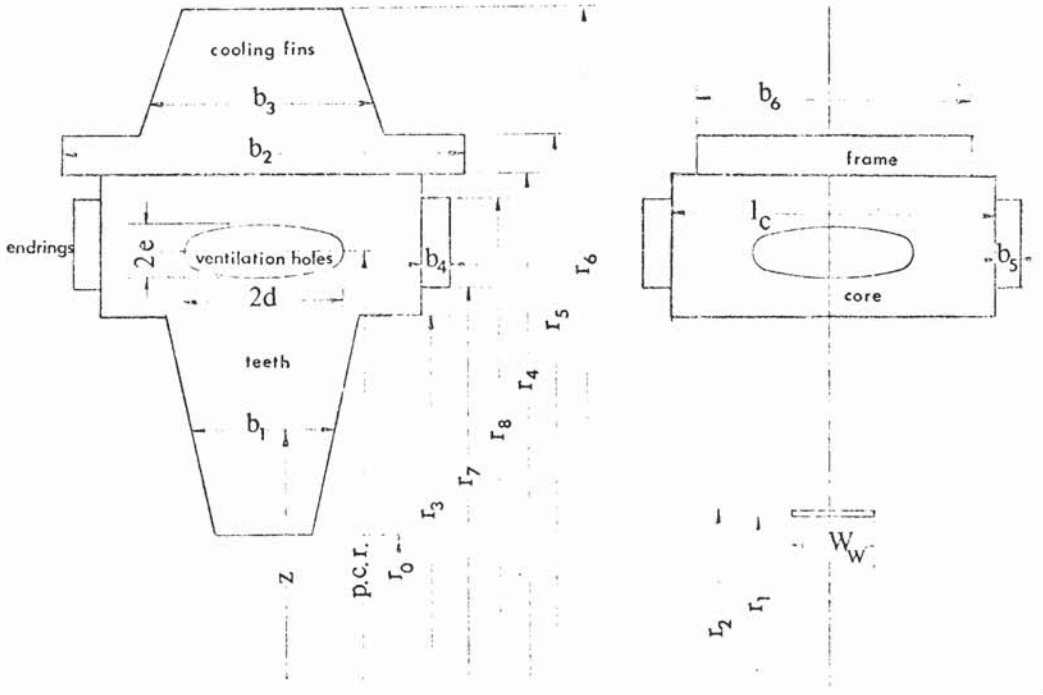

a

Mass and Inertia

b

Stiffness

Fig. 4.2.3

It is assumed that the endrings and frame are continuous circumferentially. It is obvious that the ventilation holes are discontinuous and the same procedure is used to include these holes as that adopted to account for the teeth. The nett result is that circular ventilation holes appear as elipses in the assumed cross sections of Fig. 4.2.3. Only one row of ventilation holes is shown although it is usual to have two or more. All radii in Fig. 4.2.3 are geometrical values but widths are scaled according to density ratios and Young's modulus ratios with core values as the bases. In determining the wedge width W_w the wedge material is assumed to produce all of the strain in the complete ring formed by alternate teeth and wedges. This assumption is valid as long as the teeth modulus >> wedge modulus.

Consider Fig. 4.2.3(a)

l_c = nett core length = (gross core length - ducts) x stacking factor

e = ventilation hole radius

p.c.r. = pitch circle radius of ventilation holes

$d = l_c \times e \times$ No. holes/($\pi \times$ p.c.r.)

$b_1 = l_c(1-k_1/z)$, k_1 = slot width x no. slots/2 - - parallel slot

$= l_c \times k_1/z$, k_1 = tooth width x no. slots/2 - - parallel teeth

$b_2 = l_c k_2$, k_2 = frame length x frame dens./(l_c x core dens.)

$b_3 = l_c k_3/z$, $k_3 = k_2$ x fin width x no. fins/2 - - parallel fins

$= l_c(k_2-k_3/z)$, $k_3 = k_2$ x slot width x no. fins/2 - - parallel interfin space

$b_4 = l_c \times k_4$, k_4 = 2 x endring thk, x endring dens./(l_c x core dens.)

The following are defined: $X = \int_A bzdz$, $Y = \int_A bz^2dz$, and $Z = \int_A bz^3dz$

as per equations 9 and 11 so that $R = Y/X$ and $R_p = Z/Y$. Only the equations for tapered teeth and parallel fins with one row of ventilation holes are quoted here for the sake of brevity.

$$X = l_c[(r_5^2-r_4^2)k_2/2+(r_4^2-r_3^2)/2 + (r_3^2-r_0^2)/2-k_1(r_3-r_0)+k_4(r_8^2-r_7^2)/2 + k_3(r_6-r_5) - \pi edp.c.r./l_c] \quad (23)$$

$$Y = l_c[(r_5^3-r_4^3)k_2/3+(r_4^3-r_3^3)/3+(r_3^3-r_0^3)/3-k_1(r_3^2-r_0^2)/2+k_4(r_8^3-r_7^3)/3 + k_3(r_6^2-r_5^2)/2 - \pi ed(p.c.r.^2 +e^2/4)/l_c] \quad (24)$$

$$Z = l_c[(r_5^4-r_4^4)k_2/4+(r_4^4-r_3^4)/4+(r_3^4-r_0^4)/4-k_1(r_3^3-r_0^3)/3+k_4(r_8^4-r_7^4)/4 + k_3(r_6^3-r_5^3)/3 - \pi ed(p.c.r.^3+3e^2p.c.r./4)/l_c] \quad (25)$$

Consider Fig. 4.2.3(b)

$b_5 = l_c x k_5$, k_5 = 2 x endring thk.x endring mod./(l_c x core mod.)

$b_6 = l_c x k_6$, k_6 = frame length x frame mod./(l_c x core mod.)

$W_w = l_c x k_7$, k_7 = fit x $2\pi r_1$ x wedge mod./(l_c x core mod. x no. slots), fit $\leqslant$ 1.0 according to tightness of fit of wedges in the grooves.

Following the definitions in equations 6,7, 8

$$A = l_c[(r_2-r_1)k_7+(r_4-r_3)+(r_5-r_4)k_6+(r_8-r_7)k_5- \pi ed/l_c] \quad (26)$$

$$a = l_c[r_2^2-r_1^2)k_7+(r_4^2-r_3^2)+(r_5^2-r_4^2)k_6+(r_8^2-r_7^2)k_5-2\pi ed\ p.c.r./l_c]/2A \quad (27)$$

$$r = A/l_c[k_7\ell n(r_2/r_1)+\ell n(r_4/r_3)+k_6\ell n(r_5/r_4)+k_5\ell n(r_8/r_7) - 2\pi p.c.r.\ d(1-\sqrt{1-(e/p,c,r,)^2})/l_c e] \quad (28)$$

Having obtained R, R_p, A, a and r the quantities δ, ε and σ can be calculated and equations 17 and 20 solved for resonant frequencies where the tooth flexure is not significant i.e. $\xi = \psi = 1.0$.

It should be noted in passing that experimental work on large machines shows that frame endplates can be considered to be coupled to the complete system only at low frequencies.

4.2.3 Tangential Displacement Mass Factor

Two factors were introduced into the equations of motion of the elementary ring to account for flexing of the teeth. In the forces obtained by considering the tangential displacements of an elementary ring section the mass per unit periphery m appears thus:

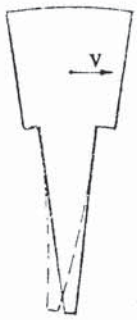

$$Q + N' = ma\ddot{v} \ ;$$

dots denoting differential with respect to time.

This equation is adequate until the teeth begin to flex. When this happens the force for a given tangential displacement increases by a mass factor ψ.

Frohne[14] proposed such a factor but did not publish any expressions, although Verma[21] has reported using Frohne's work. The following theory is specifically for tapered teeth - parallel teeth being a particular case.

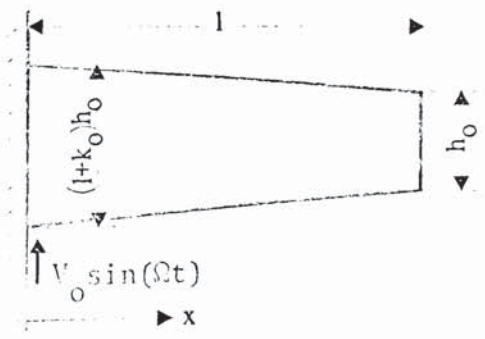

Consider an encastre beam vibrated at the root with a given displacement $V_o \sin(\Omega t)$ and let the beam transverse vibration be $v(x,\Omega)$. Then the tooth mass factor ψ_t:

$$\psi_t(\Omega) = -\int_0^{\ell} h(x)\ddot{v}\ (x,\Omega)\ dx/\ell h_o(1+k_o/2)\Omega^2 \sin(\Omega t)V_o \qquad (29)$$

$h(x)$ is the height of the beam as a function of x and for a linearly tapered beam $h(x) = h_o(1+k_o-k_o x/\ell)$ (30)

In order to obtain a solution for ψ_t with reasonable accuracy and simplicity the Euler equations of motion for a straight beam were chosen to obtain $v(x,\Omega)$. The use of these equations leads to an inaccurate calculation of the tooth transverse vibration resonant frequency. To overcome this deficiency the resulting $v(x,\Omega)$ is scaled in the frequency domain using an accurately calculated resonant frequency. This scaling also allows the use of an empirically obtained tooth resonant frequency, should this be required.

Euler's equation is usually written thus:

$$\frac{d^2v}{dx^2} = k^4 v, \text{ where } v = A_1\sin(kx)+A_2\cos(kx)+A_3\sinh(kx)+A_4\cosh(kx) \qquad (31)$$

with end conditions $v = V_o\sin(\Omega t)$ and $v' = 0$ at $x = 0$

and $v'' = 0$ and $v''' = 0$ at $x = \ell$

the terms A_1, A_2, A_3 and A_4 are:

$$A_1 = V_o\sin(\Omega t)[\sinh(k\ell)\cos(k\ell)+\cosh(k\ell)\sin(k\ell)]/[2+2\cos(k\ell)\cosh(k\ell)]$$
$$= \text{say, } V_o\sin(\Omega t)\ A_1^*$$

$$A_2 = V_o\sin(\Omega t)[\cosh(k\ell)-A_1^*[\sin(k\ell)+\sinh(k\ell)]]/\ [\cos(k\ell)+\cosh(k\ell)]$$

$$A_3 = -V_o\sin(\Omega t)A_1^*$$

$$A_4 = V_o\sin(\Omega t)[1-\cosh(k\ell)-A_1^*[\sin(k\ell)+\sinh(k\ell)])/[\cos(k\ell)+\cosh(k\ell)]] \qquad (32)$$

From equations 32 and 30 the numerator of equation 29 becomes

$$I = -\Omega^2 V_o \sin(\Omega t) h_o \int_o^{\ell} [1+k_o-k_o x/\ell][A_1^* \sin(kx)+A_2^* \cos(kx)+A_3^* \sinh(kx)+A_4^* \cosh(kx)]dx$$

$$= -\Omega^2 V_o \sin(\Omega t) h_o [(1+k_o)A_1^*(1-\cos(k\ell))/k$$

$$+ (1+k_o)A_2^* \sin(k\ell)/k+(1+k_o)A_3^*(\cosh(k\ell)-1)/k$$

$$+ (1+k_o)A_4^* \sinh(k\ell)/k - k_o A_1^*(\sin(k\ell)-k\ell\cos(k\ell))/k^2\ell$$

$$- k_o A_2^*(\cos(k\ell) - 1+k\ell\sin(k\ell))/k^2\ell$$

$$- k_o A_3^*(k\ell\cosh(k\ell) - \sinh(k\ell))/k^2\ell$$

$$- k_o A_4^*(k\ell\sinh(k\ell) + 1-\cosh(k\ell))/k^2\ell] \qquad (33)$$

In calculating the overall tangential displacement mass factor ψ the influence of the core has to be added so that

$$\psi = (\psi_t \times \text{tooth mass} + \text{core mass})/(\text{mass of core plus teeth}) \qquad (34)$$

The use of the Euler equations is justified by the good agreement of the calculations with measurements - See Chapters 5 and 6. A more elaborate, and presumably more accurate, treatment of the tangential displacement mass factor ψ could be produced using Bessel function solutions of the beam equations[31].

It is well known that equation 31 prescribes resonant frequencies when $\cos(k\ell)\cosh(k\ell) = -1$. The first resonance occurs when $k\ell = 1.8751$. Since k is a function of $\Omega^{\frac{1}{2}}$ the tangential displacement factor is scaled in the frequency domain by putting $k\ell = 1.8751\ (\Omega/\Omega_t)^{\frac{1}{2}}$ in equation 33. The tooth resonant frequency Ω_t is obtained previously using methods which allow the inclusion of secondary effects such as root flexibility, shear, rotary inertia and taper - see Section 4.4.

If the expression for ψ is evaluated at various frequencies Ω the result is a function similar in form to $1/(1-(\Omega/\Omega_t)^2)$. In order to minimise computer execution time the expression for ψ is evaluated for any machine at regular fractions of the tooth resonant frequency and stored in tabular form and used with an interpolation routine. A specific interpolation routine is used with the foreknowledge that the function has a form similar to that above. This technique requires virtually no more computer storage facilities but produced a time saving if 3 or more modes are being calculated.

4.2.4 Rotational Inertia moment factor

In the equation of moments of an elementary ring section, as developed in Section 4.2.1, the moment of inertia J_r appears:

$$M' + N'a = maR\ddot{v} - J_r(\ddot{w}' - \ddot{v})/R$$

The term J_r can be termed the rigid moment of inertia. When the teeth begin to flex the inertia moment increases above the rigid value by a factor of ξ - the rotational inertia moment factor.

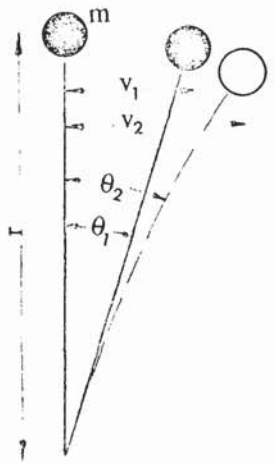

In the lumped parameter system opposite the moment exerted by the mass m when the light beam is rigid equals:

$$M = J_r\ddot{\theta} = mr^2\ddot{\theta}_1$$

When the beam is allowed to flex

$M = mr^2\ddot{\theta}_2$ which can be rewritten as

$$M = mr\ddot{v}_2 \text{ or } M = \int_x m(x)x\,\ddot{v}_1(x)dx \qquad (35)$$

Consider an encastre beam of length ℓ built in at A such that OA = p x ℓ i.e. the beam is pivoted about O. Again the mode of vibration is obtained using the Euler equations for straight beams. Let the root of the beam have a displacement $V_o \sin(\Omega t)$. From the Euler equation (31) and with the following end conditions it is straightforward to obtain expressions for $A_1 - A_4$,

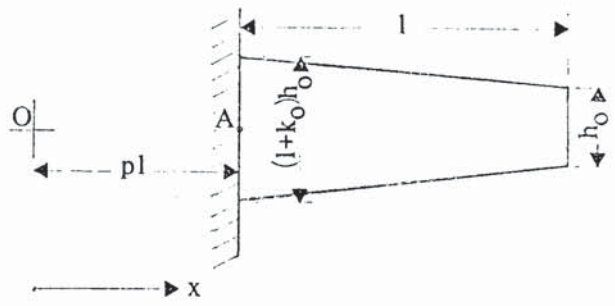

$$v = V_o \sin(\Omega t) \text{ and } v' = V_o \sin(\Omega t)/p\ell \text{ at } x = p\ell, \ (y = 0)$$

$$v'' = 0 \text{ and } v''' = 0 \text{ at } x = (p+1)\ell, \ (y = \ell)$$

In order to simplify the following expressions they are written with reference to a new variable $y = x - p\ell$

Equation 31 thus becomes:

$$v = A_1\sin(ky) + A_2\cos(ky) + A_3\sinh(ky) + A_4\cosh(ky) \qquad (36)$$

and $A_1 = y_o \sin(\Omega t)\ (1/kp\ell - A_3^*)$

$A_2 = y_o \sin(\Omega t)\ (1-A_4^*)$

$$A_3 = y_o \sin(\Omega t)\,((\cos(k\ell)/kp\ell - \sin(k\ell))(\cos(k\ell)+\cosh(k\ell))$$
$$- (\sin(k\ell)/kp\ell + \cos(k\ell))(-\sin(k\ell)+\sinh(k\ell)))/(2+2\cos(k\ell)\cosh(k\ell))$$
$$= y_o \sin(\Omega t) A_3^*$$

$$A_4 = y_o \sin(\Omega t)\,((\sin(k\ell)/kp\ell+\cos(k\ell)) - A_3^*(\sin(k\ell)+\sinh(k\ell)))/$$
$$(\cos(k\ell) + \cosh(k\ell))$$
$$= y_o \sin(\Omega t) A_4^* \qquad (37)$$

From equation 35 and assuming that $m(x) \alpha h(x)$ and that

$$h(x) = h_o(1+k_o - k_o y/\ell)$$

$$M_t = -\Omega^2 V_o \sin(\Omega t) h_o \int_o^{\ell} (1+k_o - k_o y/\ell)(A_1^* \sin(ky) + A_2^* \cos(ky) + A_3^* \sinh(ky) + A_4^* \cosh(ky))(y+p\ell)\,dy \qquad (38)$$

$$= -\Omega^2 V_o \sin(\Omega t) h_o ((1+k_o(1+p))(I_1+I_2+I_3+I_4) - (I_5+I_6+I_7+I_8)k_o/\ell)) \qquad (39)$$

Where

$$I_1 = A_1^*(\sin(k\ell) - (p+1)k\ell\cos(k\ell) + kp\ell)/k^2$$

$$I_2 = A_2^*(\cos(k\ell) - 1 + k\ell(1+p)\sin(k\ell))/k^2$$

$$I_3 = A_3^*((1+p)k\ell\cosh(k\ell) - \sinh(k\ell) - pk\ell)/k^2$$

$$I_4 = A_4^*((1+p)k\ell\sinh(k\ell) - \cosh(k\ell) + 1)/k^2$$

$$I_5 = A_1^*(2(1+p)k\ell\sin(k\ell) + (2-(1+p)^2k^2\ell^2)\cos(k\ell) - 2 + p^2k^2\ell^2)/k^3$$

$$I_6 = A_2^*((2k\ell+2pk^2\ell^2)\cos(k\ell) + ((1+p)^2k^2\ell^2 - 2)\sin(k\ell) - 2kp\ell)/k^3$$

$$I_7 = A_3^*(((1+p)^2k^2\ell^2 + 2)\cosh(k\ell) - 2k\ell(1+p)\sinh(k\ell) - 2 - p^2k^2\ell^2)/k^3$$

$$I_8 = A_4^*(((1+p)^2k^2\ell^2 + 2)\sinh(k\ell) - 2k\ell(1+p)\cosh(k\ell) + 2pk\ell)/k^3$$

The tooth rotatory inertia moment factor ξ_t, is defined as M_t divided by the inertia moment exerted by the rigid beam vibrated about O with a root displacement of $V_o \sin(\Omega t)$, and obtained from equation 35.

$$\xi_t = -M_t/(\Omega^2 V_o \sin(\Omega t) h_o \int_{p\ell}^{p\ell+\ell} ((1+k_o(1+p) - k_o x/\ell)x^2/p\ell)\,dx)$$

since $v(x) = V_o x/p\ell$

$$\xi_t = \frac{((1+k_o(1+p))(I_1+I_2+I_3+I_4) - (I_5+I_6+I_7+I_8)k_o/\ell)}{((1+3p+3p^2)/3 + (1+4p+6p^2)k_o/12)\ell^2/p} \qquad (40)$$

PAGE

NUMBERING

AS ORIGINAL

4.3 ZERO ORDER VIBRATION

This type of vibration is often the cause of noise in rotating electrical machines but its calculation offers no real difficulty for most large machines. The two main areas of application where the classical equation for the resonant frequency becomes inaccurate are (a) radially deep-cored machines, and (b) machines with axial ventilation holes and/or segmental laminations.

In studying Záček's Bessel function solution for this mode of vibration (see Kuhl[27] page 133) it was found that a very much simplified expression could be used. Love's classical solution is:

$\Omega_o = \frac{1}{a}\sqrt{E/p}$ and the proposed equation is

$$\Omega_o = \frac{R}{a^2}\sqrt{E/p} \qquad (43)$$

where a is the radius through the centroids of the ring section and R is the radius of the centre of gravity of the ring, as previously. Kuhl[27] has verified Zaceks' theory experimentally, obtaining errors of $\leq 0.25\%$. A contraction of Kuhl's table 5 is shown below to indicate the accuracy of equation 43.

h/a	.0909	.1395	.2439	.3589	.4865	.6667	.7879	.9677	1.172
*	1.000	1.005	1.004	1.012	1.020	1.038	1.053	1.080	1.109
**	1.001	1.002	1.005	1.011	1.020	1.037	1.052	1.078	1.115

* Záček's Bessel function solution divided by Love's classical solution.

** Present theory divided by classical theory (equals R/a)

It is evident from the above table that equation 43 is accurate for all $h/a < 1.0$. Electrical machines are seldom, if ever, made with such deep cores. The effect of teeth is accommodated by increasing the density ρ by an amount equal to the mass of the complete laminations divided by the mass of the core.

The effect of segmentation is to reduce this resonant frequency and the experimental work reported in Chapter 5 shows that this effect can be readily predicted using an artificially low value of E.

4.4 RESONANT FREQUENCIES OF TEETH

The teeth of electrical machines are basically encastre beams integral with the core, which is deep enough to be considered as an infinite half space. The teeth are sufficiently short for secondary effects to be important. Teeth differ in two main respects from the simple encastre beam. Firstly, the teeth have a non-uniform cross section - the depth of the teeth tapering linearly along the length. Secondly, the teeth are partially supported by the wedges that are introduced between teeth to retain the winding. Pavlovsky[19] says that the influence of the windings also provides support along the length of the teeth.

The general tooth configuration is shown in Fig.4.4.1.

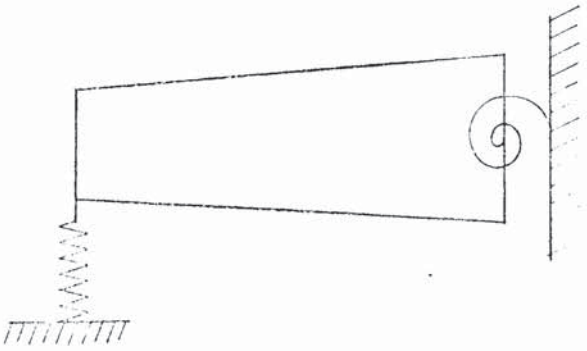

Fig. 4.4.1

The spring at the tip of the tooth is there to represent the support produced by the wedge. The mass of the wedge is sufficiently small to be ignored. In the physical system the wedges are connected to the next tooth. In the representation of Fig.4.4.1 the wedge spring is built in. The coil spring at the base of the tooth represents the root stiffness. All electrical machine teeth are integral with the core so that the root stiffness is at a maximum. Despite this fact it has been found that the root flexibility is usually the most significant second order effect in determining tooth resonant frequencies. The amount of support material

that vibrates due to the root flexibility is assumed small so that the massless coil spring shown above represents the effects. Other secondary effects are less ameanable to calculation. The most common of these are extra mass at the tip of the teeth and set back wedge grooves. The first of these is most common in small machines and the latter occurs in both small and large high-speed machines.

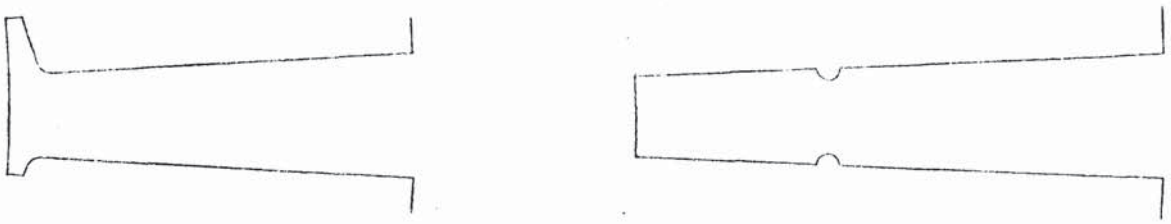

In looking for a method for calculating resonant frequencies taking the above constraints into account, as well as shear and rotary inertia, a number of criteria were applied. It was considered desirable to have a non-numerical solution so that the resulting equations could be used in a design office. This ruled out the possibility of a Bessel function solution of the differential equations. It was hoped to reduce the secondary influences to a series of correction terms presented in graphical form.

An analytical integral equation approach[32] was chosen. This method gives a lower bound approximation to the fundamental resonant frequency. Penny and Reed[32] have applied their theory to seven types of beams, including four with different types of taper, and shown very good agreement with the accepted Bessel function solutions. Gains and Volterra[33] have developed a similar approach and included shear and rotary inertia effects. Their example is that of a truncated wedge as found in electrical machines. The method is further extended to account for root flexibility and wedge support.

4.4.1 The Influence of Root Flexibility

MacBain and Genin[34,35] have used O'Donnells'[36] work on root stiffness to obtain resonant frequencies of uniform cantilever beams excluding and including the effects of shear and rotary inertia. These authors obtain an implicit function solution for the simple case and a complex numerical solution when shear and rotary inertia are included.

In order to produce a correction term for root flexibility a solution is required for the tapered tooth excluding secondary effects.

No secondary effects

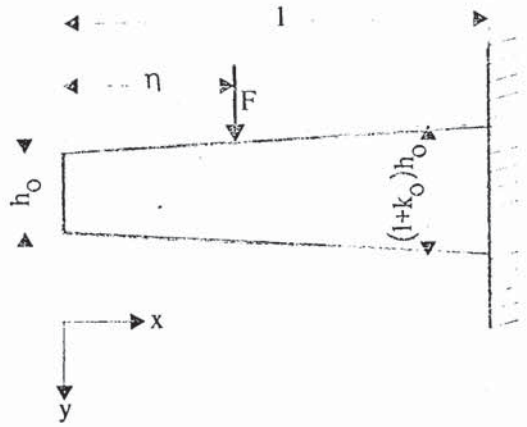

Fig. 4.4.2

Penny and Reed's theory can be re-stated as

$$1/\Omega_t^2 = \int_x K(x,x)dx$$

where $K(x,x) = a(x,x)\cdot m(x)$

and $m(x)$ is the mass of the beam as a function of x and $a(x,x)$ is the particular flexibility influence coefficient obtained from the general coefficient $a(x,\eta)$.

N.B. that Ω_t is the approximate resonant frequency, being a first lower bound.

From Fig.4.4.2, and with a force F operating at point η, bending moments can be equated thus:

$$EI_x y'' = F(x-\eta) \text{ for } \eta \leq x \leq \ell, \text{ where}$$

$$I_x = I_o(1+k_o x/\ell)^3$$

Integrating twice and substituting boundary conditions gives

$$EI_o y/F\ell^3 = (\ell n[(\ell+k_o\ell)/(\ell+k_o x)])/k_o^3 + (\ell+\eta k_o+2\eta k_o^2-2\ell k_o^2)/$$

$$(2k_o^3\ell(1+k_o)^2) + x(\ell+2\ell k_o-\eta k_o)/(2k_o^2\ell^2(1+k_o)^2)$$

$$- (\ell+\eta k_o)/(2k_o^3(1+k_o x) = EI_o a(x,\eta)/\ell^3 \qquad (44)$$

The function a(x,x) is obtained by substituting x for η in equation(44).

With $m(x) = \rho A_o (1+k_o x/\ell)$, and $a(x,\eta) = y/F$

$$1/\Omega_t^2 = \int_o^\ell K(x,x)dx = \frac{\rho A_o \ell^4}{EI_o}\left(\frac{1+1.5k_o+k_o^2/3+k_o^3/12}{2k_o^3(1+k_o)^2} - \frac{\ell n(1+k_o)}{2k_o^4}\right) \qquad (45)$$

In the limit as $k_o \to 0$ equation 45 tends to $\rho A_o \ell^4/12EI_o$

i.e. $\Omega_t = 3.464\sqrt{EI_o/\rho A_o}/\ell^2$, which agrees with Penny's expression for a uniform beam. For all tapers found in electrical machines this lower bound is in error by an approximately constant 1.5%.

Including root flexibility

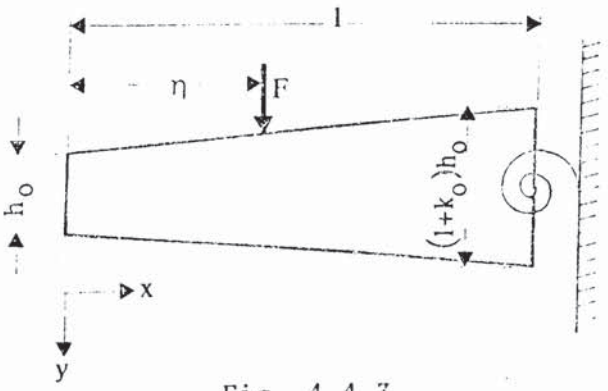

Fig. 4.4.3

In taking into account the root flexibility the boundary conditions at $x = \ell$ are:

$y' = -F(\ell-\eta)/k_b$ and $y = 0$,

where k_b is the stiffness of the base spring.

Integrating twice and substituting these new boundary conditions gives

$$1/\Omega_t^2 = \int_0^{\ell} k(x,x)\,dx$$

$$= \frac{\rho A_o \ell^4}{EI_o}\left[\frac{1+1.5k_o+k_o^2/3+k_o^3/12}{2k_o^3(1+k_o)^2} - \frac{\ell n(1+k_o)}{2k_o^4} + \frac{EI_o(1+k_o/4)}{3\ell k_b}\right] \quad (46)$$

The flexibility of the root spring is obtained from stress analysis of the boundary between the tooth and the ring. O'Donnell shows that the effective rotation θ_m at the built in end of a cantilever due to a moment load M equals:

$$\theta_m = CM/\pi Eh^2$$

The quantity h is the effective depth of the beam at the root. Various values of the constant C are given depending on the assumptions made about the stress/strain distribution across the root section. For the case of steel with $\nu = 0.29$ the values of 18, 16.49, 15.17 and 16.67 are quoted. The spring stiffness k_b is obtained from the above expression.

$$k_b = M/\theta_m = \pi Eh^2/C \quad (47)$$

O'Donnell shows that small fillets reduce slightly the deflection for a given moment, and that there is a small additional rotation due to the shear load at the root. The value of $C = 16.49$ $(18(1-\nu^2))$ was chosen after comparing calculated and measured frequencies. In this comparison fillet radii and rotation due to shear were ignored. The comparison is shown graphically in Fig.4.4.4 together with a normalised correction curve for root flexibility.

It was found that the effect of root flexibility could be represented by one curve for all normal linear tapers. This curve is

given in Fig.4.4.4 together with the constituent points obtained for three different tapers. The use of this curve together with Fig.4.4.5 (the correction coefficient for shear and rotary inertia effects, Cs) produces the following simplified version of equation (46) for hand calculations.

$$f_t = 810.5\ h_o\ (1+1.16\ k_o)\ C_s C_r/\ell^2 \text{ kHz (mm dimensions)} \quad (48)$$

This expression is surprisingly accurate. It should be noted that the influence of root flexibility is more pronounced in tapered beams than equivalent straight beams, and even with a length/depth ratio of 10 the correction term is already -8%. It is fortuitous that tapered teeth in electrical machines have previously been treated as equivalent parallel beams. Artificially low resonant frequencies are thereby calculated which approximate roughly to the measured values (secondary effects being ignored).

4.4.2 The Influence of Wedge Support

The fit of the wedges in the wedge-grooves is very variable and the relative dimensions of wedges and teeth vary over a wide range. Because of the complexity of the influence of wedges on tooth resonant frequencies simple empirical factors are inadequate. In the following analysis the wedges are assumed to be solidly connected to the teeth. The spring constant contains a factor to account for the fit of the wedges. Each tooth is assumed to be supported by one wedge, at the tip, which is built in. In reality the wedge is attached to the adjoining teeth. In the following analysis the influence of wedge support is treated separately from other secondary factors so that the following figure depicts the assumed configuration.

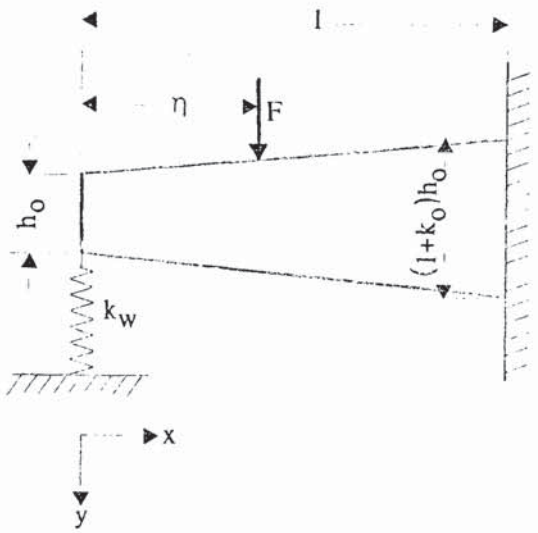

It should be noted that the wedge is assumed to be acting at the tip of the tooth. This assumption is used to simplify the derivation of the flexibility influence coefficient. Refer to Figure 3.1.1 for a typical wedge and groove layout. The influence coefficient must be considered in two parts:

$0 \leq x \leq \eta$ and $\eta \leq x \leq \ell$

$0 \leq x \leq \eta$

Equating bending moments gives

$EI_x y'' = y_o x k_w$ where y_o is the tip deflection

k_w is the wedge spring constant

Now $I_x = I_o (1+k_o x/\ell)^3$ and by integrating twice

$$\frac{EI_o y}{\ell^3} = \frac{k_w y_o}{k_o^3} \ell n(\ell+k_o x) + \frac{y_o \ell k_w}{2k_o^2(\ell+k_o x)} + Ax + B \qquad (49)$$

$\eta \leq x \leq \ell$

Equating bending moments gives

$EI_x y'' = F(x-\eta) - k_w y_o x$

and integrating twice

$$\frac{EI_o y}{F\ell^3} = \frac{-1}{k_o^3} \ell n(\ell+k_o x) - \frac{(\ell+k_o\eta)}{2k_o^3(\ell+k_o x)} + \frac{k_w y_o}{Fk_o^3} \ell n(\ell+k_o x) + \frac{k_w y_o \ell}{2Fk_o^3(\ell+k_o x)} + Cx + D$$

(50)

Substituting boundary conditions at $x = \ell$ into equation 50 and the associated equation for slope leads to the following expressions for C and D:

$$C = [2F\ell(1+k_o)+k_w\ell y_o-F(\ell+k_o\eta)-2k_w\ell y_o(1+k_o)]/2Fk_o^2\ell^2(1+k_o)^2 \quad (51)$$

$$D = \frac{1}{k_o^3}\ell n(\ell+k_o\ell) + \frac{\ell+k_o\eta}{2k_o^3(\ell+k_o\ell)} - \frac{k_w y_o}{Fk_o^3}\ell n(\ell+k_o\ell) - \frac{k_w y_o \ell}{2Fk_o^3(\ell+k_o\ell)}$$

$$+ [-2F\ell(1+k_o)-k_w\ell y_o+F(\ell+k_o\eta)+ 2k_w\ell y_o(1+k_o)]/2Fk_o^2\ell(1+k_o)^2 \quad (52)$$

The substitution of equations 51 and 52 into equation 50 leads to an implicit equation for deflection since the R.H.S. contains the tip deflection, y_o. By equating equations 49 and 50 at $x = \eta$, and also the corresponding slope equations, expressions are obtained for A and B. Equation 49 is then evaluated at $x = 0$ to obtain the tip deflection y_o.

$$y_o = \frac{\dfrac{\ell n\dfrac{(\ell+k_o\ell)}{(\ell+k_o\eta)}}{k_o^3} + \dfrac{\eta}{2k_o^2(\ell+k_o\eta)} - \dfrac{k_o(3\ell-2\eta)+(2\ell-\eta)}{2k_o^2\ell(1+k_o)^2}}{\dfrac{EI_o}{\ell^3} + \dfrac{k_w}{k_o^3}\ell n(1+k_o) - \dfrac{k_w}{2k_o^2(1+k_o)} - \dfrac{k_w(1+2k_o)}{2k_o^2(1+k_o)^2}} \quad (53)$$

Bringing together equations 53, 52 and 51 and substituting them into equation 50 produces an unwieldy expression for $\frac{EI_o}{\ell^3}\ a(x,\eta)$. From this expression the particular influence coefficient $a(x,x)$ is obtained and the first resonant frequency determined from the relationships:

$$1/\Omega_t^2 = \int_x K(x,x)dx; \quad K(x,x)=a(x,x)m(x), \quad m(x) = \rho A_o(1+k_o x/\ell)$$

The resulting expression is very cumbersome and falls short of the intention to produce equations suitable for the design office. Since the step from equation 50 to the expression for Ω_t involves only straightforward integration, albeit tedious, the long expression for Ω_t is not reproduced here. It was evaluated using a computer and reduced to the curve shown in Fig.4.4.6. This is a correction curve similar to those in Figs.4.4.4 and 4.4.5 and is intended to be used as a further multiplier C_w in equation 48. Thus:

$$f_t = 810.5h_o\ (1+1.16k_o)\ C_s C_r C_w/\ell^2 \text{ kHz (mm dimensions)} \qquad (54)$$

Although wedges normally increase tooth resonant frequencies by only a small amount, there are configurations where the wedges can produce an increase of 100% and more. Increases of this order are typical with bonded wedges, such as magnetic wedges. A normalised correction curve cannot be produced for such large corrections and the expression above for Ω_t must be evaluated.

In producing a wedge spring stiffness k_w for any particular machine the fit of the wedge in the groove has to be included. Thus

$$k_w = \frac{3.0\ E_w \text{ x wedge depth x fit}}{\text{wedge width}} \qquad (55)$$

where E_w is the elasticity modulus of the wedge material, and

fit = factor ≤ 1.0 accounting for the quality of the fit of the wedge.

4.5 HIGH DAMPING MATERIAL WEDGES

In designing machines to avoid elactromagnetically produced noise the approach of mismatching forcing and resonant frequencies has been universally adopted. If sufficient damping can be introduced into the stator of an electrical machine then attempts at mismatching frequencies can be abandoned. In investigating various possibilities for added damping a number of restrictive criteria were applied. A simple, low cost method was required which could reasonably be tried in a production machine without excessive costs. In addition to these general requirements the materials to be used must; have the desired properties in the frequency range 100 - 3000 Hz, be easily handled, temperature stable, nonmetalic, and reasonably inexpensive.

The following account gives the theoretical investigation into the use of high damping plastic wedges to produce highly damped overall systems. With present day materials this approach is not capable of producing overall loss factors of β greater than $\doteq .10$. The advent of new materials may change this situation. The target value is $\beta > 0.5$.

The winding retention wedges that are a normal part of large machines are ideally situated to impart a large amount of damping to the stator core of a machine when it vibrates.

The strain experienced by a wedge when the core assumes a bending deflection is amplified due to the large displacement from the neutral layer. This means that although the bulk of the wedges is small the damping may be large. The damping energy per cycle is proportional

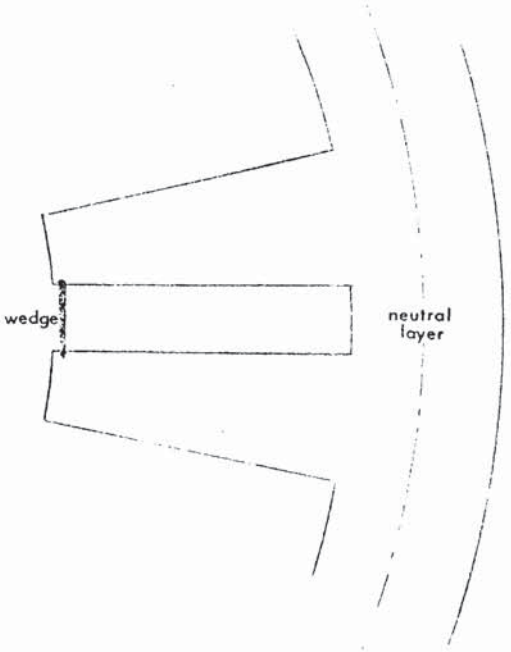

to the loss modules x strain ratio. (ref.37). In the measurements reported in section 5.3.8 the strain ratio γ is 19.95 for a 2.44 mm deep wedge. This is the normal size of wedge used at present. If wedges were designed for a damping function then a 5 mm wedge could be expected - and easily accommodated. This would mean that γ would have a maximum value of approximately 40 for normal electrical machines. The above calculations relate to a machine with a tooth length/core depth ratio as high as any normal large machine. This ratio determines γ. Present day viscoelastic polymers have loss modulii which peak at approximately 1/200 times the storage modulus of steel[37]. The frequency and temperature at which the loss modulus is a maximum depends on the type of polymer or copolymer. If the storage modulus of wedges are ignored the maximum value of $\beta = \gamma/200 = 0.2$. If allowances are made for reduced performance when 'damping wedges' are fitted on a production basis a maximum realiseable value for β is 0.1. A normal value would be 0.025.

The loss produced in wedges in simple extension falls short of the required value by approximately one order of magnitude. With wedges assuming a shearing motion the loss could be increased. The width/depth ratio of a wedge is typically 3 to 1 - assuming that 'damping wedges' are twice the depth of conventional wedges. The loss modulus

in shear is approximately 1/3 the value for simple extension. The increased shearing area is offset by the reduced modulus. By laminating the wedge as shown opposite it is possible to magnify the shearing area by a factor of 2 or 4, depending on the number of laminations. An overall increase in β of 2 or 4 can be obtained, therefore, at the expense of the simplicity. This increase is not sufficient to meet the target value of $\beta > 0.5$.

Since the desired loss cannot be produced by normal extension or shear it was decided to investigate the effect of wedge longitudinal resonance. It was hoped that the increased strain amplitudes associated with a resonance condition would lead to extra loss.

4.5.1 Longitudinal Wedge Vibration

The general equation of motion of a simple beam subject to longitudinal vibration is:

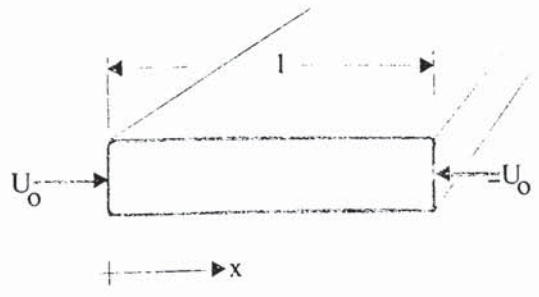

$$u = (A\cos\alpha x + B\sin\alpha x)e^{j\omega t} \quad (57)$$

where $\alpha = \omega \sqrt{\rho/E}$

For a displacement excitation at each end of a wedge equal to $U_o e^{j\omega t}$ and $-U_o e^{j\omega t}$ equation 57 reduces to:

$$u = U_o(\cos\alpha x - (1+\cos\alpha\ell)\sin\alpha x/\sin\alpha\ell)e^{j\omega t} \quad (58)$$

Assuming that the viscoelastic nature of wedges allows the use of a complex modulus, the stress and strain amplitudes as functions of x are:

$$\text{strain } \varepsilon = \partial u/\partial x = (-A\alpha\sin\alpha x + B\alpha\cos\alpha x)e^{j\omega t} \tag{59}$$

$$\text{stress } \sigma = E\varepsilon = (E_1+jE_2)(-A\alpha\sin\alpha x+B\alpha\cos\alpha x)e^{j\omega t} \tag{60}$$

Now work done $w = \int_T \sigma\dot{\varepsilon}\, dt$ and a convenient period of time T for comparison purposes is one period, $2\pi/\omega$. Equations 59 and 60 are conjugate pairs of equations and only the real or imaginary component equations are needed for the evaluation of work done. If the equation for w is evaluated at either end of the wedge ($x = 0$ or ℓ) then the curves shown in Fig.4.5.1 result. These have been drawn for various values of $\beta = E_2/E_1$ with the work done per cycle scaled by the value obtained at zero frequency, and the frequency scale shown in units of the first longitudinal resonant frequency.

It is apparent from Fig.4.5.1 that there is considerable gain in loss (work) to be obtained at frequencies above 1.3 times the first longitudinal resonant frequency. Unfortunately the material and geometric dimensions of wedges found in electrical machines give resonant frequencies in the region of 15000 Hz. This is outside the range of interest. The value of elasticity modulus needed to reduce this frequency to, say, 2000 Hz would give a wedge that was too elastic to retain the windings - its primary function. Since use cannot be made of a resonance condition to magnify the work done, any damping wedges must operate below their first longitudinal resonant frequency. From Fig.4.5.1 it can be seen that the most useful operating range is below 0.25 x first longitudinal resonant frequency since the loss per cycle deteriorates at highest frequencies.

To summarise it can be said that with present viscoelastic polymers the amount of damping that can be imparted to a stator core system by damping wedges is not sufficient for their general use. Any significant advances towards producing fully damped cores awaits the advent of improved damping materials. Experimental evidence of the use of polymethylmethacrylate wedges is given in Section 5.3.8.

4.6 ITERATION TECHNIQUES

Since the expression for core resonant frequencies - equation 4.17 - contains terms which are frequency dependent some form of iterative technique is needed to obtain solutions of the expression. The well known step and half step technique is used to obtain the set of resonant frequencies above the tooth resonant frequency. A novel technique has been developed for obtaining resonant frequencies for the set of modes below the tooth resonant frequency.

The efficacy of the method is that it enables an interpolation technique to be used thereby requiring only three evaluations of equation 4.17 to obtain a solution for any mode. In evaluating 4.17 the frequency dependent terms are obtained using the frequency X, say, and the resulting resonant frequency is Y, say. The suffices of X and Y denote the number of the evaluation. The value of X_1 is taken as the calculated resonant frequency of the next lowest mode, which has just been calculated. To start the sequence X_1 is taken as 0. Because X_1 is below the required resonant frequency the value of Y_1 will be above it. If X_2 is now made equal to Y_1 the resulting Y_2 is below the required resonant frequency.

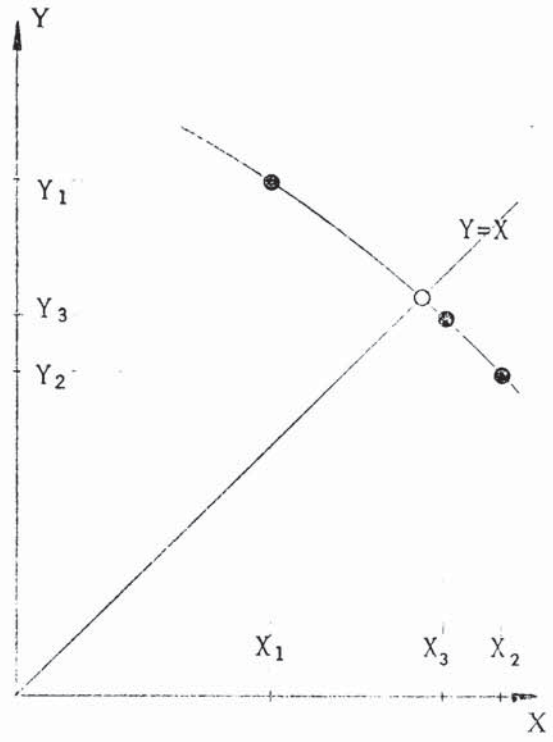

The points (X_1, Y_1) and (X_2, Y_2) straddle the required resonant frequency, i.e. $Y = X$. A third value of X is chosen between X_1 and X_2 to produce an extra point (X_3, Y_3). A convenient value for X_3 has been found to be $(X_1 + 3X_2)/4$. The required resonant frequency is then the intersection of the parabola formed by the three points and the straight line $Y = X$.

In the computer program written to calculate resonant frequencies a check has been included to test this technique and the errors involved are generally <0.1%.

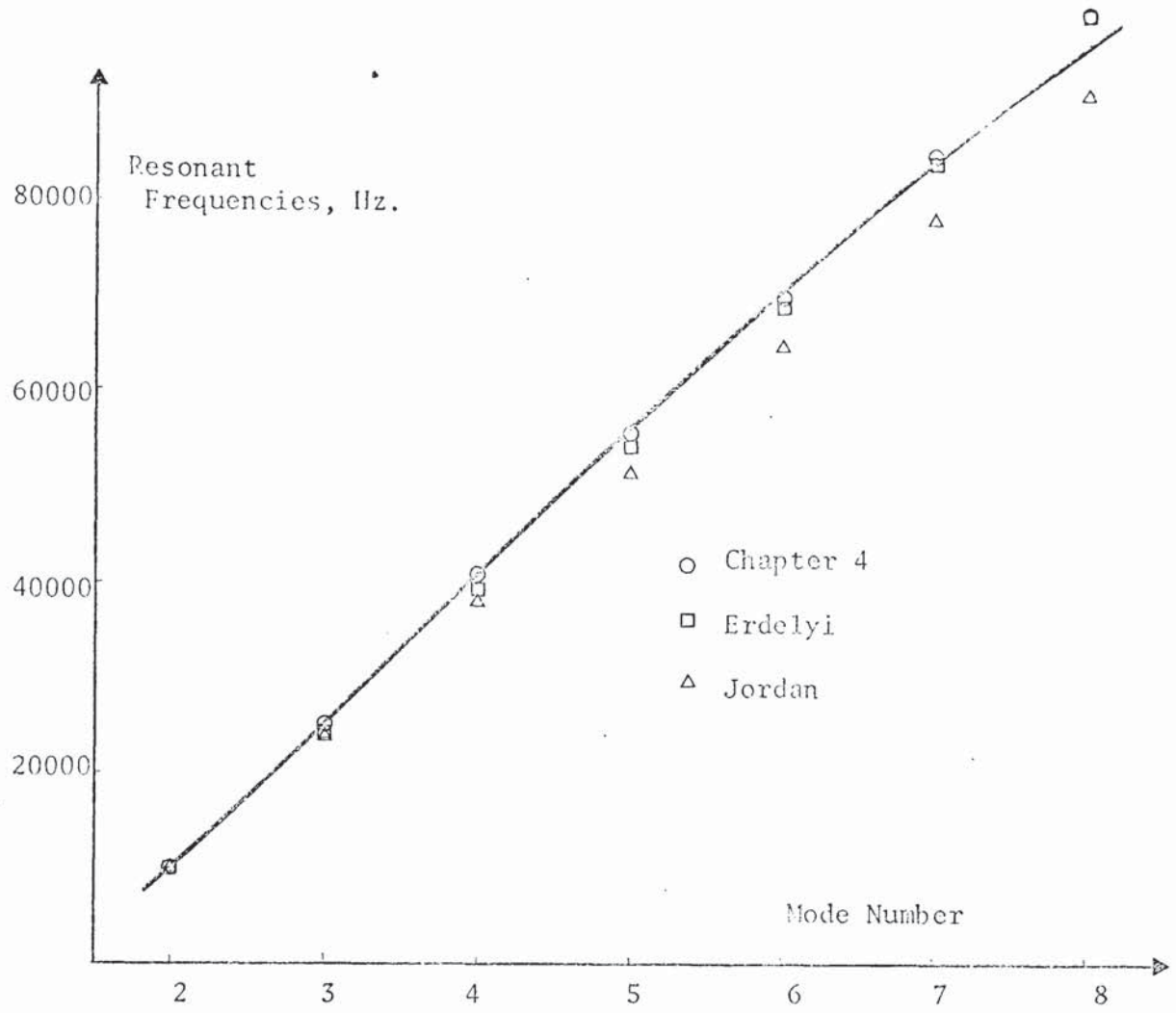

Mode	Measurements	Erdelyi	Jordan	Bucken	
2	1723	1711	1724	1726	
3	4820	4788	4821	4836	Total error bands
4	9170	9045	9108	9152	(95% confidence)
5	14535	14362	14460	14557	
6	20850	20626	20758	20940	
7	27400	27725	27880	28187	
8	36000	35551	35709	36186	Erdelyi = 9.33%
2	10715	10324	10450	10908	
3	25400	24341	24011	25632	Jordan = 18.70%
4	41000	39311	37944	40902	
5	56450	54458	51656	55954	Bucken = 4.98%
6	70950	69544	65081	70691	
7	84150	84500	78264	85153	
8	96800	99315	91259	99402	

OD = 90mm, ID = 80.163mm and 45 mm.

COMPARISON OF RING THEORIES WITH KUHL'S MEASUREMENTS

Fig. 4.1.1

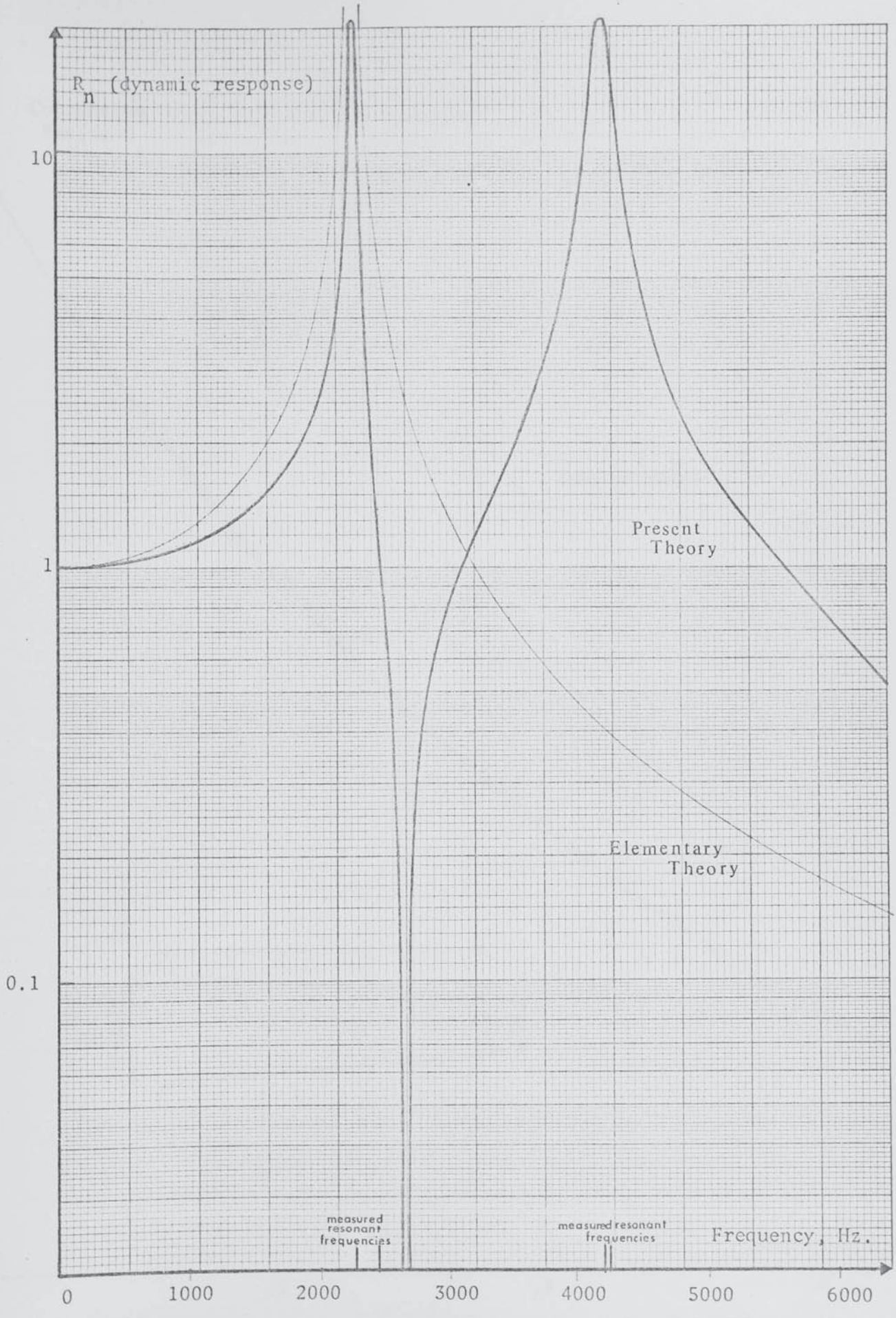

DYNAMIC RESPONSE TO MODE 8 FORCE WAVE

Fig. 4.2.2

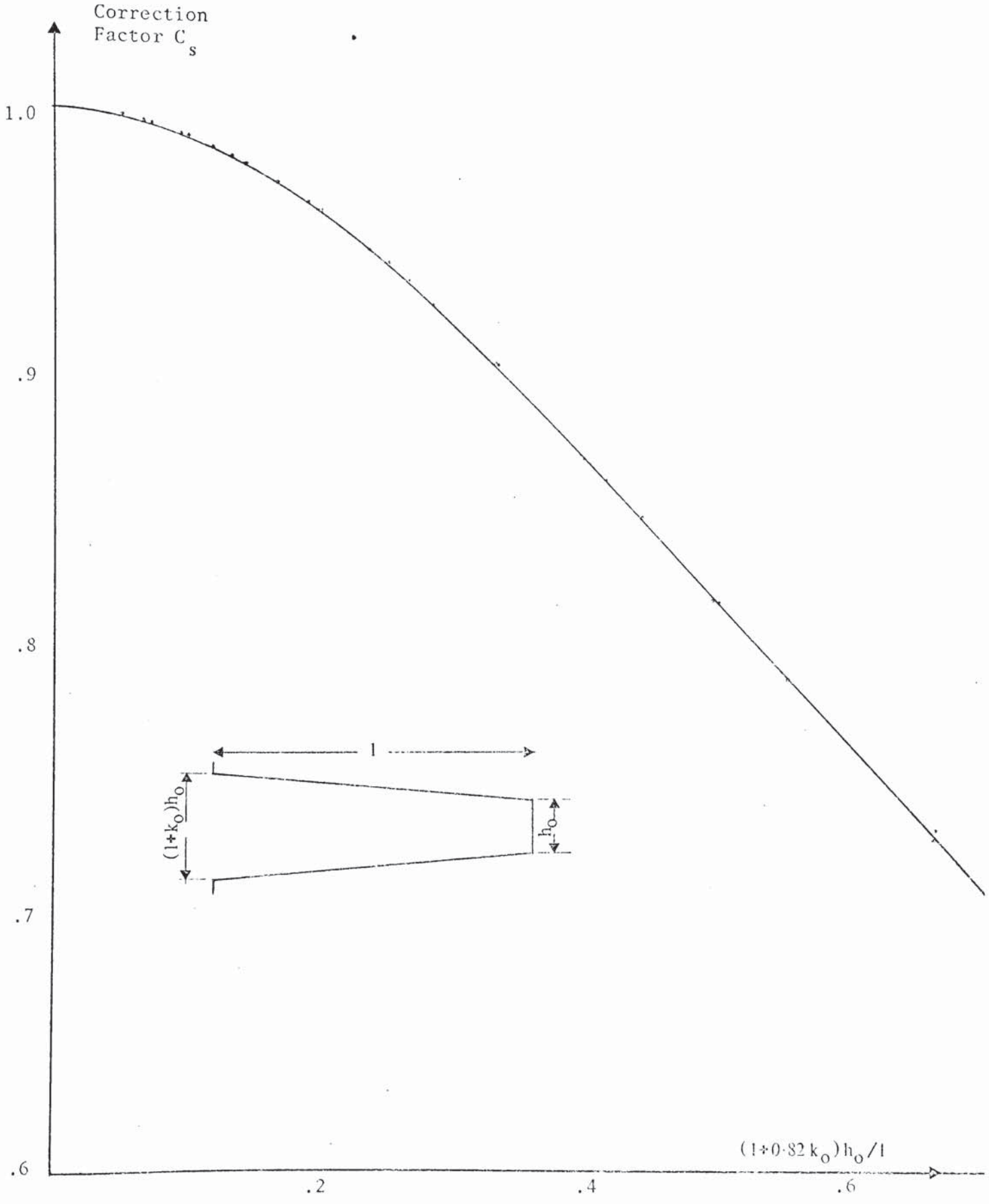

SHEAR AND ROTARY INERTIA CORRECTION CURVE (TOOTH RESONANCE)

Fig. 4.4.5

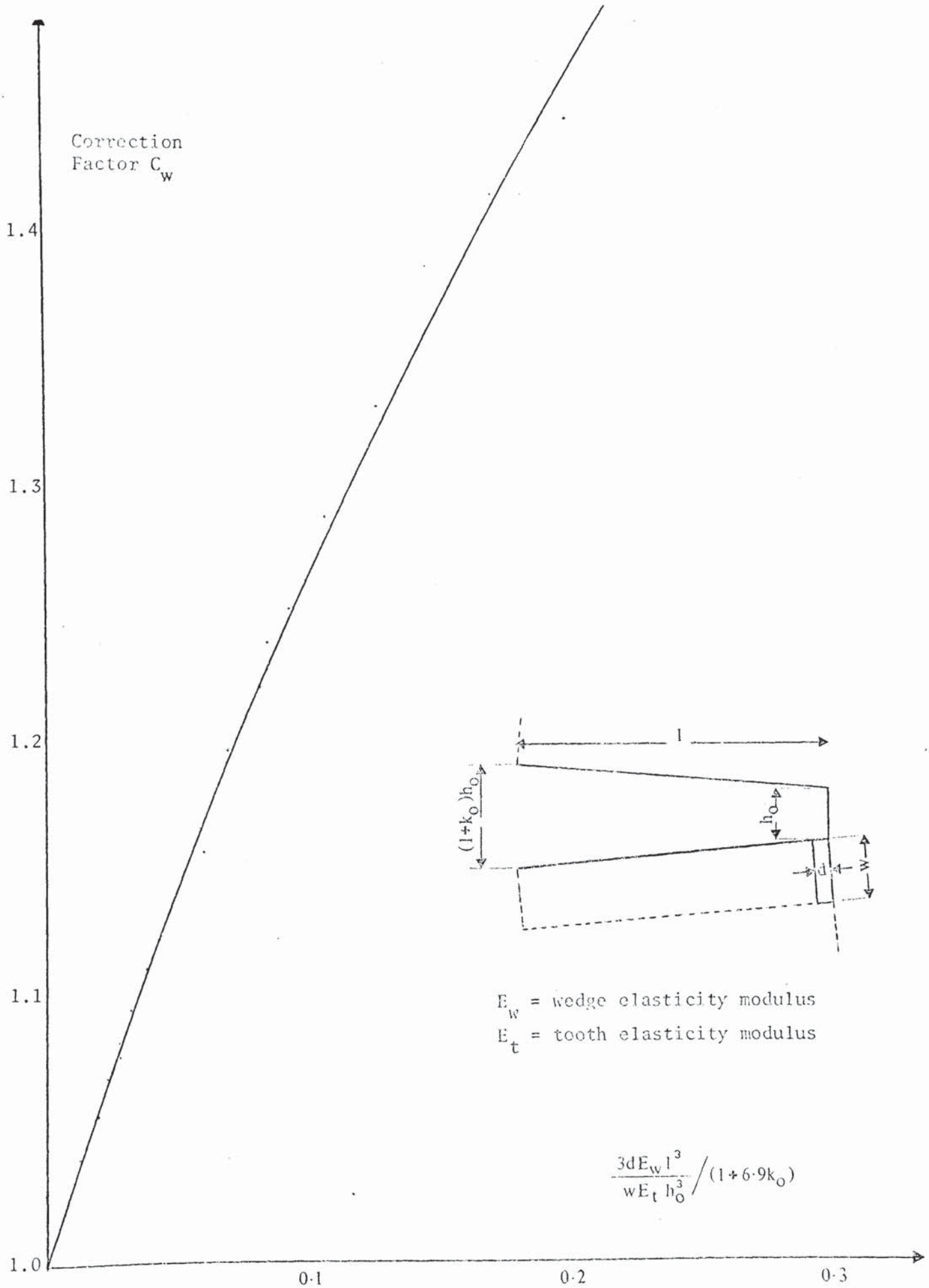

WEDGE SUPPORT CORRECTION CURVE (TOOTH RESONANCE)

Fig. 4.4.6

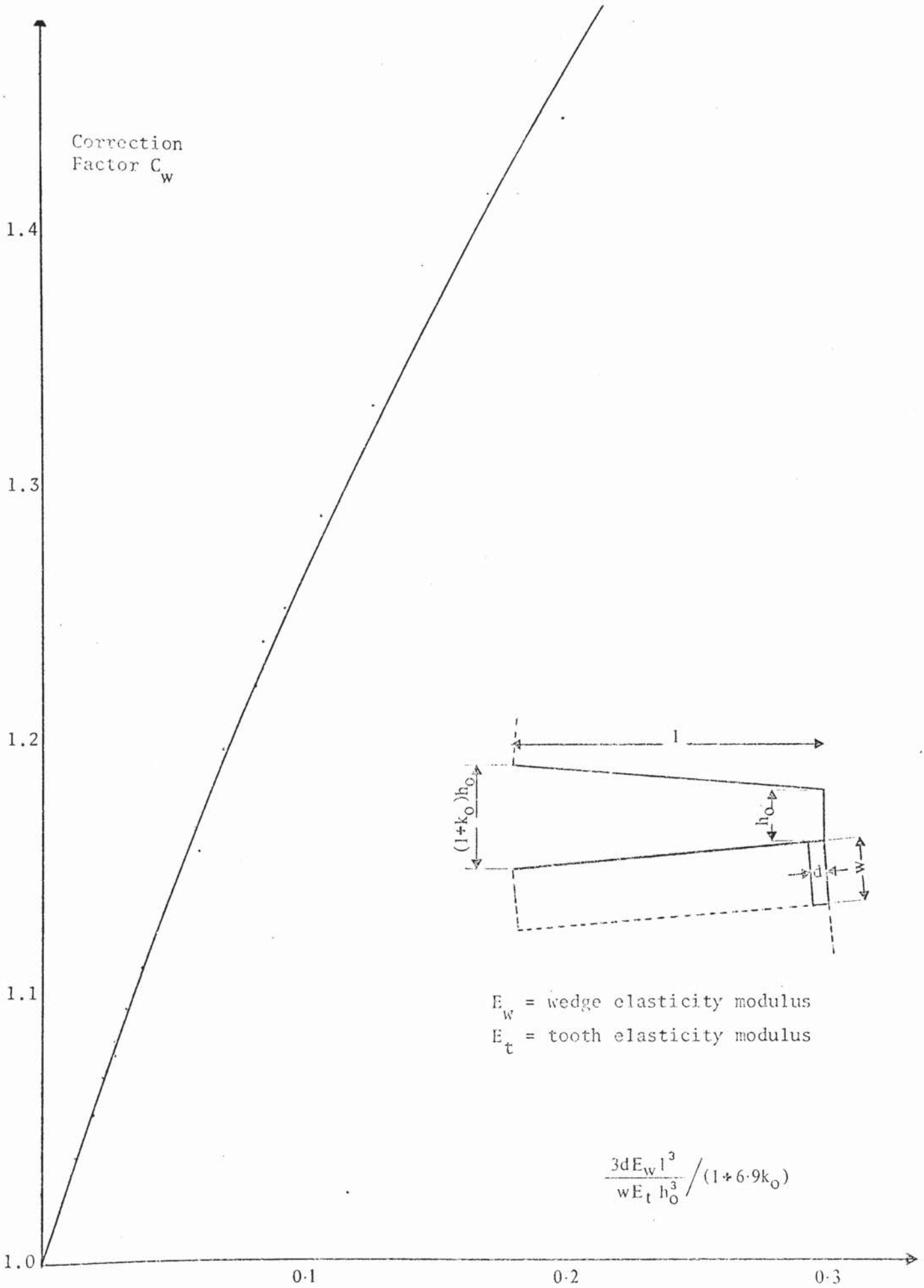

WEDGE SUPPORT CORRECTION CURVE (TOOTH RESONANCE)

Fig. 4.4.6

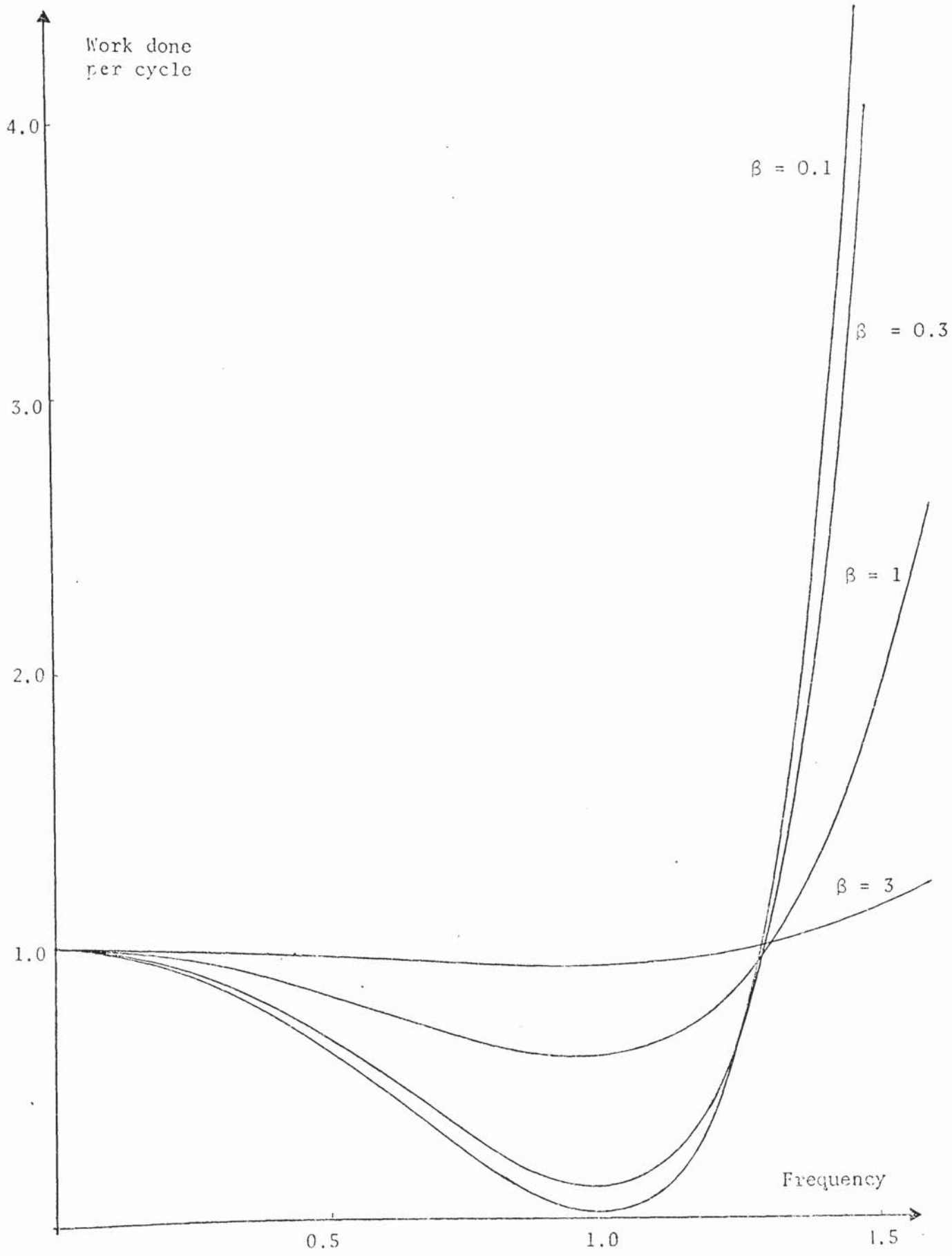

ENERGY DISSIPATED BY DAMPING WEDGES

Fig.4.5.1

CHAPTER V

MEASUREMENTS OF STATOR CORE RESONANT FREQUENCIES

(SAMPLE TESTS)

Since the principal elements (dynamically) of an electrical machine are the laminations, it has been possible to devise a method for measuring resonant frequencies using only a small number of laminations[11, 18]. Correspondence between such measurements and similar measurements on a complete machine has always been assumed. To test this assumption for the case of large machines a full set of measurements was made on a production machine in its various stages of manufacture and compared with the method above (the 'short core' method). The complete machine measurements are reported in Chapter 6. Quite apart from this correlation exercise a large number of short core measurements have been made to gain an understanding, and measure the influence, of various features on core resonant frequencies. The short core method is ideally suited to this since the cost and time involved in preparing a sample for test is small; the feature of interest is easily controlled, the sample may be tested to destruction if necessary, and the method can be applied in the factory ahead of the bulk of production giving time for remedial action if necessary. The majority of the measurements reported in this chapter relate to two designs of laminations which have the same outside diameter. Laminations of these designs were built into a production machine as part of the experimental work of this investigation.

5.1 THE SHORT CORE METHOD

The first obvious features of the method are that only a short stack of laminations is used (25mm to 50mm deep) and that the source of excitation is an electro-mechanical vibrator. A diagramatic presentation of the core, the vibrator and the measurement accelerometers and force transducer is given in Fig.5.1.1. For large machines the vibrator was attached to the core through a jig bolting on to two adjacent teeth. For small machines a bolt was bonded to the outside of the stack of laminations and the vibrator attached through this bolt. The most convenient means of attaching accelerometers was found to be the commercially available tripod magnet. Various methods of clamping the laminations were tried and investigated for aberations of the measurements.

It was found that bolts at the bottom of every fourth or so slot had negligible influence on resonant frequencies and were simple to use. Tightness of the bolts had no measurable influence on resonant frequencies of rings and very small influence on segmented cores. The cores were mounted horizontally on rubber to provide a resilient mounting. No benefit seemed to accrue from bolting the vibrator to a baseplate so this practice was discontinued.

The procedure used for isolating resonant frequencies is to sweep through the frequency range 0 Hz to 10000 Hz keeping the applied force constant - by monitoring the force transducer output - and measuring the acceleration at the point of attachment of the vibrator. A typical acceleration trace is shown in Fig.5.1.2. Having obtained this curve, each of the peaks is examined in detail to determine the mode of vibration.

This is done by holding the frequency at the peak value and traversing the second accelerometer round the outside of the core. Zones round the periphery are marked as being in phase or out of phase with the reference accelerometer. The number of zones equals twice the number of modes. This approach was found to be quicker and more reliable than locating nodal points. Generally speaking the peaks are sufficiently sharp for the points of maximum velocity and maximum acceleration to be sensibly coincident. The phase difference between the force and acceleration signals was checked at each resonance peak and the 3dB points measured. Sometimes it was not possible to measure a 3dB point because of the proximity of the next resonance.

After the theory detailed in Chapter 4 was developed the prior knowledge of calculated resonant frequencies greatly facilitated the isolation of measured values.

5.2 TOOTH RESONANT FREQUENCY MEASUREMENTS

It was explained in Chapter 3 that tooth resonance is a major influence in determining core resonant frequencies. The method of measuring tooth resonant frequencies is given below. It is based on the knowledge that the tip deflection of an encastre tooth is considerably greater than the base deflection.

Miniature accelerometers are attached to the base and tip of a tooth with wax. Acceleration measurements are then made at various frequencies. The output from miniature accelerometers is small and it was found helpful to make these measurements at or near to core

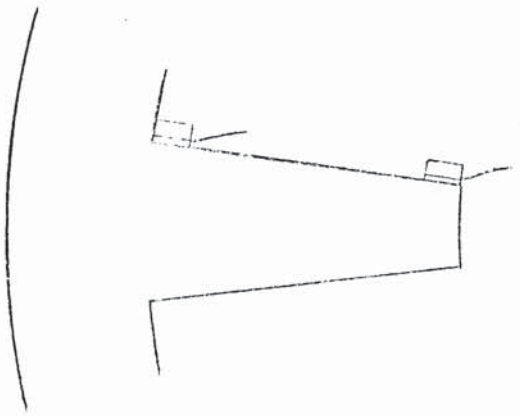

resonant frequencies where the vibration levels are magnified. The ratios of the two accelerometer outputs produce curves like those of Fig.5.2.1. The first of these shows clearly the peak at the resonant frequency. The second curve is more typical. The main peak is reasonably clear but there are several side peaks. The dips in this curve correspond with core resonant frequencies. It has been possible to use this fact to measure certain high mode core resonant frequencies near to the tooth resonance which do not show up using accelerometers attached to the back of the core.

5.3 MEASURED VALUES OF CORE RESONANT FREQUENCIES

All the following measurements were made using the short core method, unless otherwise indicated. Considerable use was made of Kuhl's measurements to verify the plain ring theory which formed the basis of that developed in Chapter 4. These measurements were made with solid rings. In order to confirm the theory for laminated rings, measurements were made on a set of machine laminations from which the teeth were removed. The laminations are those shown in Fig.3.3.5. The measured and calculated resonant frequencies are:

Mode	2	3	4	5	6	7	
Measured freq.Hz	229	633	1198	1884	2684	3584	
Calculated freq.Hz	228	635	1195	1886	2690	3589	
Mode	8	9	10	11	12		
Measured freq.Hz	4514	5624	6664	7743	9048	Error band=2.26%	
Calculated freq.Hz	4565	5603	6689	7812	8963	(95% confidence)	

These figures confirm the excellent agreement found in Chapter 4 (Fig.4.1.1) and further verify the plain ring theory.

5.3.1 The Effects of Wedges

Early in the initial exploratory measurements it was found that tooth resonant frequencies were important in large machines and that the retaining wedges can increase these frequencies considerably. This fact has not been reported in any of the published work in this field and extensive tests were instituted to investigate the effect. The first of the two main lamination designs was chosen for these tests. This design has long teeth and the effect of wedges is pronounced. The dimensions of these laminations are given in Fig.3.3.1. The measurements and calculations with various wedges are given in Fig.5.3.1. The first two curves in this figure are values obtained without wedges and are included as reference values. There are two sets of resonant frequencies - one below the fundamental tooth resonant frequency and one above it. The resonant frequencies shown graphically are repeated in tabular form. Curve and row numbers correspond.

Wedges in production machines are normally a slight clearance fit in the wedge grooves but they are blocked-up using strips of insulation

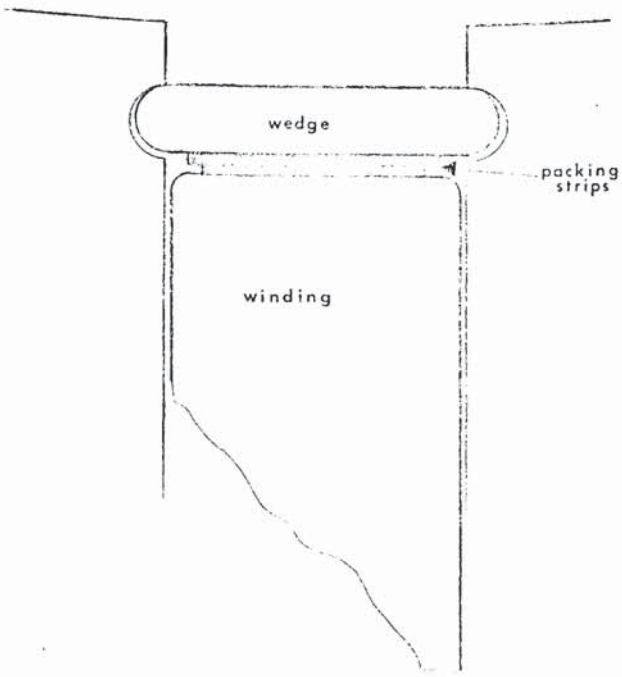

to produce a tight fit in the radial direction. As a first approximation to the real situation, oversize wedges were introduced into the grooves to produce an interference fit. The measured resonant frequencies for this configuration are given in curve 3 of Fig.5.3.1. The resonant frequencies have increased by approximately 24% at the low mode numbers and 100% at the high numbers. This means that the core stiffness has been increased by 55% and the fundamental tooth resonant frequency has doubled. The wedges for this test were made from bonded fabric. High temperature machines use glass-reinforced epoxy wedges which have a much higher modulus of elasticity E_w. The mass of the wedges was negligible compared with the mass of the laminations. The measured increases in resonant frequencies were large and unexpected and two further tests were made to investigate the influence of the method used to fit the wedges into the grooves. The same wedges were used in these three tests and the concept of a fit factor is introduced to describe the type of fit. The two practical limits of 'fit' are the blocked-up clearance wedge, shown above, and the epoxy-adhesive bonded wedge.

In order to produce the blocked-up wedge configuration without the added complication of a massive winding, a dummy wooden winding was

produced. The mass of the wood was only 3.6% of the mass of the laminations. The measurements are given in curve 4 of Fig.5.3.1. High mode number resonant frequencies were not measurable because of the high damping in this arrangement. The low mode number frequencies are increased by approximately 9% and the fundamental tooth frequency is increased by 35%. There appears to be a direct relationship between the increased stiffness of the core and the increase in tooth resonant frequency caused by the wedges. In this and the previous test the zero order resonant frequency is only affected by the mass of the wedges since the hoop stiffness is virtually unaltered.

In the next test the wedges were made to have a clearance of 0.1mm and then bonded to the grooves using a common epoxy adhesive, cured at room temperature. This is the method used in industry when magnetic slot wedges are installed. The increasing use of magnetic slot wedges makes this test significant in its own right. The measurements are given in curve 5 of Fig.5.3.1. Working backwards from these measurements the fit factor is 0.7. This seems a reasonable value since the bond is bound to be imperfect. The tooth resonant frequency is increased by 177% and the core resonant frequencies are increased by upwards of 33%.

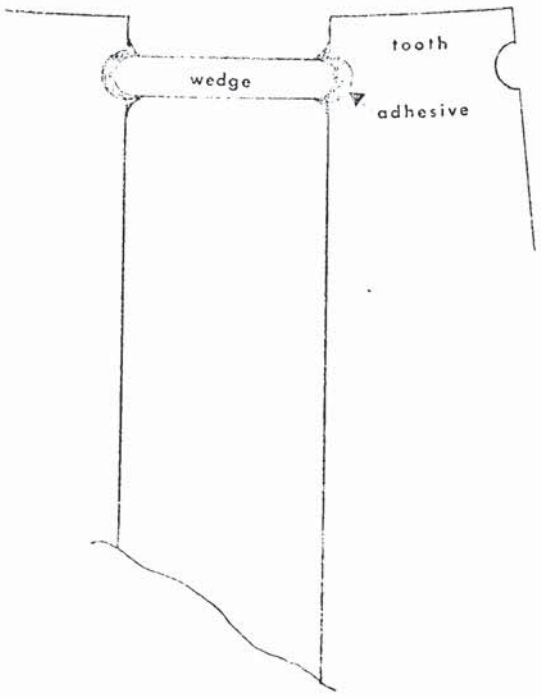

Considerable care was taken in bonding the wedges to the grooves so it was decided to produce another short core with what could be called 'production quality' bonded wedges. Glass-reinforced epoxy wedges were used for these measurements which are given in curve 6 of Fig.5.3.1. The value of fit factor deduced from these measurements is 0.42. This reduction is only partly due to the bond quality. The maximum elasticity modulus of the adhesive is only 40% of the wedge modulus for glass reinforced wedges.

These tests show clearly that wedges are important in determining core and tooth resonant frequencies. For bonded wedges the contribution is of first order magnitude. The theory developed in Chapter 4 includes the effects of wedges i.e. the increase in core stiffness and the elevation of the fundamental tooth resonant frequency. The calculations in Fig.5.3.1 show excellent agreement with measurements, especially for the modes where the resonant frequencies are below approximately 50% of the tooth resonant frequency. The errors are nowhere very large but there are discernible trends in these errors. The primary reason for the errors is the deficiency in the assumed modal shape of the tooth vibration and the effect this has on the inertia and tangential mass factors ξ and ψ. The calculated values of the tooth resonant frequencies are sufficiently accurate but the classical Euler theory for encastre beam deflection is evidently too simple.

The classical theory for beam deflection is for parallel beams. The deflection curve at some fraction of the fundamental resonant frequency is represented by curve 'a' on the next page. For tapered

beams, as found in large electrical machines, the deflection at the thin end is increased above the value for straight beams as shown by curve 'b'. This increased deflection would mean larger values of ξ and ψ so that factors based on curve 'a' produce core resonant frequencies above the actual values when tooth flexure becomes important. This is true unless the support provided by the wedges at the tips of the teeth produce the deflection curve 'c'. In this case the values of the two factors ξ and ψ based on curve 'a' are too high and result in core resonant frequencies below the actual values. These trends are well illustrated by the measured and calculated core resonant frequencies in Fig.5.3.1. The correlation between the wedge parameters and the increase in tooth resonant frequency is given in Fig.5.3.2 together with the theoretical curve. The values of wedge stiffness used to plot the measured points were obtained using fit factors derived from the core resonant frequency measurements. The use of bonded wedges is increasing, especially in induction machines. More extensive tests to determine tooth resonant frequencies with such wedges would enable a more critical appraisal of the theory developed (Section 4.4.2). It may be found that thick wedges should be considered to constrain the rotational as well as the translational movement of the tooth tip.

Elasticity moduli for the various wedge materials were obtained using a vibrating beam method. Extensometer methods were tried but these

gave poor results. A stroboscope was used to measure the resonant frequencies of very long clamped/free beams and the moduli deduced from them. Different samples of the same material gave a spread of values (approximately ± 15%).

Since the wedges in a machine can have such a dramatic effect on resonant frequencies they may provide a means of adjustment, should a machine be in resonance. It should be noted that this large influence of wedges on the fundamental tooth resonant frequency contradicts Pavlovsky's[19] theory. He shows than when a machine is wound and wedged the fundamental tooth resonant frequency remains sensibly constant.

5.3.2 The Effects of Segmentation

Machines with outside diameters greater than approximately one metre are normally segmented i.e. the laminations are produced as segments of a ring. It has been stated by Uner and Jordan[15] that measurements show that the segmented core can be assumed equivalent to a complete ring. This statement is based on two live measurements on a complete machine and the theory developed by these authors.

From the measurements given below it is apparent that segmentation has a significant effect on resonant frequencies and that the near cancellation of two opposite effects has lead to an erroneous conclusion by Uner and Jordan.

The principal measurements made to investigate segmentation were made on laminations that were originally complete rings. This approach was chosen so that a direct comparison of measurements was possible. The second of the main lamination designs was chosen for this test. The laminations were machined into six segments with a 1.5 mm spacing between segments. The core was clamped together in the normal way with two complete ring laminations at the top and bottom of the core. The dimensions of the laminations and the various measurements are shown in Fig.5.3.3. At frequencies unaffacted by tooth flexure the resonant frequencies are approximately 8.0% below the non-segmented values. At higher modes the resonant frequencies become assymptotic to the same tooth resonant frequency so that the difference in resonant frequencies reduces to zero. It was also observed that slightly different resonant frequencies could be obtained by changing the position of the vibrator. The difference is small as can be seen from the measurements in Fig.5.3.3. Further small differences in resonant frequencies were obtained with different clamping pressures.

The effects of segmentation can be accommodated in the calculation method by using an artificially low value of elasticity modulus E. Such a value applies to the core but not the teeth since the tooth resonant frequency is not affected by segmentation. The calculations with a reduced value of E are given in Fig.5.3.3. Variations in measured resonant frequencies with clamping pressure mean that the correlation between measured and calculated frequencies is generally poorer with segmental laminations compared with ring laminations.

Two more sets of segmental laminations were tested. These cores were of large diameter and designed for segmental construction. The measured and calculated resonant frequencies are given in Fig.5.3.4. The first of these cores was constructed in two ways. In addition to the normal 50% overlap between layers the core was also built up so that the discontinuities were spread evenly round the core rather than at 12 points (there being 6 segments in each ring). It was found that the two configurations produced the same results, within the limits of measurement accuracy and repeatability. The good agreement between calculated and measured frequencies for all three segmental designs verifies the use of a reduced elasticity modulus.

5.3.3 Axial Ventilation Holes and Duct Spacers

Axial ventilation through holes in the core is used most frequently in small and medium size machines. A small proportion of large machines use this form of ventilation and so a set of laminations with two rows of ventilation holes was tested. The differences in calculated values with and without ventilation holes is small. These are shown in Fig.5.3.5. The measurements confirm the accuracy of the calculation method for all but the zero order mode. In this mode of vibration the ring expands and contracts and the holes reduce considerably the stiffness to this type of deformation. The averaging of the effect of holes to produce an elipsoidal void round the whole circumference of a lamination is not very accurate when evaluating the breathing mode resonant frequency. The stress/strain behaviour in this mode is analogous to a perforated bar in tension. Further work is needed to refine the calculation method to account for the effect of ventilation holes on the zero mode resonant frequency.

For this particular design of laminations the nett effect of ventilation holes was to increase flexural mode resonant frequencies. That is, the reduction in mass of the core was greater than the reduction in stiffness.

It has been common practice to include the mass of windings when calculating core resonant frequencies. It is shown in Chapter 6 that windings in large machines do not contribute to live machine resonant frequencies. The only extra mass that should be included is that due to the duct spacers. These spacers are usually welded to the last laminations in each packet. They are constrained to move with the core and teeth but add no stiffness. The spacers reduce tooth resonant frequencies as well as core resonant frequencies so that the latter are doubly affected.

Measurements on a core with duct spacers were made using a short core comprising two half packets sandwiching a lamination with spacers attached. The dimensions of the laminations used are given in Fig.3.3.1. The measurements and calculations with and without duct spacers are given in Fig. 5.3.6. The tooth resonant frequency has been reduced by approximately 10%. A similar figure is obtained for the complete machine reported in Chapter 6. Since most machines have similar ratios of tooth width to spacer width and the influence is small, an empirical factor is appropriate in accounting for the effect of duct spacers on tooth resonant frequencies.

5.3.4 Thick Ring Machines

The theory developed in Chapter 4 is for thick rings with teeth, i.e. secondary effects have been taken into account. In the measurements and calculations quoted above the machines have had relatively shallow cores. Two sets of measurements were made on deep-cored machines to check the theory as applied to non-thin cores. In the first of these measurements the teeth were short so that their effect was not dominant. The measurements are given in Fig.5.3.7. There are six modes below the tooth resonant frequency where the influence of tooth flexure is negligible and the agreement between calculations and measurements for these modes is excellent. The small errors at higher modes are principally due to the error in the calculated tooth resonant frequency.

The second deep-cored machine has long teeth, with the additional complication of set back wedge grooves. The teeth also have a large taper ratio so that this machine represents the normal limit of calculation difficulty. Set back wedge grooves are not accounted for in the calculations so that it is to be expected that the measured tooth resonant frequency will be below the calculated value. The measurements and calculations are given in Fig.5.3.7. Until further experimental or theoretical work is forthcoming the effect of set back grooves can be accounted for by an empirical factor (0.9). This value is based on one set of measurements but is not included in the above calculations since it must be considered as a temporary measure only.

These two sets of measurements illustrate one of the measurement problems encountered, i.e. the great difficulty of isolating core resonant frequencies when these are within approximately ±5% of the tooth resonant frequency. The resonant frequencies for adjacent modes are so close together that the peaks in the response curve merge into one. Even when this is not so the material damping can be such as to prevent the teeth flexing sufficiently to add enough inertia to realise a resonance condition. This applies particularly to the low order modes above the tooth resonant frequency. The calculations for the second core were limited to mode 6 since the computer program only stores rotary inertia and circumferential mass factors for frequencies up to four times the tooth resonant frequency.

5.3.5 Clamping Rings

The laminations in a large machine are clamped together using rings at each end of the core which are keyed or welded to the frame. If the clamping rings are complete (not segmented) then they can add stiffness to the core structure. The theory developed can account for end clamping rings. The following measurements (Fig.5.3.8) were made on a long core (without duct spacers) using the short core method. The endring dimensions were chosen so that their effect was pronounced.

The measurements show clearly that the endrings affect the resonances at low frequencies only. The increase of 31% for the first mode resonant frequency quickly diminishes to negligible proportions for higher modes. The endrings are effectively uncoupled above 600 Hz and begin to uncouple at 200 Hz.

The calculations with endrings show good agreement only at those modes where the endrings remain coupled (modes 2 and 3 in this example). This uncoupling effect was also observed for this and another design of laminations built into the production machine frame (Chapter 6). The gradual uncoupling of the endrings was observed by mapping the modal patterns axially as well as circumferentially. This uncoupling effect was not amplitude dependent since the same resonant frequencies were measured with vibration amplitudes differing by an order of magnitude. For frequencies above the uncoupling frequency the resonances should be calculated ignoring end clamping plates.

5.3.6 Tooth Resonant Frequencies

The measured and calculated tooth resonant frequencies for various laminations are given in Fig.5.3.9. These cover a wide range of linearly tapering teeth and include one rotor tooth with a root depth smaller than the free end depth. The calculations shown use the theory developed in Chapter 4. The root flexibility and shear correction factors C_r and C_s have been obtained from the equations that underlie Figures 4.4.4 and 4.4.5. Extra correction factors for effects such as tip overhand and set back wedge grooves have not been included in these calculations. The measurements were made using the short core method without wedges or duct spacers.

Semi-closed stator slots are common in small machines and the proposed method overcalculates tooth resonant frequencies for the configuration over the page.

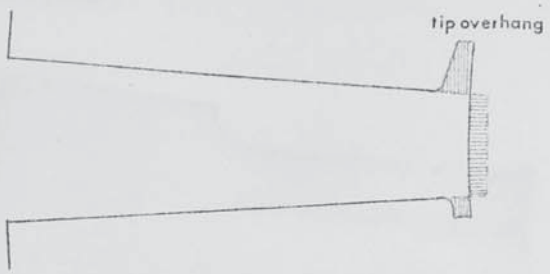

In order to improve the calculation, teeth with overhangs are assumed equivalent to slightly longer teeth where the increased area equals the tip overhang area. Until more experimental evidence is available the effect of set back grooves can be accommodated by a 10% reduction in tooth resonant frequencies.

The measured and calculated resonant frequencies show excellent agreement and confirm the overall importance of root flexibility. In the examples shown the root flexibility introduces reductions of between two and three times that obtained for the classical secondary effect - shear and rotary inertia. The overall reduction due to 'secondary' effects can be greater than 25% for teeth of normal proportions.

Previous authors have ignored secondary tooth effects and introduced further errors by assuming that tapered teeth are equivalent to parallel teeth. The compounded errors that result from this approach can be quite large. The largest error for the teeth in Fig.5.3.9 using these simplifications is +61.3%.

5.3.7 Small Machines

In addition to the frequent use of semiclosed slots the laminations in small machines often differ from large machines in that they have round bottomed slots. In order to study the differences between the two types of slots an associated research project was

undertaken by Poon[20]. This work on toothed straight beams quantified the effect of root flexibility and core stiffness with semicircular slot bottoms.

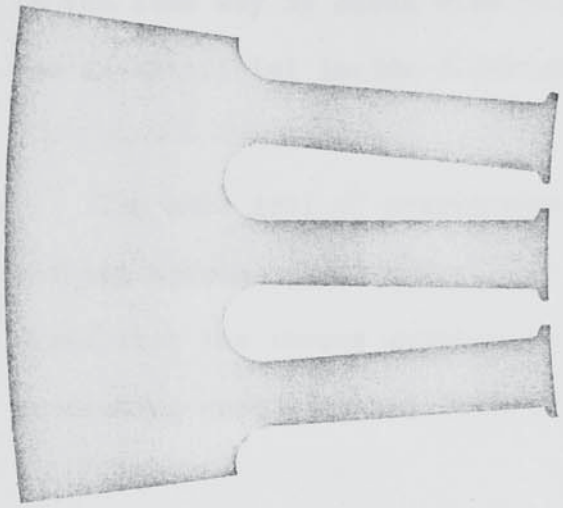

In order to check the present theory (developed for large machines) against small machines, measurements were made on the laminations shown opposite. These laminations were also valuable for checking combined axial and radial vibrations since a complete core without duct spacers was available. Measurements were made on the complete core 210mm long and a short core 22mm long. Small machine laminations of this sort are held together by a number of welds down the back of the core so there is no clamping problem nor any complication due to clamping plates. Verma and Girgis[21] make much of vibration modes which contain axial as well as circumferential variations. In the measurements on the above laminations it was not possible to excite significant vibrations with axial dimensions to the modal shapes.

The measurements are compared with calculations in Fig.5.3.10. In these calculations the inside diameter was not reduced to compensate for the rounded slots. Extra mass was added to account for the large fillets at the base of each tooth and the teeth were extended to account for the tip overhang. It was expected that the root flexibility for this type of tooth would be much reduced. In order to offset the calculated reduction the tooth resonant frequency was increased by 10%. With those

adjustments to the machine details the calculations show excellent agreement with the measurements. It can be said that, apart from the effect of root flexibility, cores with round bottom slots can be treated in the same way as cores with flat bottom slots. There is no need to use an artificial inside diameter.

Two more sets of measurements are given in Fig.5.3.10. There is nothing special about these designs. They are included as further proof that the theory developed in Chapter 4 is equally capable of predicting core resonant frequencies of small as well as large machines.

5.3.8 Damping Factors

Past machines that have been excessively noisy have usually been in a state of resonance or near resonance. When such a condition exists the vibration levels are limited only by the amount of damping in the system. It is important, therefore, to know what levels of damping are connected with the different elements that comprise the stators of electrical machines. Standard parameters have been used to determine levels of damping.

The factor Q is defined for any mode as the peak amplitude of vibration at resonance divided by the amplitude at zero frequency for the same level of force. In practice this quantity is obtained by measuring the frequencies on either side of the resonant frequency at which the vibration amplitude is 0.707 times the peak value. With a point source excitation the influence of neighbouring modes on the amplitude of vibration is not negligible and leads to inaccuracy in Q.

This is particularly so with highly damped systems and at frequencies where the resonances are close together e.g. in the region of the tooth resonant frequency. The influences of secondary dynamic effects lead to response curves which depart from the classical shape and upset the relationship between Q and the 3dB points. In Fig.4.2.2 a mode 8 response curve is drawn with a Q factor of 20. The measurements of the 3dB points lead to the conclusion that Q = 42.5 and 24.5 for the two resonant frequencies. Despite these limitations this parameter was measured at all resonant frequencies.

From a very large number of measurements, mainly on large machines, it is possible only to observe general trends. Measured values of Q varied between 5 and 350 with the majority in the band 10 to 100. The largest values were obtained with the largest cores. That the vibrator attachment and the mounting were responsible for producing reduced Q factors was clearly demonstrated in the measurements of Fig.5.3.10. With the same laminations the long core produced Q factors 10 times the values obtained with a short core. The effect of the mounting arrangement became more pronounced as the mass of the laminations decreased.

Deep cored machines had consistently high values of Q and most designs had values in the vicinity of 100 for the zero order vibration mode. In most of the cores tested there seemed to be large random changes in Q from one mode to the next. No explanation is offered for this. Similar variations occurred when the two limitations of the measurement method did not apply. Segmented cores gave rise, generally,

to lower values of Q than were obtained for the majority of complete ring laminations.

The effect of wedges on the damping factor Q was studied when making the measurements given in Section 5.3.1. The damping factors for the various types and fits of wedges are shown graphically in Fig.5.3.11 for the modes below the tooth resonant frequency. A definite trend is discernible towards higher damping with viscoelastic wedges (polymethylmethacrylate) and blocked-up wedges. For all of the other wedges the damping factors were eratic. The average damping factor for the high damping wedges was approximately 20 (equivalent to $\beta = 0.05$), which corresponds very well with the value obtained from the theory of Section 4.5.

It is to be expected that the presence of windings and the coat of varnish applied to some machines will introduce extra damping compared with the laminations alone. The production machine used as the basis of all the experimental work gave Q factors between 9.7 and 18.5 for the nine modes excited in the live machine test - see Chapter 6. It is to be expected that different designs will increase the spread of 'normal' damping factors beyond these two values. Only the systematic measurement of machines excited by the internal electromagnetics of the live machine (as described in Chapter 6) will produce reliable bounds for damping factors. At the design stage the engineer is interested in the lowest damping to be expected and until more live measurements have been made this must be assumed to be equivalent to Q = 350+.

5.3.9 Error Results

The main reason for instituting this research was to improve the error margin that had to be applied to calculated resonant frequencies of large machines when predicting noise levels.

Experience had shown that the widely used methods based on simple ring theories required a tolerance of -10%, +40% with a 69% confidence limit.

The basic error bounds for the present theory are ± 6% with a 95% confidence limit. A higher value (± 15%) should be used for the first modes above the tooth resonant frequency. These modes are usually unimportant. These figures are based on over 600 separate resonant frequencies (modes 2 to 20) measured on 15 designs of large machines, many of them configured in various ways to measure different effects. These bounds are applicable to resonances where the frame can be considered uncoupled and where the various dimensions are known precisely.

For segmental laminations the artificial value of elasticity modulus E used in calculating resonant frequencies is subject to a separate tolerance to account for clamping variations. Composite error bounds can be obtained by making calculations with the two extreme values of E and applying the 6% bounds to them. A more acceptable method is to have increased bounds of ± 8.5% for segmental laminations.

It was shown in Section 5.3.1 that the fit of wedges in a machine was an uncontrollable parameter and might reasonably range from 0.0 to

0.2 for normal wedges introduced under factory conditions. Since wedges have differing effects on machines the error bounds should be obtained by making calculations at the two extremes of wedge fit factor and then applying the basic 6% to these. For many machines the increase in error bounds due to uncertainty about wedging will be small.

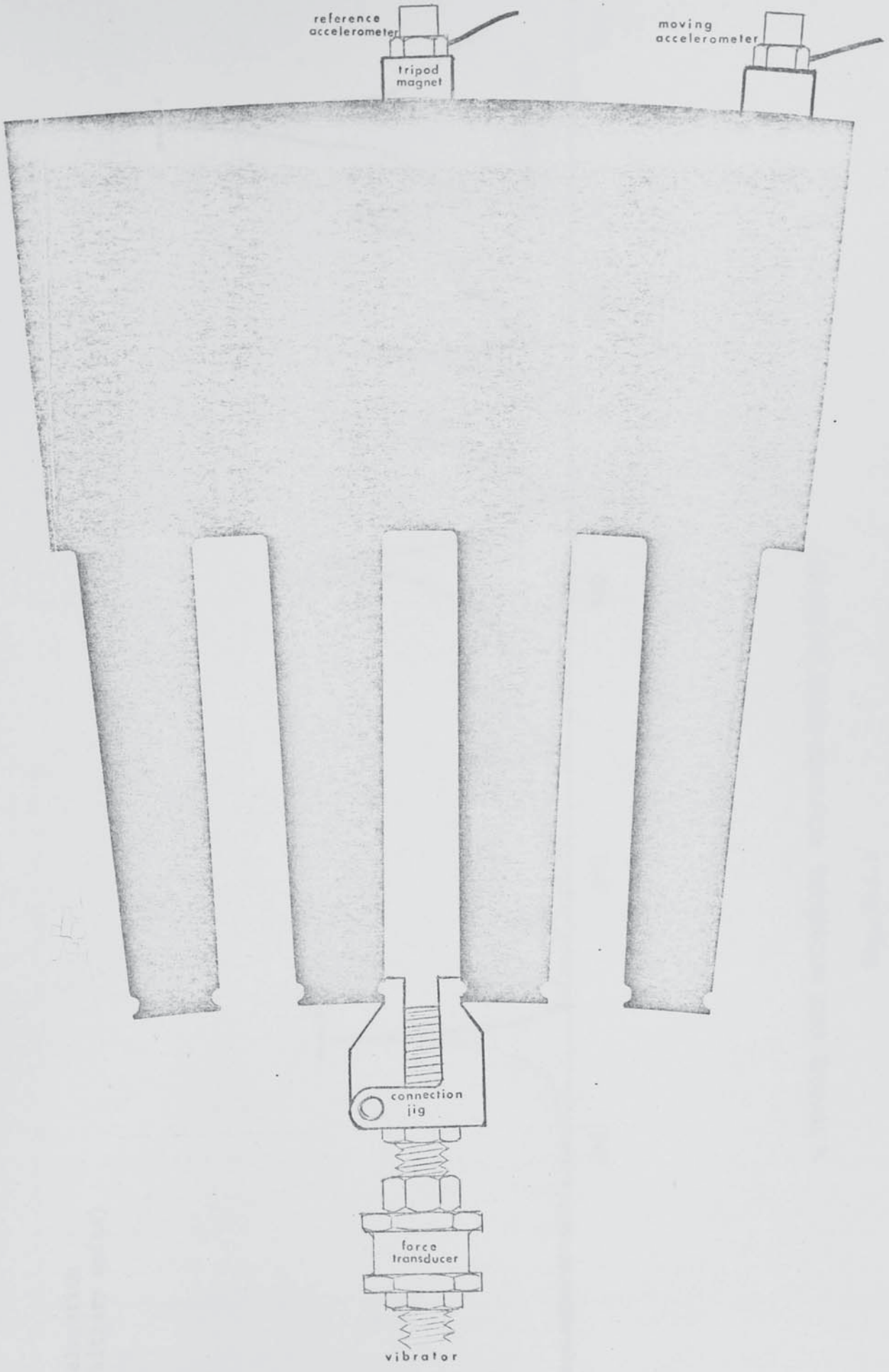

SHORT CORE MEASUREMENT SYSTEM

Fig. 5.1.1

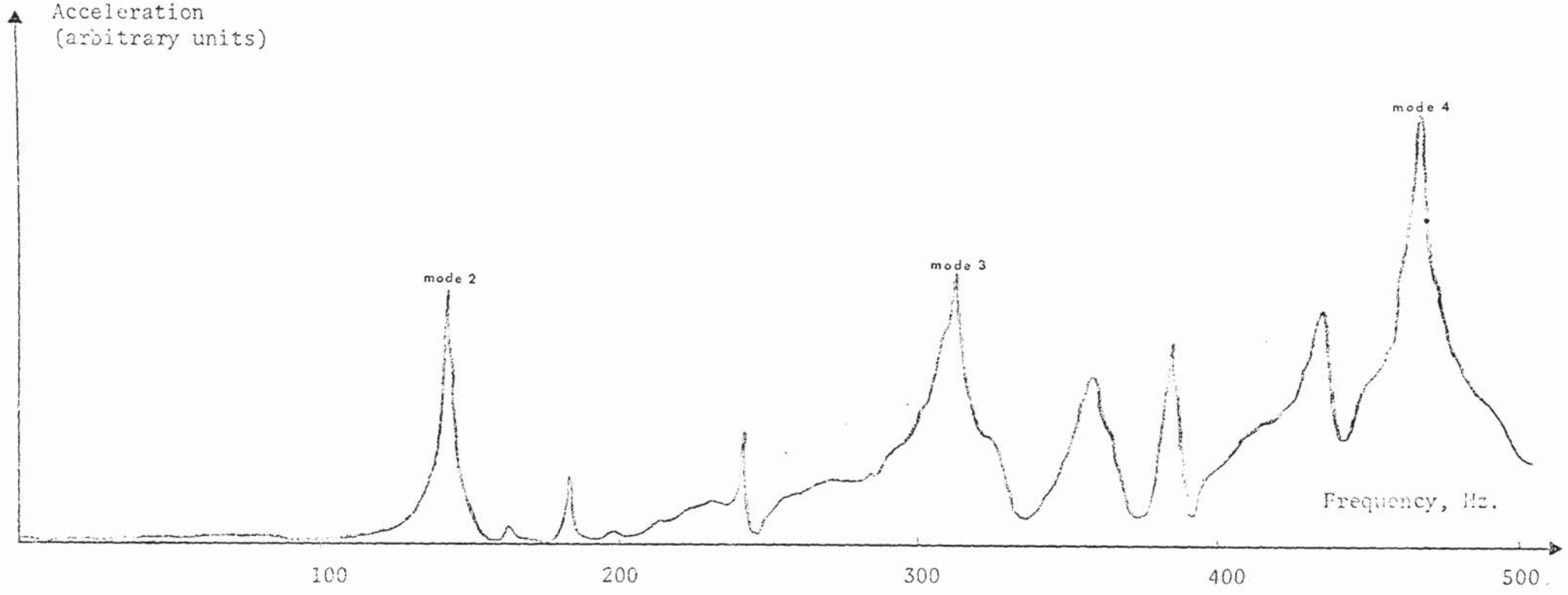

A TYPICAL CORE MECHANICAL RESPONSE CURVE (0-500 Hz)

Fig. 5.1.2

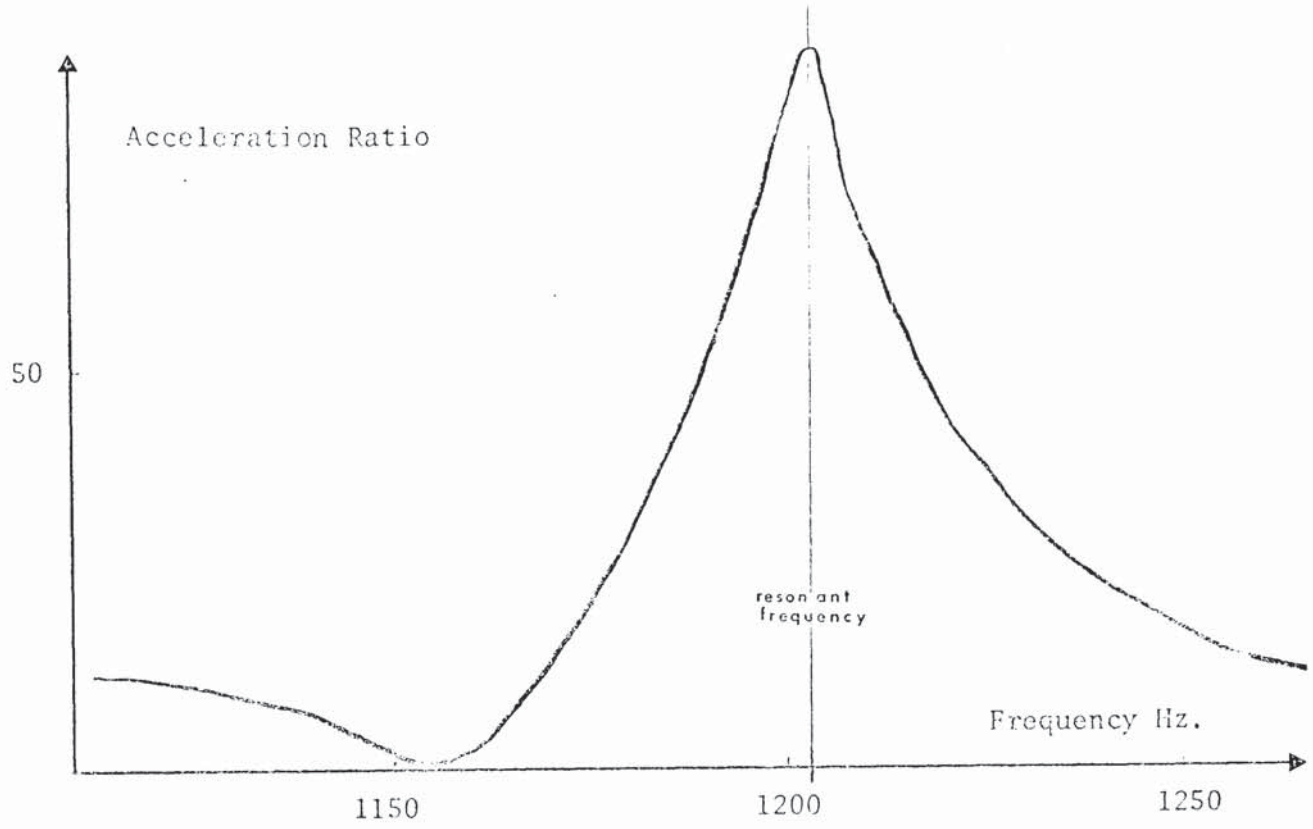

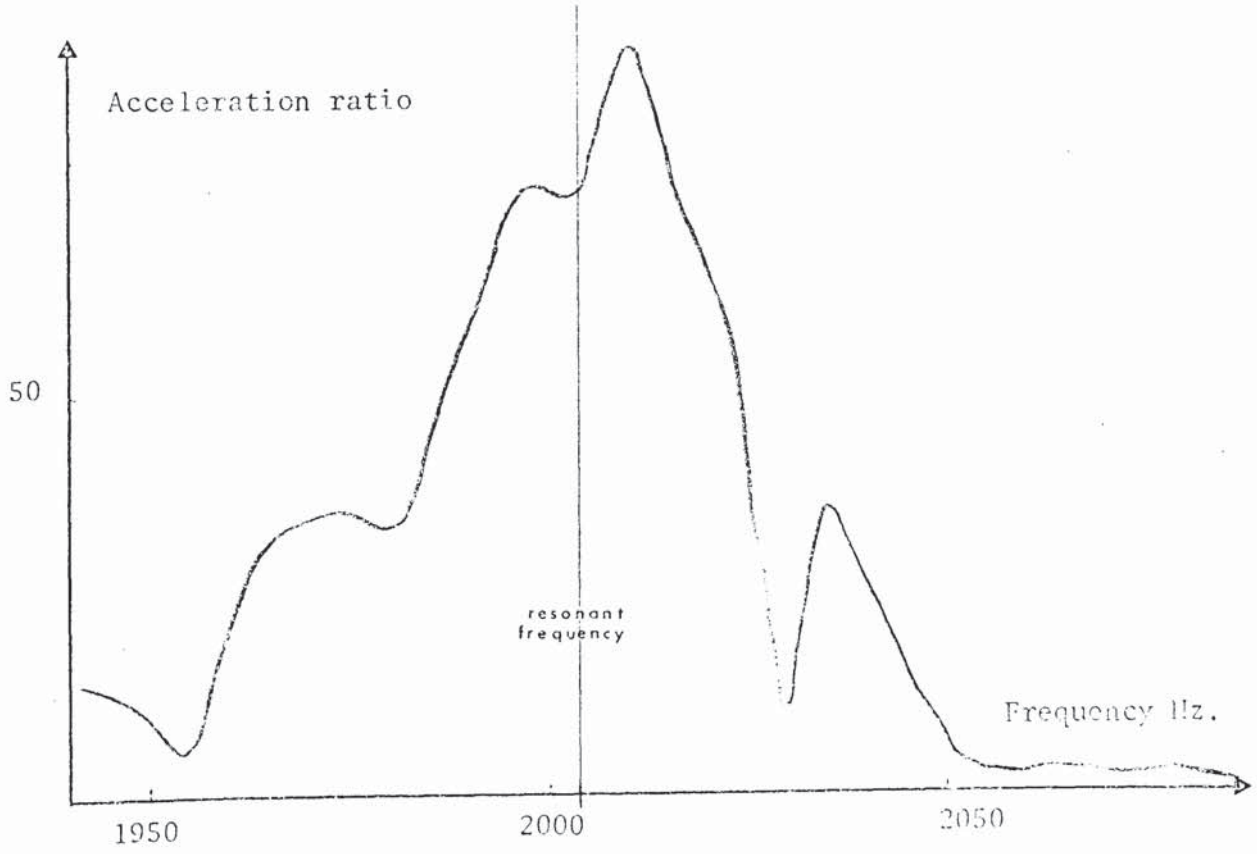

TOOTH RESONANCE CURVES

Fig.5.2.1

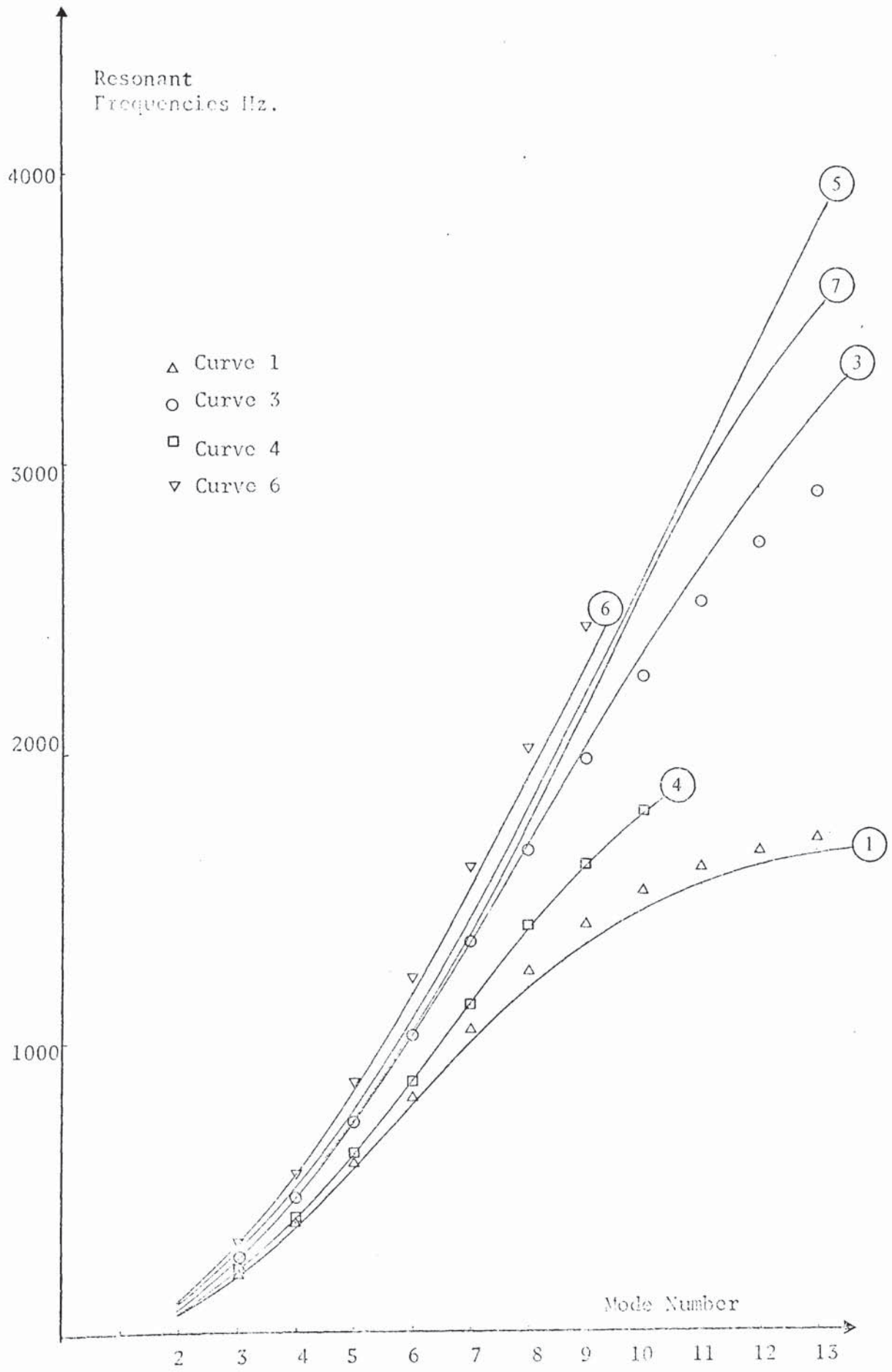

CORE RESONANT FREQUENCIES WITH WEDGES

Fig. 5.3.1

Mode		2	3	4	5	6	7	8	9	10	11	12	13	zero	tooth	
Row																
1(b)		74.7	200.8	382	572	800.8	1008	1200	1349	1463	1547	1619	1668	1349	1865	Measurements
2(a)		2095	2184	2272	2383	2522	2709	2946	3227	3609	4033	4483	4996			
3(b)		95.1	256.6	476	737	1024	1349	1697	2024	2364	2697	2926	3194	1350		
4(b)		79.2	219.4	402	620	871.2	1132	1408	1610	1807	-	-	-	1325	2500	
5(b)		103.6	280.4	507	784	1090	1432	1795	2209	2639	2956	3449	3844	1353	5163	
6(b)		116.3	311.9	556	847	1173	1538	1905	2304	-	-	-	-	1369	-	
7(b)		96.2	261.2	480	766	1042	1370	1728	2164	2578	2985	3275	3545	-	4148	
1(b)		74.4	204.6	380	590	819	1047	1249	1409	1525	1609	1666	1707	1338	1863	Calculations
2(a)		2384	2563	2691	2788	2858	2965	3149	3398	3697	4028	4376	4735			
3(b)		92.7	254	472	735	1032	1349	1671	1984	2272	2526	2740	2914	1341	3727	
4(b)		78.8	216.6	403	628	877	1139	1393	1623	1816	1967	2081	2168	1314	2516	
5(b)		99	271	503	785	1103	1447	1806	2169	2523	2860	3172	3453	1343	5242	
6(b)		111	304	562	876	1231	1617	2023	2441	2863	3280	3689	4082	1346	8199	
7(b)		95.4	261.6	486	757	1063	1392	1730	2063	2379	2666	2916	3128	1342	4211	

Wedge details:

Row	3	4	5	6	7	
depth	2.44	2.44	2.44	2.96	2.92	mm
E	8093	8093	8093	20600	5690	MN/m^2
fit factor	.5	.15	.7	.42	.7	- deduced from measurements

Lamination dimensions as per Fig.3.3.1. Letters in brackets indicate below or above tooth resonant frequency

THE EFFECT OF WEDGES

Fig. 5.3.1 (Numerical Values)

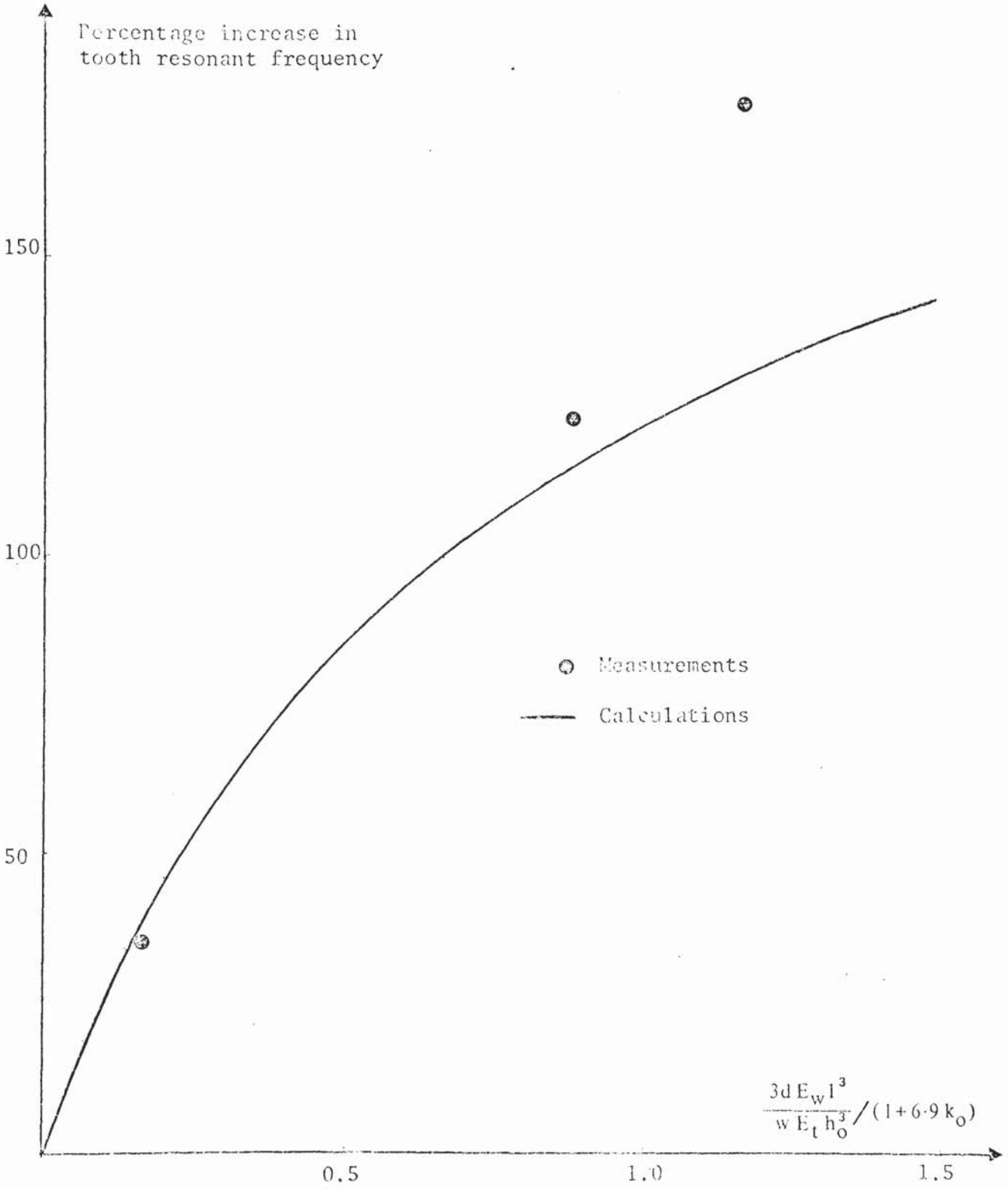

INCREASES IN TOOTH RESONANT FREQUENCIES DUE TO WEDGES

Fig. 5.3.2

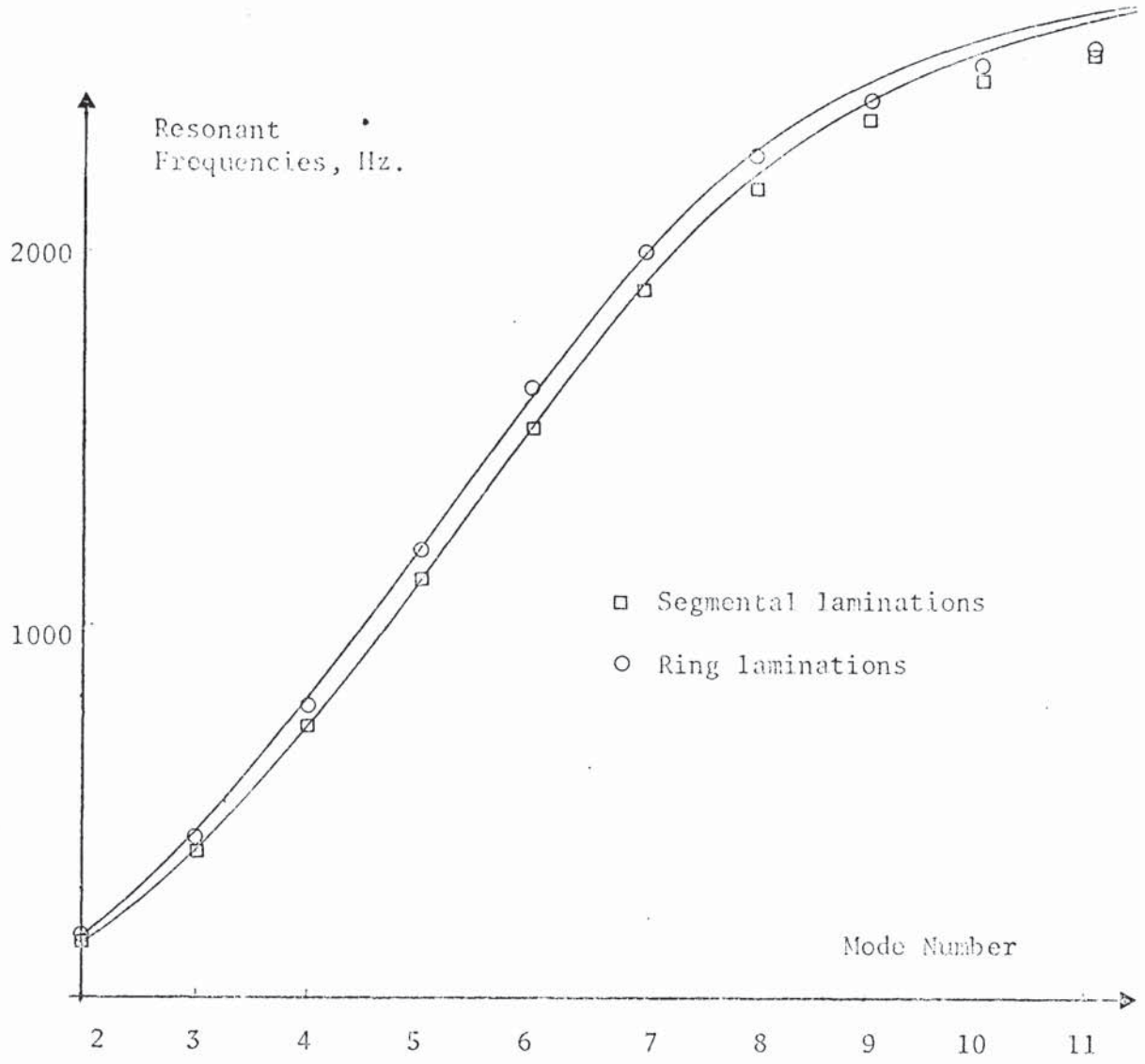

OD = 831.85mm, ID = 733.4mm, GD = 597.4mm, slots 72 x 13.97mm.

Mode	ring (b)	meas. (a)	ring (b)	calcs. (a)	segmental (b)	(b)	meas. (a)	seg. (b)	calcs. (a)
2	153	2955	156	3095	141	142*	2842	144	3095
3	443	3085	428	3222	386	392	3055	394	3221
4	806	3192	790	3308	737	740	3163	728	3308
5	1205	3318	1211	3367	1126	1134	3286	1119	3366
6	1614	3512	1645	3488	-	1475	3465	1531	3445
7	2012	3817	2015	3757	1924	1933	3758	1905	3647
8	2281	4260	2267	4193	2215	2221	4177	2180	3992
9	2461	4811	2416	4749	2410	2415	4682	2360	4466
10	2581	5538	2505	5372	2535	2536	5322	2462	5015
11	2693	6242	2553	6021	2619	2620	6024	2534	5600
0	1646		1652		1500	1507		1520	
tooth	2807		2668		2807	2807		2668	

*different circumferential position of vibrator.
Reduced modulus for segmental calculations = 174325 MN/m^2.

THE EFFECTS OF SEGMENTATION

Fig. 5.3.3

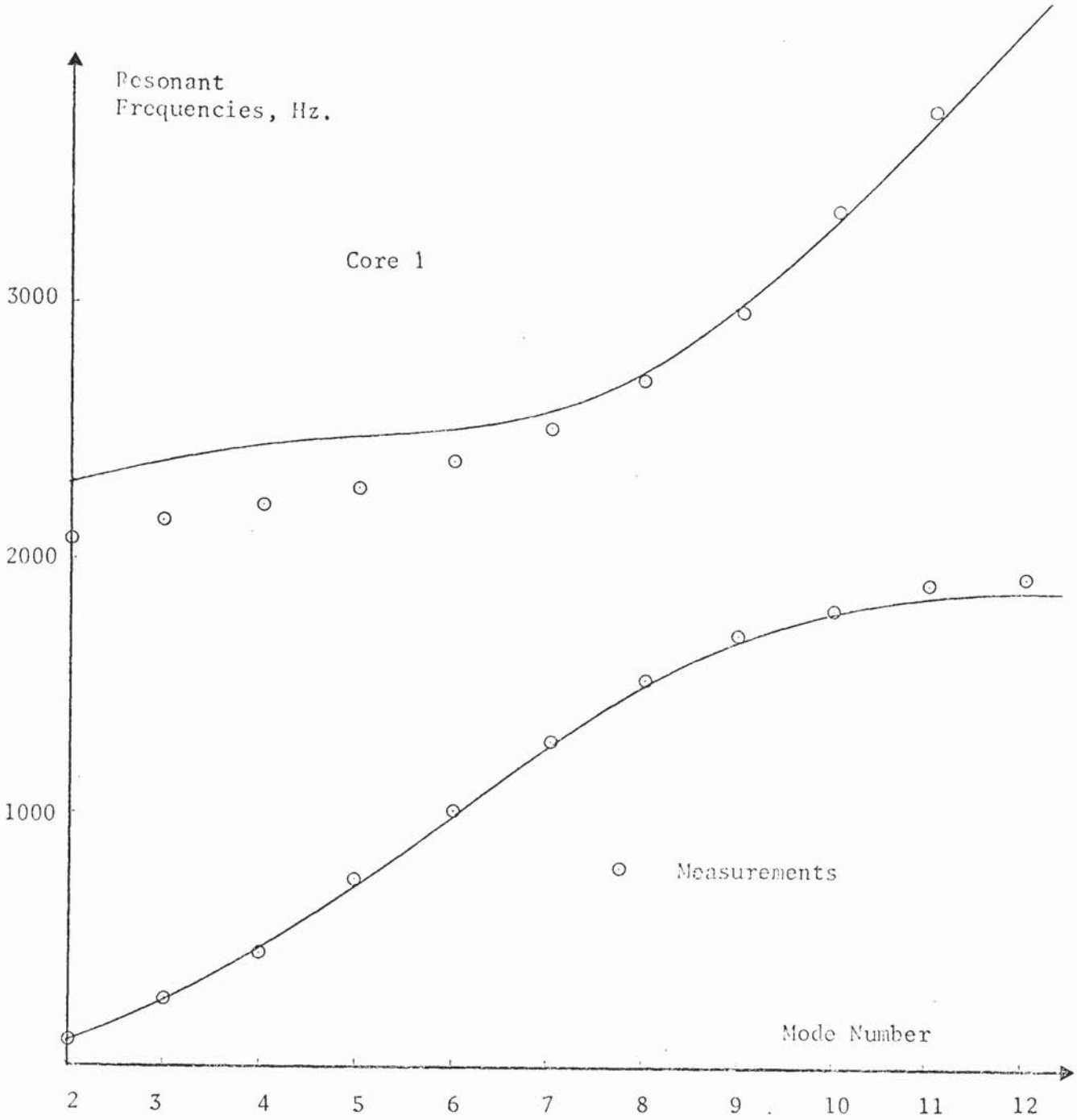

Core 1 OD = 1320.8mm, ID = 1168mm, GD = 1000mm, slots 108 x 13.4mm
Core 2 OD = 2959.1mm, ID = 2785.5mm, GD = 2600mm, slots 216 x 15.8mm.

Mode	Core 1 measurements (b)	(a)	calculations (b)	(a)	Meas. (b)	Calcs. (b)	Core 2 Meas. (b)	Calc. (b)	Mode
2	90	2074	90.2	2291	19.0	19.2	997	999	13
3	258	2141	249	2380	48.6	54	1117	1119	14
4	460	2212	463	2439	91.6	103	1215	1234	15
5	730	2278	719	2478	199	165	1328	1338	16
6	1008	2383	1001	2507	264	239	1423	1430	17
7	1287	2504	1280	2585	322	324	1506	1508	18
8	1529	2715	1517	2749	431	420	1581	1572	19
9	1710	2993	1685	3006	538	524	1627	1623	20
10	1819	3361	1791	3340	644	637	1651	1665	21
11	1910	3759	1855	3717	757	756			
12	1943	4220	1897	4116	865	877			
0	913		973		431	415			
tooth	2005		1987		1800	1861			

...ES OF SEGMENTED CORES

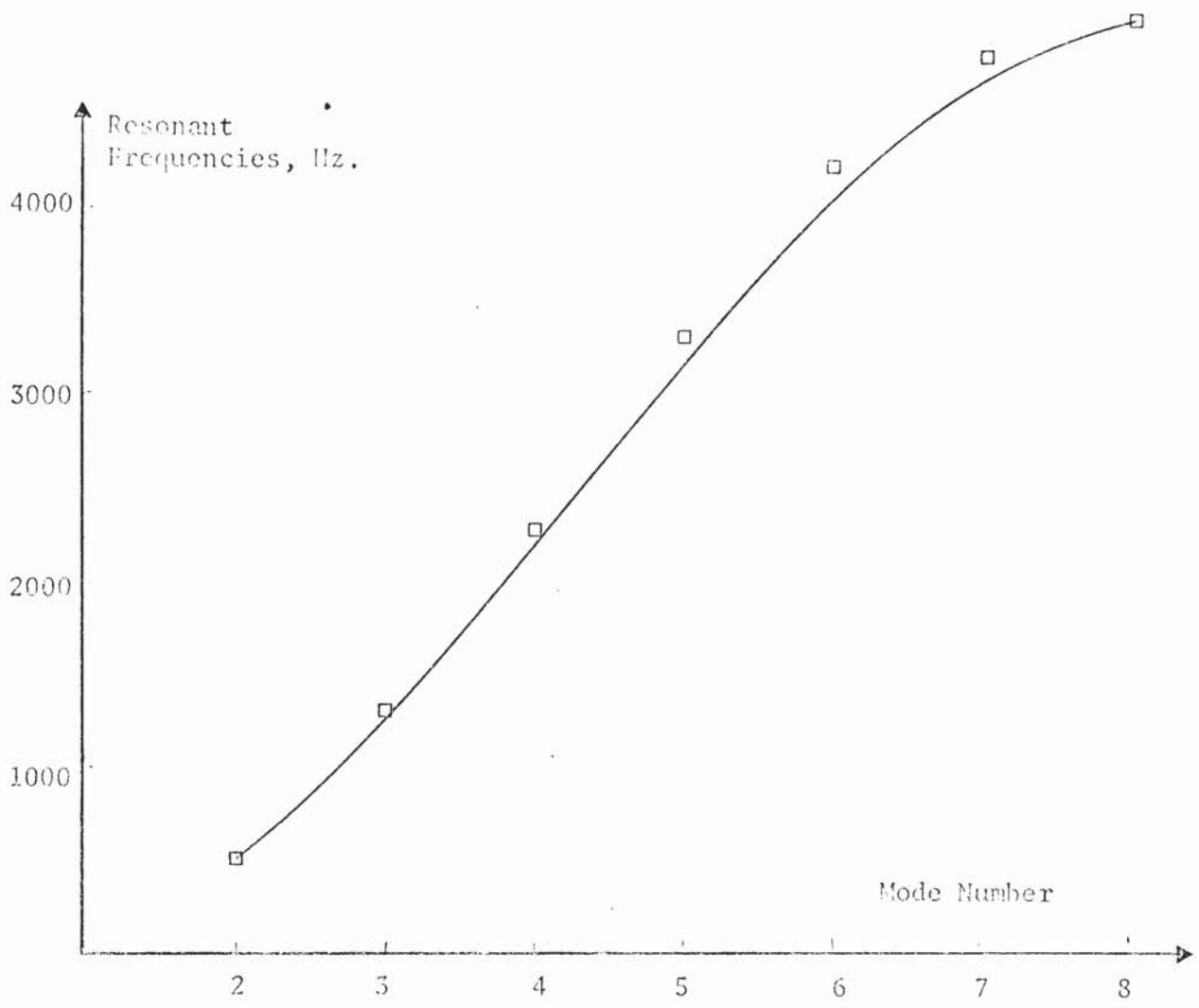

OD = 762mm, ID = 568.96mm, GD = 482.6mm, slots 60 x 13.06mm.
Two rows of ventilation holes, 2 x 35 x 15.875mm dia. on
pitch circle diameters of 699.3mm and 631.17mm.

Mode	measurements		calculations without holes		calculations with holes	
	(b)	(a)	(b)	(a)	(b)	(a)
2	494	5606	482	5480	488	5480
3	1247	5751	1273	5562	1287	5561
4	2187	5977	2245	5592	2263	5588
5	3168	6180	3282	5629	3301	5621
6	4046	6512	4213	5867	4228	5862
7	4655	7125	4766	6513	4772	6513
8	4950	8002	4946	7519	4943	7514
0	2094		2273		2260	
tooth	5070		5164		5164	

LAMINATIONS WITH AXIAL VENTILATION HOLES

Fig. 5.3.5

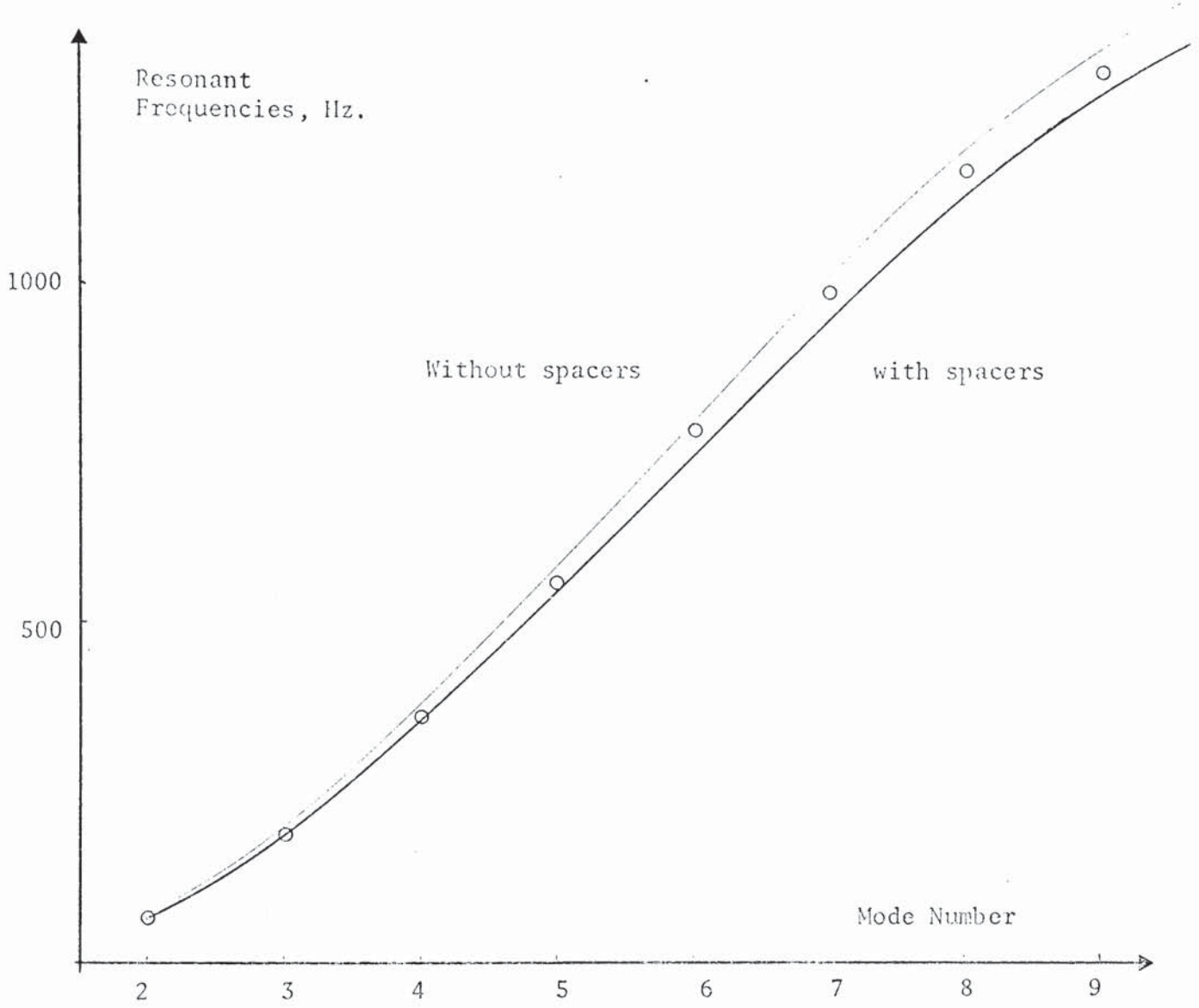

OD = 831.85mm, ID = 772.25, GD = 597.63mm, slots 72 x 13.97 mm
Stack length (nett) = 40mm, weight of duct spacers 4.5kg.

Mode.	2	3	4	5	6	7	8	9	0	tooth
meas.	74.7	201	382	572	801	1008	1200	1349	1349	1865
calc.	74.4	205	380	590	812	1047	1249	1409	1525	1863
meas.	71.5	193	364	547	-	977	1138	1281	1281	1665
calc.	71.4	196	364	565	781	993	1174	1310	1283	1667

EFFECTS OF DUCT SPACERS

Fig. 5.3.6

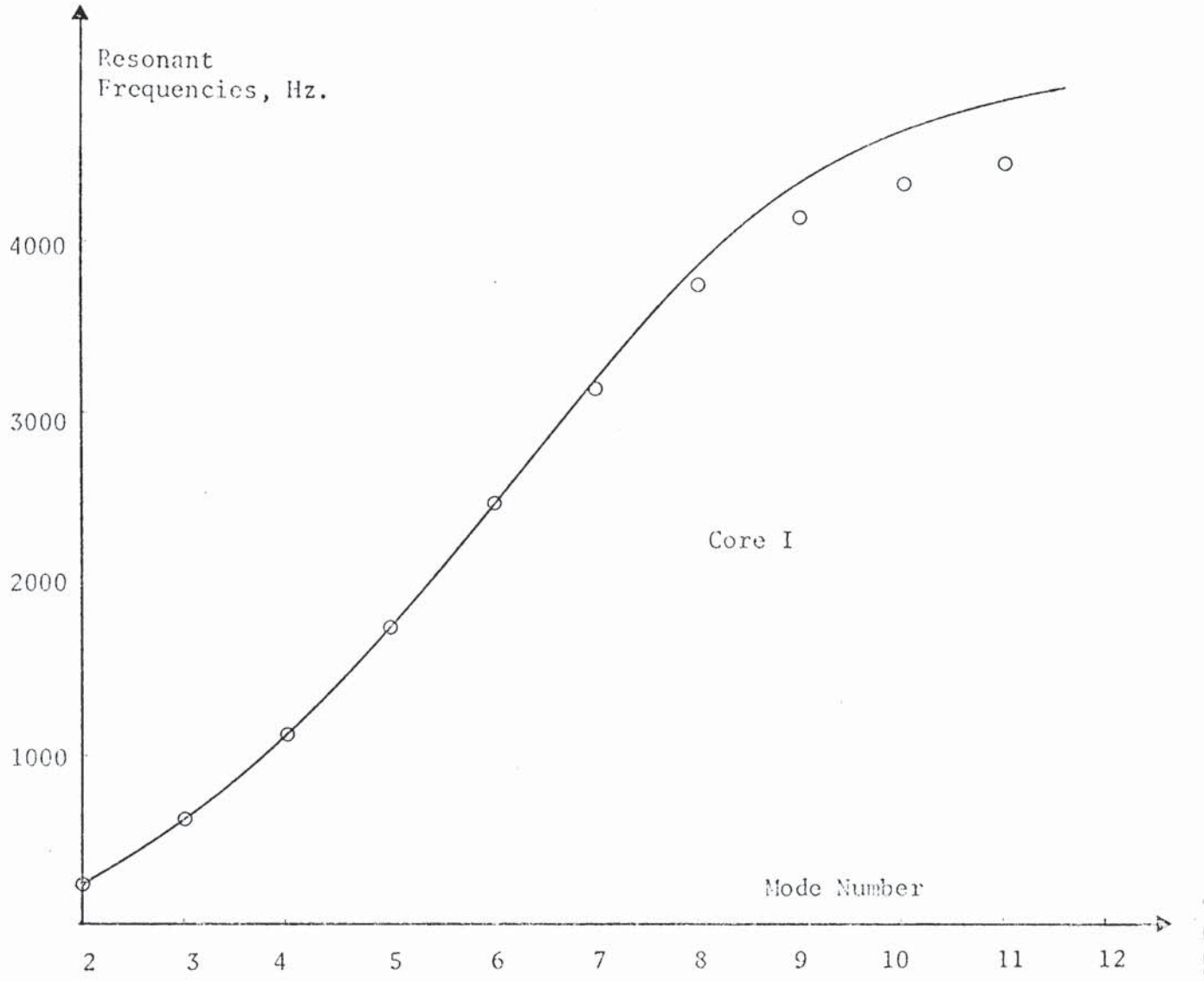

Core 1 OD = 920.5mm, ID=774.25mm, GD = 700.25mm, slots 144 x 7.315mm.
Core 2 OD = 1016. mm, ID=736.6 mm, GD = 508 mm, slots 60 x 15.58 mm.

Mode	Core 1 measurements (b)	Core 1 measurements (a)	Core 1 calculations (b)	Core 1 calculations (a)	Core 2 measurements (b)	Core 2 measurements (a)	Core 2 calculations (b)	Core 2 calculations (a)
2	-	-	227	4980	377	1505	375	1458
3	629	-	623	5073	914	1602	929	1537
4	1150	-	1150	5132	1160	2027	1254	1985
5	1777	5276	1777	5165		2799		2743
6	2445	5419	2465	5182		3640		3541
7	3191	5674	3156	5272		4458		
8	3897	5959	3753	5528		5112		
9	4342	6400	4153	6017		5499		
10	4648	7054	4353	6718	5679			
0	1738		1740		1637		1651	
tooth	5000		4627		1203		1345	

DEEP CORE MACHINES

Fig. 5.3.7

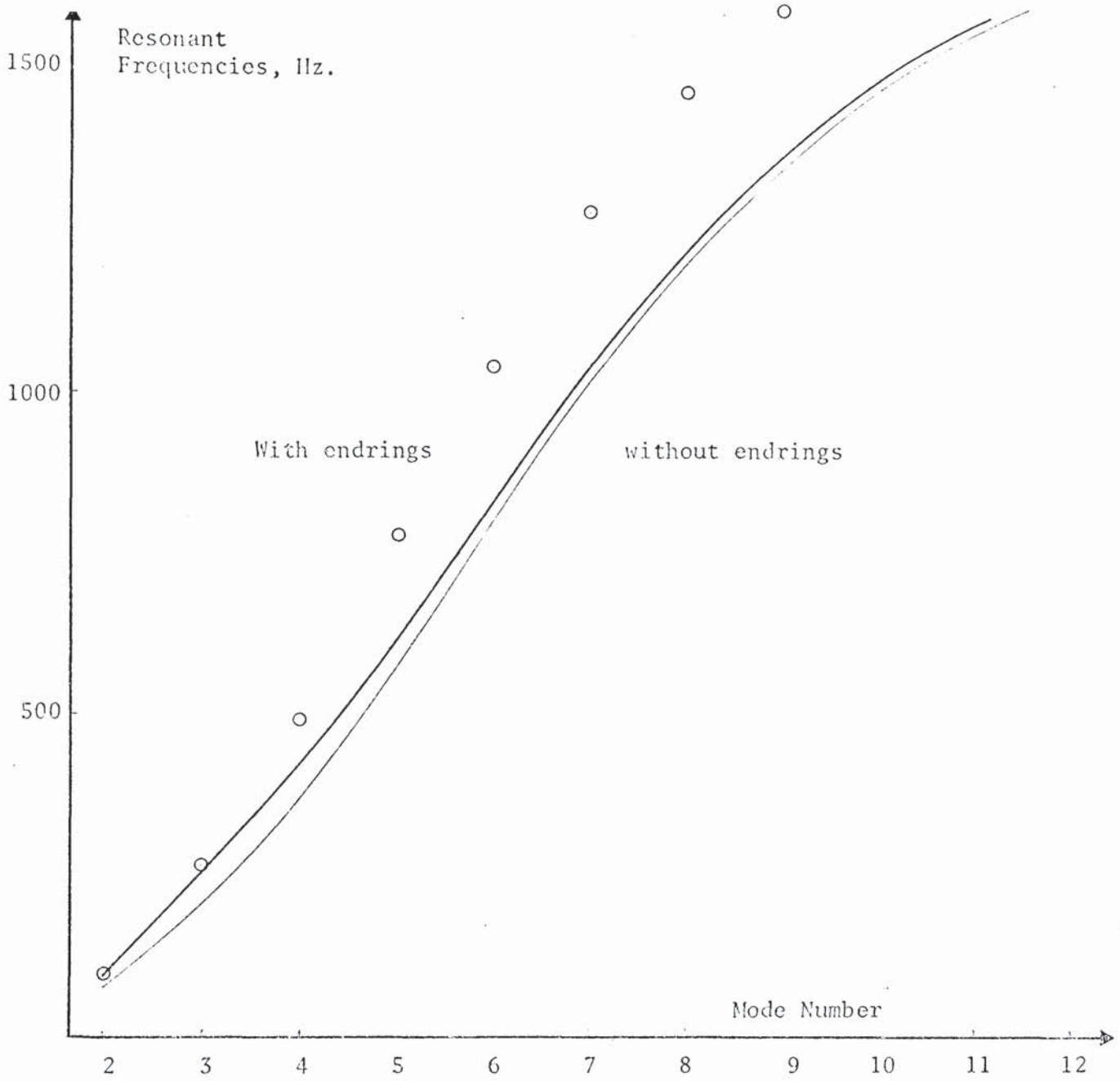

OD = 831.85mm, ID = 772.25mm, GD = 597.63mm, slots 72 x 13.97 mm
endring OD = 832 mm, ID = 745mm, axial length = 2 x 14.35 mm.

Mode	Measurements				Calculations			
	No endrings		With endrings		No endrings		With endrings	
	(b)	(a)	(b)	(a)	(b)	(a)	(b)	(a)
2	74.7	2095	97.6	2100	74.4	2384	97.3	2393
3	201	2184	255	2181	205	2563	268	2587
4	382	2272	418	2267	380	2691	495	2734
5	572	2383	613	2376	590	2788	761	2846
6	801	2522	838	2523	819	2858	1036	2968
7	1008	2709	1032	2710	1047	2965	1279	3203
8	1200	2946	1222	2962	1249	3149	1460	3534
9	1349	3227	1369	3275	1409	3398	1583	3931
10	1463	3609	1488	3640	1525	3697	1663	4364
11	1547	4033	1572	4059	1609	4028	1715	4812
12	1619	4483	1644	4522	1666	4376	1754	5268

Letters in brackets indicate below or above tooth resonant frequency

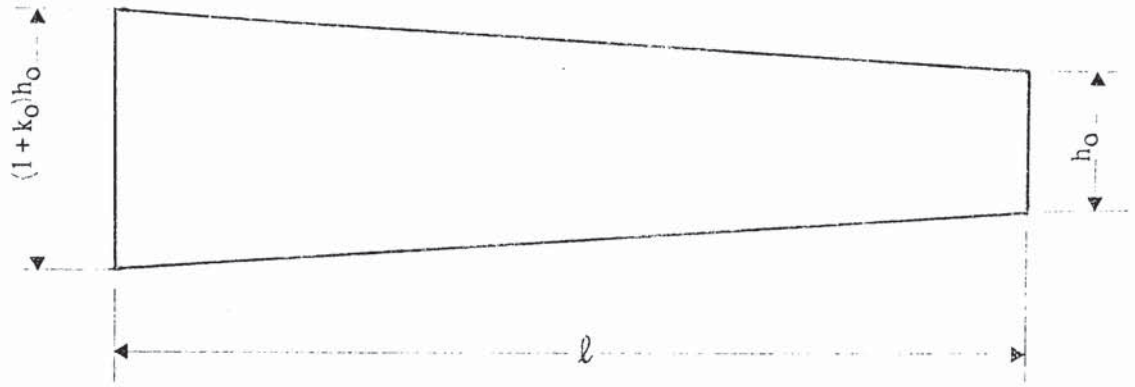

length ℓ,mm	height h_o,mm	taper k_o	shear correction C_s	root correction C_r	meas. Hz	calc. Hz	Comments
43.48	10.76	.302	.919	.817	4600	4680	semiclosed
84	15.69	.311	.950	.853	2005	1987	-
87.31	12.11	.629	.958	.874	1865	1863	-
37	7.96	.203	.945	.840	5000	4627	-
64.26	21.36	-.242	.935	.807	2340	2330	rotor teeth
43.18	12.21	.370	.887	.793	5070	5471	semiclosed
114.3	11.02	1.086	.967	.895	1203	1346	set back grooves
68	12.10	.491	.944	.851	2807	2668	-

TOOTH RESONANT FREQUENCIES

Fig. 5.3.9

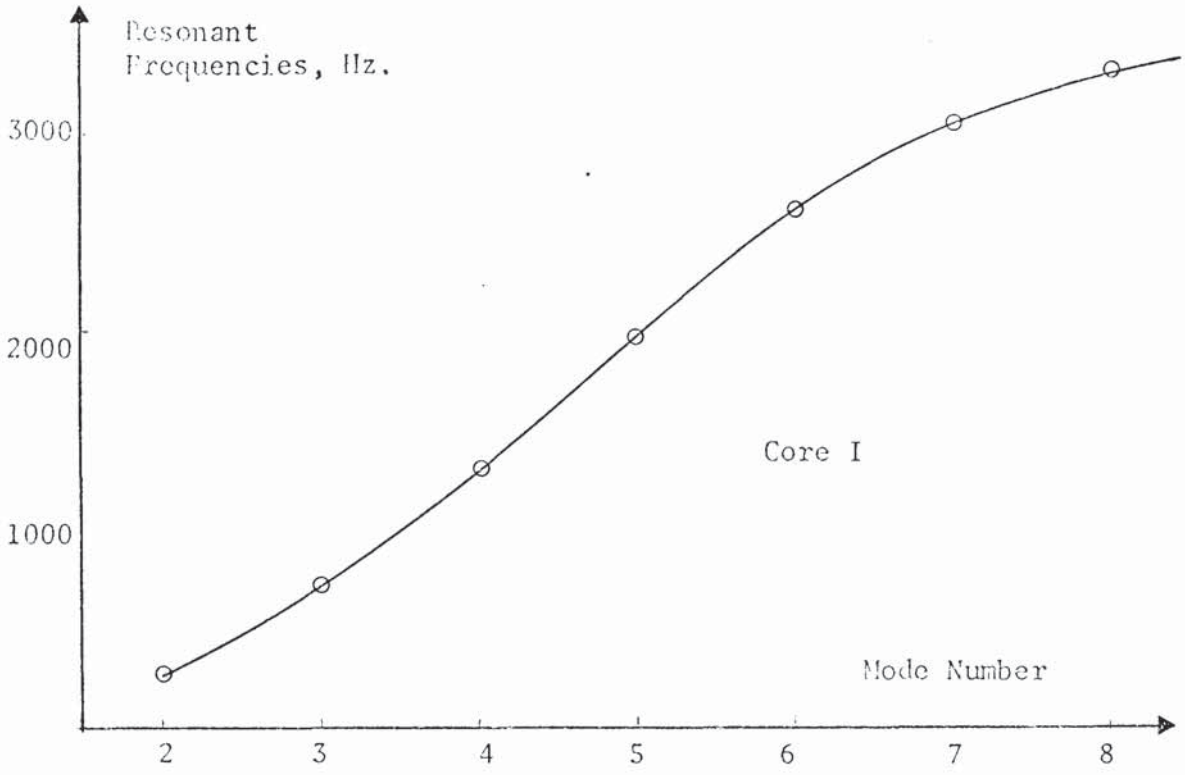

	Core 1	Core 2	Core 3
Outside dia.	473 mm	596.9 mm	596.9 mm
Inside dia.	418.08 mm	525.74 mm	494.6 mm
Airgap dia.	336.5 mm	400.1 mm	374.55 mm
Slots	72x6.17mm*	72x9.2 mm	48x11.96 mm

* parallel teeth, semiclosed slots.

Core No.	Mode	2	3	4	5	6	7	8
1,meas.	b	261	715	1308	1966	2626	3032	3307
	a	4076	4192	4352	4592	5043	5693	6635
1,calc.	b	263	719	1316	1988	2613	3054	3321
	a	4447	4678	4837	4988	5370	6041	6944
2,meas.	b	204	555	995	1467	1894	2164	2340
	a	2945	3024	3163	3384	3795	4356	5120
2,calc.	b	206	560	1016	1507	1918	2176	2315
	a	3015	3169	3276	3446	3817	4406	5128
3,meas.	b	340	906	1592	2306	2944	3315	3458
	a	4321	4481	4733	5084	5610	6433	7472
3,calc.	b	335	900	1607	2343	2929	3274	3444
	a	4197	4356	4449	4611	5053	5796	6722

SMALL MACHINE CORE RESONANT FREQUENCIES

Fig. 5.3.10

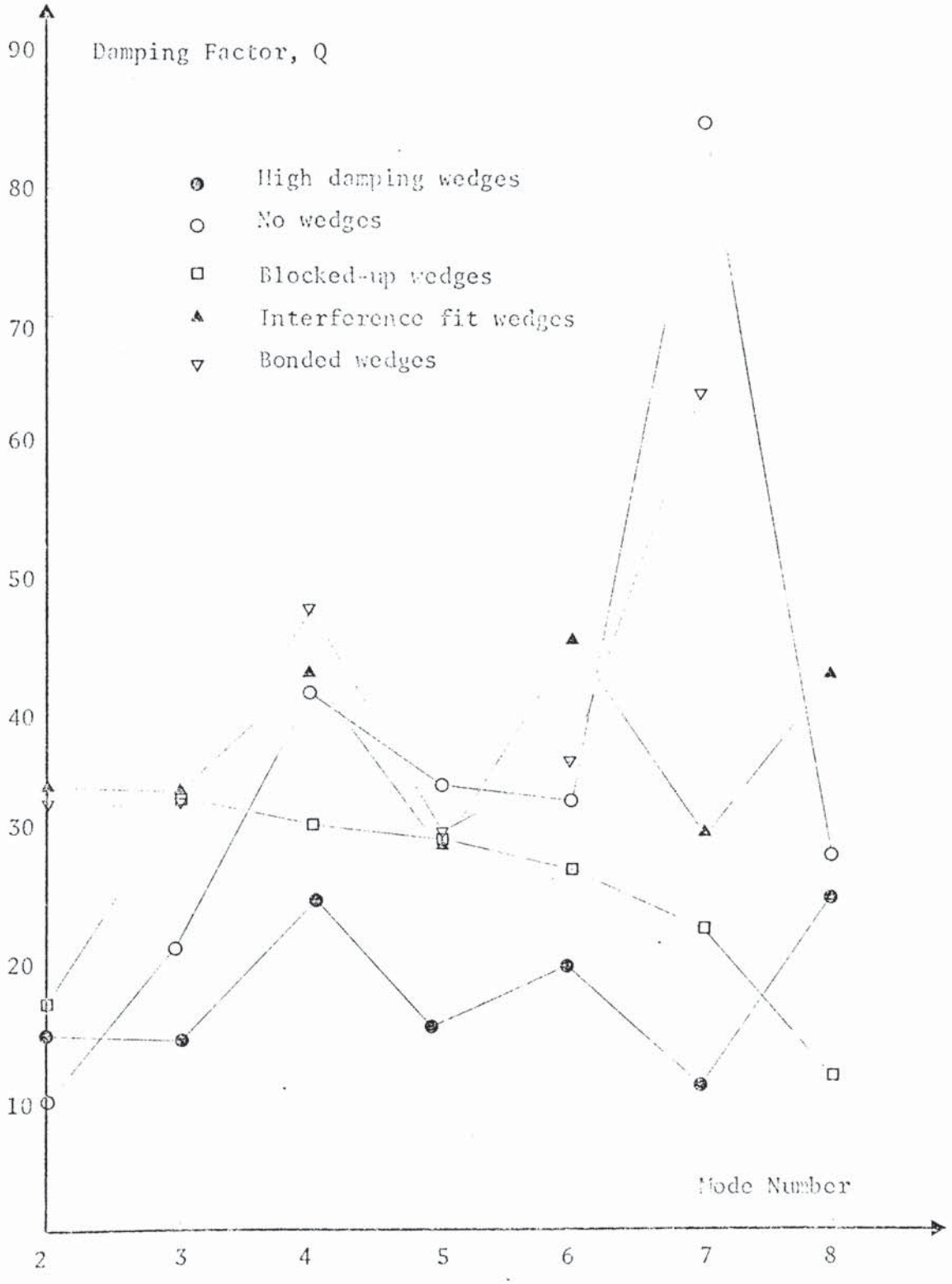

CORE DAMPING WITH DIFFERENT WEDGES

Fig. 5.3.11

CHAPTER VI

MEASUREMENTS OF COMPLETE MACHINE RESONANT FREQUENCIES

The separate effects of different features of electrical machines on stator core resonant frequencies are reported in Chapter 5, in as far as these have been measurable using the short core method. In the present chapter the measurements on complete large machines show the nett effect of all the contributing features. The laminations that formed the basis of the short core measurements were built into a production machine. This was tested at various stages of manufacture including the final test before dispatch. These tests show clearly the effects of frames and windings. Tests on other past noisy production machines are included to illustrate the level of errors produced by the theory of Chapter 4.

6.1 THE INFLUENCE OF STATOR FRAMES

Measurements were given in Section 5.3.5 showing the rapid uncoupling of clamping rings. At low frequencies the clamping rings moved with the main body of laminations and had a full effect in determining resonant frequencies. Above a certain uncoupling frequency the influence of clamping rings was negligible. The same phenomenon was observed with laminations built into a frame. Above the uncoupling frequency complete core and frame assemblies produce resonant frequencies which are very close to those of the laminations alone.

The two principal designs of laminations (Figs.3.3.1 and 5.3.3) were built into the same production frame and tested before the winding was inserted. Resonant frequencies were obtained using a vibrator connected to two adjacent teeth in the centre packet of the machine. The measurements are shown in Fig.6.1.1. With the weak laminations the frame increases resonant frequencies by 100% for the lowest mode and by less than 10% above 600 Hz. It should be remembered that this design of laminations had a very shallow core so that the influence of the frame is exaggerated. The final production laminations have a larger depth of core and the same frame increased the lowest resonant frequency by only 17%. The uncoupling frequency for this configuration is approximately 600 Hz. The other production machine measured resonant frequencies (all $\geq$ 830 Hz) confirm that calculations should be made considering the frame and/or endplates uncoupled. The nature of the slotting of normal induction motors is such that forces likely to produce significant noise have frequencies in excess of 600 Hz. This means that calculated resonant frequencies can be obtained ignoring the frame and endplates.

This generalisation is not true of synchronous machines or special induction machines (such as multi-speed machines) and for these cases the frame etc. must be considered. For resonances below the uncoupling frequency the calculated resonant frequency should be taken between the frequencies obtained ignoring and including the frame etc. The method in which the calculations should transfer from 'with the frame' to 'without the frame' must be determined from further measurements on production machines. Although the uncoupling frequency has been

approximately 600 Hz for the three sets of measurements quoted it is probable that different frame constructions will have different values. For large machines with skeleton frames the frame is best approximated to two clamping rings for calculation purposes.

During the measurements using the production frame it was found that there were a number of resonant frequencies for each mode depending on the circumferential position of the vibrator. This effect was more pronounced with the weak laminations. The varying stiffness of the main members of the frame produces a number of resonant frequencies for any mode depending on the position of the antinodes of the vibrating force. This effect is only noticeable at frequencies below the frame uncoupling frequency. An unusual example of this multiplicity of resonant frequencies was exhibited by a particular slow speed fractional-slot induction motor. A winding sub-harmonic produced a large vibration amplitude at 120 Hz. The resulting vibration was stationary although the force was rotating in space. This occurs when a given mode of vibration has different resonant frequencies for different circumferential positions of the modal shape - as can occur with frames of electrical machines. In this example the frame influence was obviously large since the measured resonant frequency and the calculated resonant frequency of the laminations alone were 129 Hz and 96.3 Hz respectively.

The measurements in Fig.6.1.1 underline the effect of duct spacers measured in Section 5.3.3. For both machines the resonant frequencies

are asymptotic to a lower tooth resonant frequency when spacers are used. In both series of measurements with frames the resonant frequencies were difficult to isolate, especially compared with the ease of making short core measurements.

6.2 THE EFFECTS OF WINDINGS

After the tests with the production laminations in the frame the machine was wound with a 6.6 kV, 8 pole, double layer consolidated winding. The total mass of the winding was 323 kg, of which 52% was embedded in the slots. The slot wedges were nominally 2 mm deep. Measurements of resonant frequencies were made, after the machine had been wound, using a vibrator attached to the inside of the core.

The results of this test were slightly ambiguous. A full set of resonant frequencies was measured below the corresponding values without a winding. In addition a number of resonant frequencies were measured that were very close to those without a winding. This second set was incomplete and unexpected. These measurements are shown in Fig.6.2.1 together with the calculated values including the winding and wedges but ignoring the frame. In these calculations the full winding mass has been used. Both the measurements and the calculations show a reduction in the region of 13% at low mode numbers due to the mass of the winding and a slightly increased tooth resonant frequency due to the wedges which offsets the reduction caused by the duct spacers. The ambiguity was further underlined by live-machine measurements which produced resonant frequencies which were virtually the same as those without a winding. It appears that it is possible to excite two resonances for each mode,

one in which the winding moves and one where the winding is stationary. With the complete machine excited using a vibrator the lower resonant frequencies are excited, although a limited number of the other resonances were also excited. With the machine excited electromagnetically the higher resonant frequencies only are excited. The difference between the two types of excitation is that one is stationary and the other rotates in space. It is assumed that the winding is unable to 'follow' the vibrations when the force wave rotates and so the machine behaves as though the winding was absent. This explains why the calculations without a winding give the best correlation with live-machine measurements. The zero order force wave does not rotate by definition so that calculations with the winding mass give the best correlation with live measurements for this mode of vibration.

Live measurements on two very different large machines are reported in Section 6.4. In one the zero order resonant frequency is measured and in the other a radial bending mode resonant frequency is measured. For these two machines the best correlation with measurements is obtained by calculations including the winding for the zero order mode, and excluding the winding for the radial bending mode.

These conclusions about the influence of the winding on resonant frequencies apply to large machines and may not apply to small machines. The reality of the influence of windings in small machines will be revealed only in live-machine measurements. Almost all of the measurements given by the various authors have been vibrator excited. It has always been assumed that windings add mass and lower resonant frequencies. The measurements referred to above are consistent and

reasonably conclusive that this is not so for radial bending modes, but true for the zero order (breathing) mode only.

6.3 THE LIVE-MACHINE METHOD OF MEASURING RESONANT FREQUENCIES

It is well recognised that the only definitive measurements of core resonant frequencies are those made on complete machines which are energised and rotating, and that regular measurements are very desirable. In the past, occasional measurements of this sort have been made by analysing the noise spectra emitted from machines. To make these measurements requires additional tests and can often only be justified when a machine fails to meet its noise specification and remedial work has to be done.

A number of useful measurements have been made using this technique and these are reported in Section 6.4 together with some of the dangers inherent in the methods used.

The technique of noise spectral analysis has two disadvantages which make it unsuitable for routine testing to obtain resonant frequencies. Noise analysis is only suitable for machines which produce electromagnetically generated noise levels well above background levels. This means that a machine may excite a number of resonant frequencies during such a test but none of them at a sufficient level to be measurable. The other important disadvantage is that a separate test is required which often has to be carried out at an unusual hour to minimise background noise. Most manufacturers are very hard pressed to meet delivery dates by the time a machine gets to the test department and 'inessential' tests are very difficult to implement.

A test technique has been used which is based on core vibration measurements and can be incorporated into an existing standard test so that testing time is not increased. The use of vibration rather than sound measurements means that minor vibration peaks can be isolated. It also means that background noise levels are unimportant.

6.3.1 The Test Method

The test involves supplying the machine with a varying supply frequency and making back of core vibration measurements. In order to minimise the test time and enable the use of digital signal analysis, the vibration signals are recorded with an F.M. instrument tape recorder.

One of the first tests the complete machine undergoes is the bearing test. The machine is run for approximately two hours to bed the bearings. The resonance test is carried out during this time. Unusual windage or bearing noises that sometimes occur during this test are of no consequence since only vibrations are being measured.

The supply frequency is varied between the minimum set by the supply alternator speed-control and the test machine overspeed capabilities. At each frequency the voltage is adjusted so that the quotient of supply frequency and voltage is constant and equal to the rated voltage divided by the rated frequency. This is done to keep the flux levels constant. One or more piezoelectric accelerometers are attached to the back of the core using a tripod magnet. A high speed recording of approximately 10 seconds duration is made of the accelerometer outputs, suitably amplified, at each frequency. A number of accelerometers may be used to check on

modal shapes but it has been found that the electromagnetics of machines (and particularly induction machines) are such that each frequency of vibration is associated with a unique mode number. It is usually necessary to have only one accelerometer. Analysis of the accelerometer signals can be greatly facilitated by recording a reference signal on the tape before and after the main body of measurements. This is done with all of the amplifier and tape recorder settings as per the main series of measurements and with the accelerometers attached to a calibrated vibration table.

Each measurement is analysed by replaying the recordings, usually at a reduced speed, and digitising the accelerometer signals using an A/D convertor. Digital Fourier transforms of the signals, plotted automatically, condense and abstract the information into a manageable form. From these plots it is relatively easy to obtain the amplitudes of the different components of acceleration and to plot a response curve for those components that span a resonance. Having a reference signal on the tape means that each transform can be scaled easily before plotting. It also means that measurements can be stored in a self contained format with no need to attach notes and labels regarding calibration factors etc. This is an important advantage if the test is to be carried out by personnel who are not familiar with the parameters being measured.

It is useful to monitor accelerometer signals using an oscilloscope so that obvious peaks in one component can be recorded using a finer variation of the supply frequency. It is important to note, however, that some resonance peaks will not be obvious from the oscilloscope and

a full range of measurements should always be made. It is to be expected that most resonances measured in this way will not be associated with a discernable noise peak. In the measurements reported in the next section only one of the nine measured resonant frequencies was associated with an obvious noise peak.

6.3.2 An Example of the Test Technique

The production machine used throughout this research was designed with a 58 slot rotor. This machine was tested in its production form using the technique described. It was also tested with a 60 slot rotor which was designed especially for this research to produce a very high noise level caused by the near coincidence of a major force wave and the corresponding resonant frequency. The tests described are more detailed than that proposed in the previous section since these were prototype tests. The tests with the two rotors were duplicates so that the results only of the test for the 58 slot design are given. It is significant that this 'quiet' machine produced five of the nine resonant frequencies measured in these tests.

The 60 slot rotor machine produced a large mode 4 force at 850 Hz when supplied at 50 Hz. This produced a large level of vibration and high sound pressure levels (SPL) - 120 dB at the core surface. Measurements were made to determine the axial variations in the mode of vibration. It was found that these measurements could be analysed using a voltmeter instead of the digital analysis because of the predominance of this vibration component. The axial variations in vibration amplitudes were small and confined to the end packets. This

confirms the conclusion in Section 6.1 that above approximately 600 Hz the frame is uncoupled.

In the measurements two accelerometers were used together with two precision microphones. The accelerometers were calibrated using a reference table vibrating at 250 Hz and 9.81 m/sec^2 (peak). The microphones were calibrated using a Pistonphone. They were fixed near to the core in a radial position and used to compare vibration and sound pressure levels.

Measurements were made at supply frequencies varying between 34 Hz and 60 Hz in steps of 2 Hz using a four channel tape recorder. Some of the signal levels were such as to require changes of sensitivity. These were achieved using precision range switches (built into the tape recorder) and the voice channel of the recorder to note them. The adjustment of the supply between each set of measurements was very straightforward. The frequencies were set only approximately and the requirement concerning the supply frequency/voltage quotient was automatically met by leaving the supply alternator excitation constant.

Measurements were also made at constant frequency (50 Hz) and varying supply voltage to study the effects of saturation harmonic flux densities. Background and windage noise levels were measured with the machine stationary and rotating at the rated speed and de-energised.

The signal analysis was carried out using a suite of programs developed for a mini-computer at the University of Aston in Birmingham

by C.S.Sunnersjö. Each Fourier transform was made using a 1024 point sample with the tape-relay speed and the A/D convertor sampling rate adjusted to give a real time sampling frequency of 10 kHz. This produced an upper frequency-resolution limit of 5 kHz. In order to improve the selectivity of the transforms the samples were pre-processed with a Hanning window.

Typical Fourier transforms (FTs) are shown in Fig.6.3.1. These two measurements were made with the supply frequency equal to 44 Hz and 48 Hz and show how the various component accelerations vary with proximity to the corresponding resonant frequency. Resonant frequencies were obtained from the whole family of FTs by plotting component amplitudes as functions of frequency. The resulting curves for the mode 4 resonant frequency are given in Fig.6.3.2. For this machine there are two significant mode 4 force waves with frequencies of $\doteqdot$ 17 x supply and $\doteqdot$ 19 x supply. Both forces excite this resonance when the supply is varied from 36 Hz to 60 Hz. In each case a smooth curve results and the resonant frequency is easily deduced. In addition to the predominant mode 4 vibrations three other components pass through resonances. These are the zero order, mode 4, and 8 above the tooth resonant frequency. Each of these is marked in Fig.6.3.1 together with the associated resonant frequencies. No measurements have previously been published which show machines exciting modes above the tooth resonant frequency.

The FTs for the production rotor (58 slots) contain large numbers of components of vibration, five of which passed through the associated resonant frequencies. The values of the resonant frequencies measured

in this way are given in Fig.6.2.1. The FTs for 44 Hz and 50 Hz supply are shown in Fig.6.3.3. When the microphone signals were analysed it became clear that the sound pressure measurements produced signals containing a lot of extraneous information which obscured the components of interest. Also, some of the components of vibration were inefficient radiators of sound so that these were not discernable at all. Vibration modes 2, 8, 9 and 10 (Fig.6.3.3.) give unreliably small sound pressure levels. The complete noise spectrum at 50 Hz is shown in Fig.6.3.4 together with the bearing and windage noise (machine at full speed but de-energised) and the background noise. The windage and background measurements were made at the end of the measurements so that comparisons must be made with caution. The superiority of vibration measurements over sound pressure measurements for obtaining core resonant frequencies is obvious.

In addition to the measurements of resonant frequencies it was also possible to glean important information about certain flux densities. From Fig.6.3.2 it is clear that the magnitude of the second mode 4 force is 5.50% of the main force. The fluxes that produce these two forces (one at 850 Hz and the other at 950 Hz) are listed in Fig.6.3.5. The rotor slot harmonic flux density produced by a first order stator slot harmonic is common to both forces so that the ratio of the other pair of fluxes should equal 5.5%. This means that the saturation harmonic should be 5.5% of the fundamental flux density. The fundamental is known accurately so these results give an indirect measurement of the saturation harmonic flux density. There are two saturation based forces that add vectorially to produce the mode 4, 950 Hz force. Using

the noise analysis program mentioned in Chapters I and 2 the calculated ratio of the two forces is 4.9%. This compares favourably with the measured value of 5.5% and establishes the accuracy of the saturation flux harmonics calculation.

From the resonance peak of the mode 4 vibration (Fig.6.3.2) it is possible to deduce the damping factor Q and use this to find the core deflection at zero frequency. This gives a deflection of 1.25μm for the 850 Hz vibration component. Static core deflections are calculated using beam theory and previously obtained flux densities. If the beam theory part of this calculation can be considered accurate then the calculated and measured static deflections give a direct measure of the accuracy of the flux densities. The static deflection calculated by the noise analysis program is 1.16 μm. This calculation involves directly a mutual rotor slot harmonic and the good agreement confirms the values given in Chapter 2.

The origins of the various important component vibrations produced by the 58 slot rotor (Fig.6.3.3) are given in Fig.6.3.5. This list serves to show that some of the more 'exotic' flux densities can be significant. Saturation, eccentricity and the slotting harmonics feature in a large proportion of these components. There has been a tendency in the past to ignore such effects.

6.4 OTHER PRODUCTION MACHINE MEASUREMENTS

The following accounts apply to large machines tested live in a manufacturers works. The accepted[15] method for measuring pure tone noise components is to use a precision microphone coupled through a high selectivity filter to a direct reading sound pressure level meter. Test equipment of this type is available commercially. With the microphone fixed in one position the machine supply frequency is varied as much as possible and components of interest in the noise spectrum traced and measured (usually in units of dB). This technique was used in the following measurements as that proposed in Section 6.3 had not then been adopted as the preferred method.

6.4.1 A 12 Pole Synchronous Motor

This machine was tested at full voltage (6.6 kV) uncoupled and with the excitation winding current adjusted to the calculated full load value. The machine emitted a pure tone noise at 1000 Hz when the supply frequency was 50 Hz. The noise peak varied as shown in Fig. 6.4.1 when the supply was varied between 46 Hz and 60 Hz. The shape of this curve is somewhat unsatisfactory and results from the interference caused by standing waves. The machine was tested with a moderate amount of test equipment near the machine which produced reflections and thereby complicated the noise field. Despite these complications the resonant frequency was easily discernable and equal to 1091 Hz. The irregularities in Fig. 6.4.1 could have been removed by making a large number of measurements at each speed and averaging the results. With ad-hoc measurements such as these the time available prohibits such detail.

The calculated resonant frequency excluding the winding mass is 1136 Hz. (4.12% high). In this calculation the nominal wedge dimensions have been used and an average wedge fit factor assumed. The calculation was repeated including the winding mass to check the conclusion in Section 6.2 that live machine resonances (apart from the zero mode) are best calculated with the winding mass excluded. Including the winding mass produced an error of -9.26% in the calculated value (990 Hz). The smaller error confirms the conclusion drawn.

6.4.2 A 48 Pole Synchronous Motor

The tests on this machine were carried out with the machine acting as a short circuited generator. It was during other tests under these conditions that the pure tone noise component was most noticeable. Back of core vibration measurements were made to discern the modal shape of the displacement causing the noise. These confirmed that a zero order force wave created by a high order saliency harmonic was giving rise to the 600 Hz noise. Variable speed measurements produced the displacement curve shown in Fig. 6.4.2. The secondary peak at 540 Hz observed using noise measurements only had been mistaken for the resonant frequency. The measured resonant frequency obtained from the complete sweep of frequencies using vibration measurements is 307 Hz. This value is well below the frame uncoupling frequency and it is to be expected that the frame influence will be significant. The calculated resonant frequency ignoring the frame but <u>including</u> the winding is 280.4 Hz, which indicates that the frame is indeed coupled and adds stiffness to the core. It seems reasonable also to assume that the non uniformity of the frame gives rise to the two secondary peaks in Fig. 6.4.2 - the flux levels were kept constant throughout this test.

The initial erroneous conclusions drawn about this machine and the distortion of measurements caused by standing waves, as illustrated by Fig. 6.4.1, underline the inefficiency of the sound pressure measurements in determining resonant frequencies. In addition to these problems a microphone in a fixed position is likely to be phased differently, relative to the peaks in the sound pressure waves, as the frequency is varied. This has the effect of modulating the measured sound pressure levels.

6.5 A NOISE PROBLEM CIRCUMVENTED

Routine noise calculations on a synchronous motor indicated a possible source of noise caused by a very high order saliency harmonic. The then current method for calculating resonant frequencies showed a reasonable margin between the forcing frequency and the corresponding core resonant frequency, especially considering the etherial nature of the noise source. The theoretical work described in Chapter 4 was nearly complete as this machine was starting manufacture and new calculations were carried out. The calculated resonant frequency for this mode was 1507.9 Hz, with the winding and wedges ignored. The laminations had been made, unfortunately, but not built into the machine frame. It was decided to measure the core resonant frequencies in the factory using the short core method. The measured and calculated resonant frequencies for a large number of modes are shown in Fig.6.5.1. The measured mode 18 resonant frequency was 1506 Hz. The correspondence between the calculated and measured resonant frequencies provided convincing evidence that the new theory was reliable and a way of overcoming the problem was sought using the theory as the main aid.

Three possible solutions were considered.

(1) Increasing the resonant frequencies by using thick bonded wedges produced a calculated change of +27.1%. This approach was favoured by the author since it required no modifications to the laminations, with the consequential loss of time and electrical performance. Also, it would have provided eloquent proof of the influence of wedges, which have previously been ignored.

(2) Reducing the resonant frequencies by removing 12.5 mm from the bottom of the slots gave a change of -20% for mode 18.

(3) Removing the same amount from the back of the core gave a reduction of 9.4%.

The first solution was ruled out mainly because the bonding of wedges makes subsequent winding repairs almost impossible - should they be necessary. The third solution was preferred as the press operations needed no special dies and considerably less time, and therefore money.

The profile of the modified laminations is given in Fig. 6.5.2. A short core was constructed using these laminations and the resonant frequencies measured - see Fig. 6.5.1. The expected reduction was only partly achieved. The mode 18 measured and calculated resonant frequencies were 1421 Hz and 1365 Hz respectively - an error of -3.9%. The laminations were built into the frame and the resonant

frequencies were measured again before the winding was inserted. These measurements show clearly the uncoupling phenomenon discussed in Section 6.1. For mode 18 the frame influence is very small. The resonant frequency was 1462 Hz.

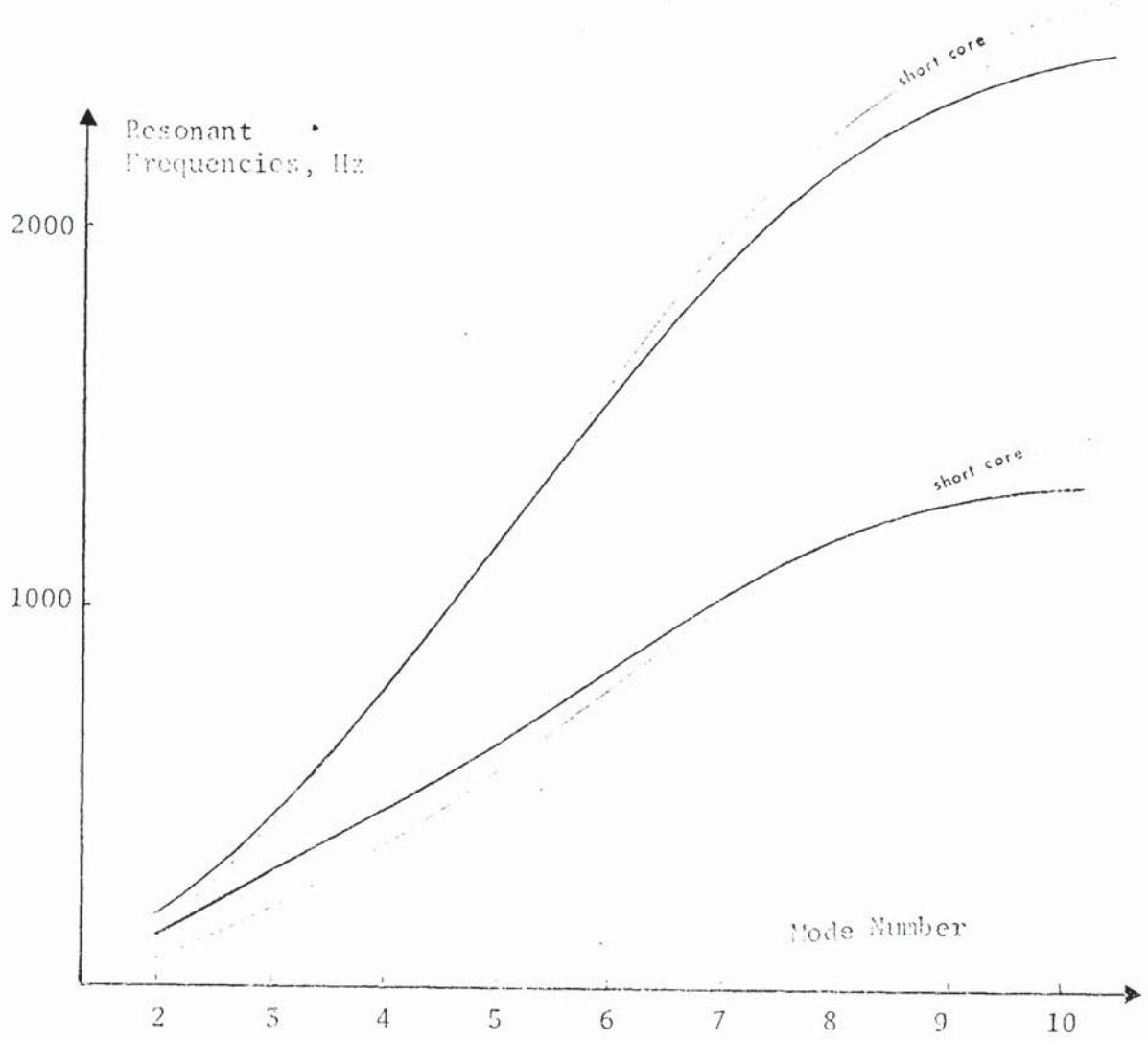

Measurements

Mode	short core	in frame	short core	in frame
2	74.7	143.3	152.9	178.7
3	200.8	312.5	443.3	456.9
4	382.4	467.4	805.8	789
5	571.9	639.2	1205	1188
6	800.8	833	1614	1575
7	1008	1042	2012	1920
8	1200	1187	2281	2198
9	1349	1282	2461	2350
10	1463	1338	2581	2455
0	1349	1460	1646	

See Figs. 3.3.1 and 5.3.3 for dimensions

THE INFLUENCE OF FRAMES ON RESONANT FREQUENCIES

Fig. 6.1.1

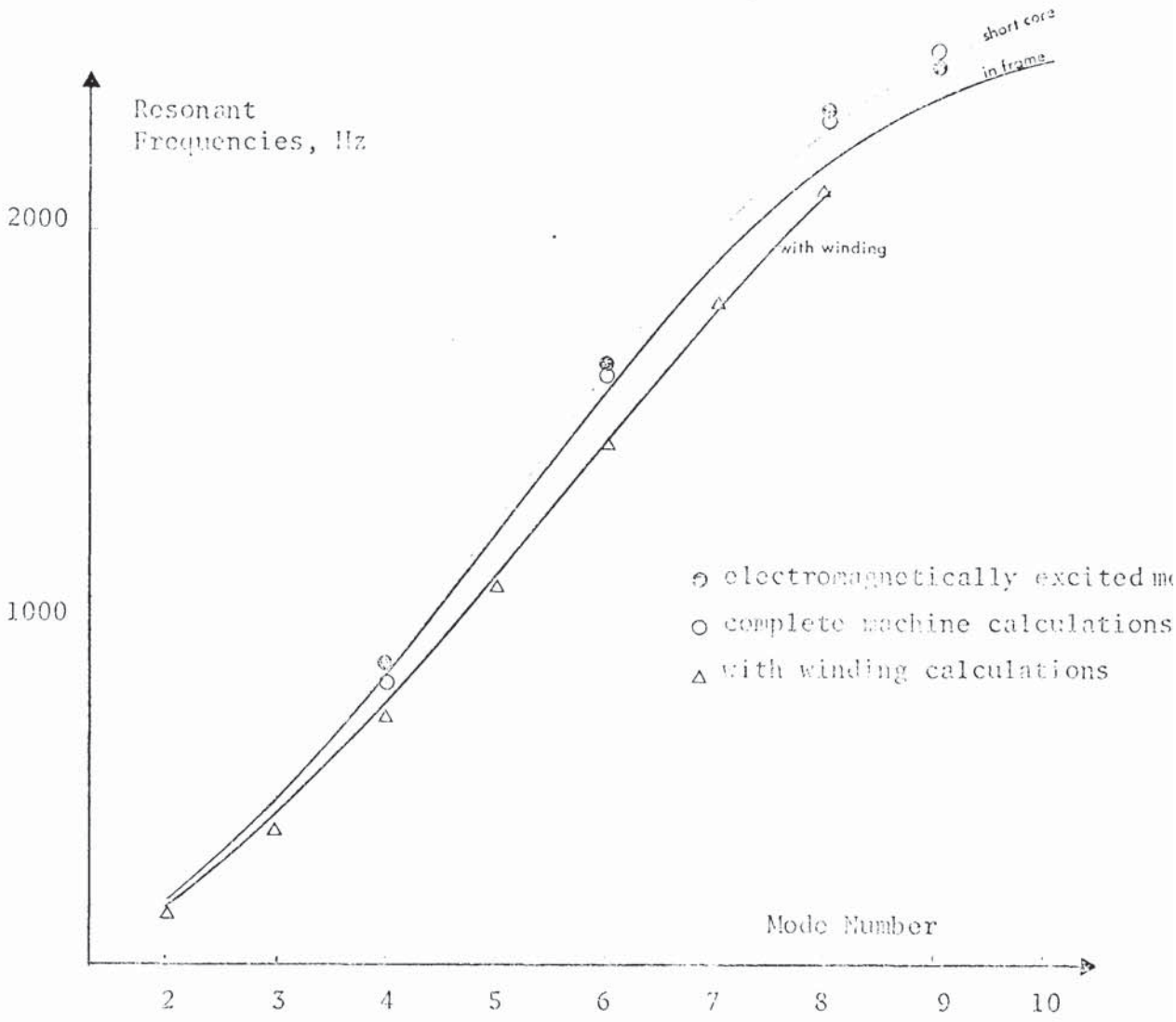

Mode	Measurements				Calculations *			
	short core	live machine	short core	in frame	with wdg.	live machine	with wdg.	without wdg.
	a	a	b	b	b	b	b	b
2	2955	2700	153	179	168/177		132	151
3	3085		443	457	411/455		362	414
4	3192	3210	806	789	720	830	669	765
5	3318		1205	1188	1065		1032	1177
6	3512	3520	1614	1575	1428	1640	1424	1610
7	3817		2012	1920	1815		1805	2002
8	4260	4200	2281	2198	2105	2310	2125	2291
9	4811		2461	2350		2450	2352	2479
10	5535		2581	2455			2501	2586
0			1646		1428	1450	1390	1592

* wedge fit factor 0.05, spacer & winding mass 323 kg & 60 kg, core length 543mm

RESONANT FREQUENCIES OF THE COMPLETE MACHINE

Fig. 6.2.1

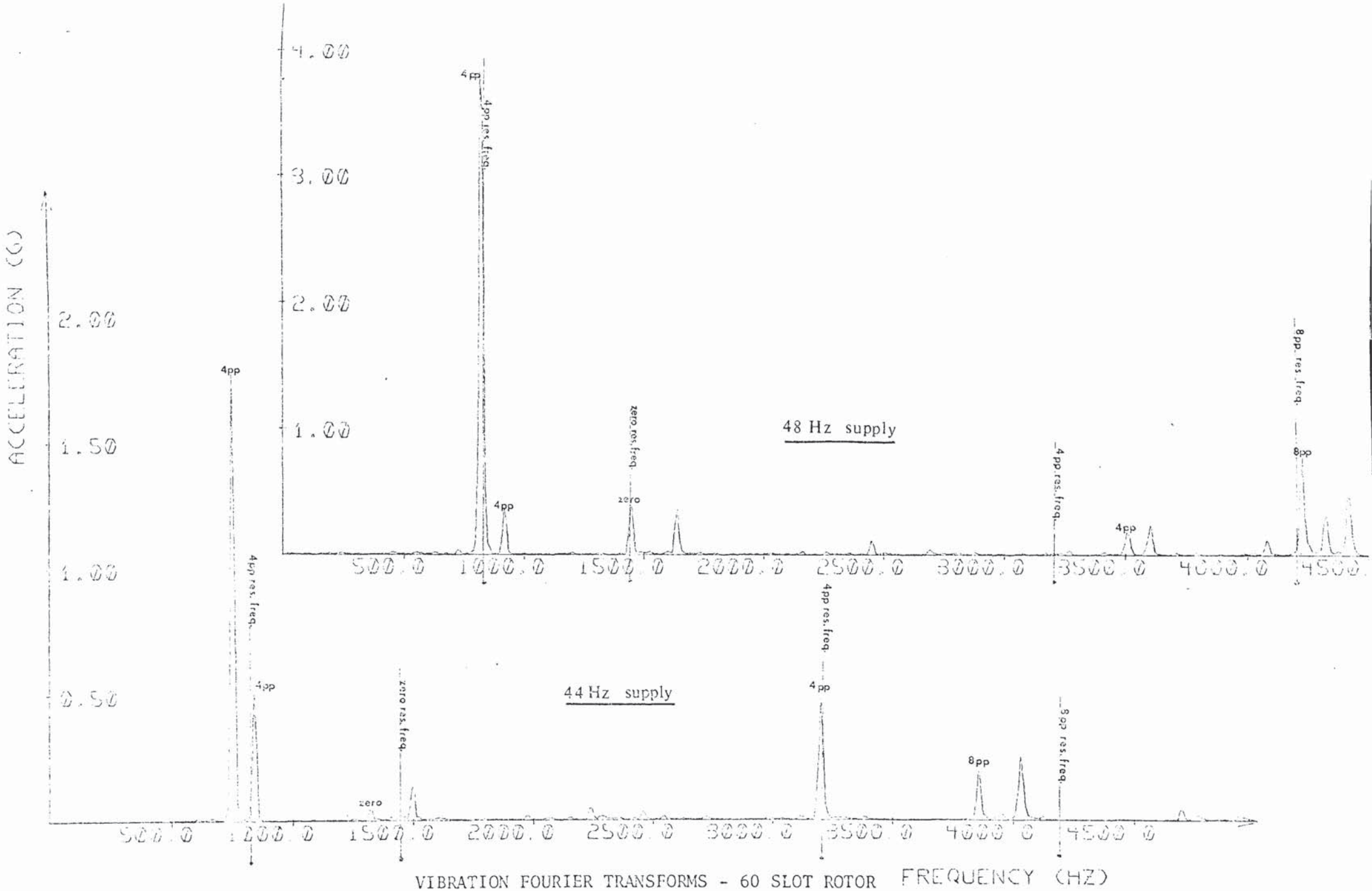
ACCELERATION (G)
4.00
3.00
2.00
1.00
2.00
1.50
1.00
0.50
4pp
zero
8pp
4pp res.freq.
zero res.freq.
8pp res.freq.
48 Hz supply
44 Hz supply
500.0
1000.0
1500.0
2000.0
2500.0
3000.0
3500.0
4000.0
4500.0
VIBRATION FOURIER TRANSFORMS - 60 SLOT ROTOR
FREQUENCY (HZ)

Fig. 6.3.1

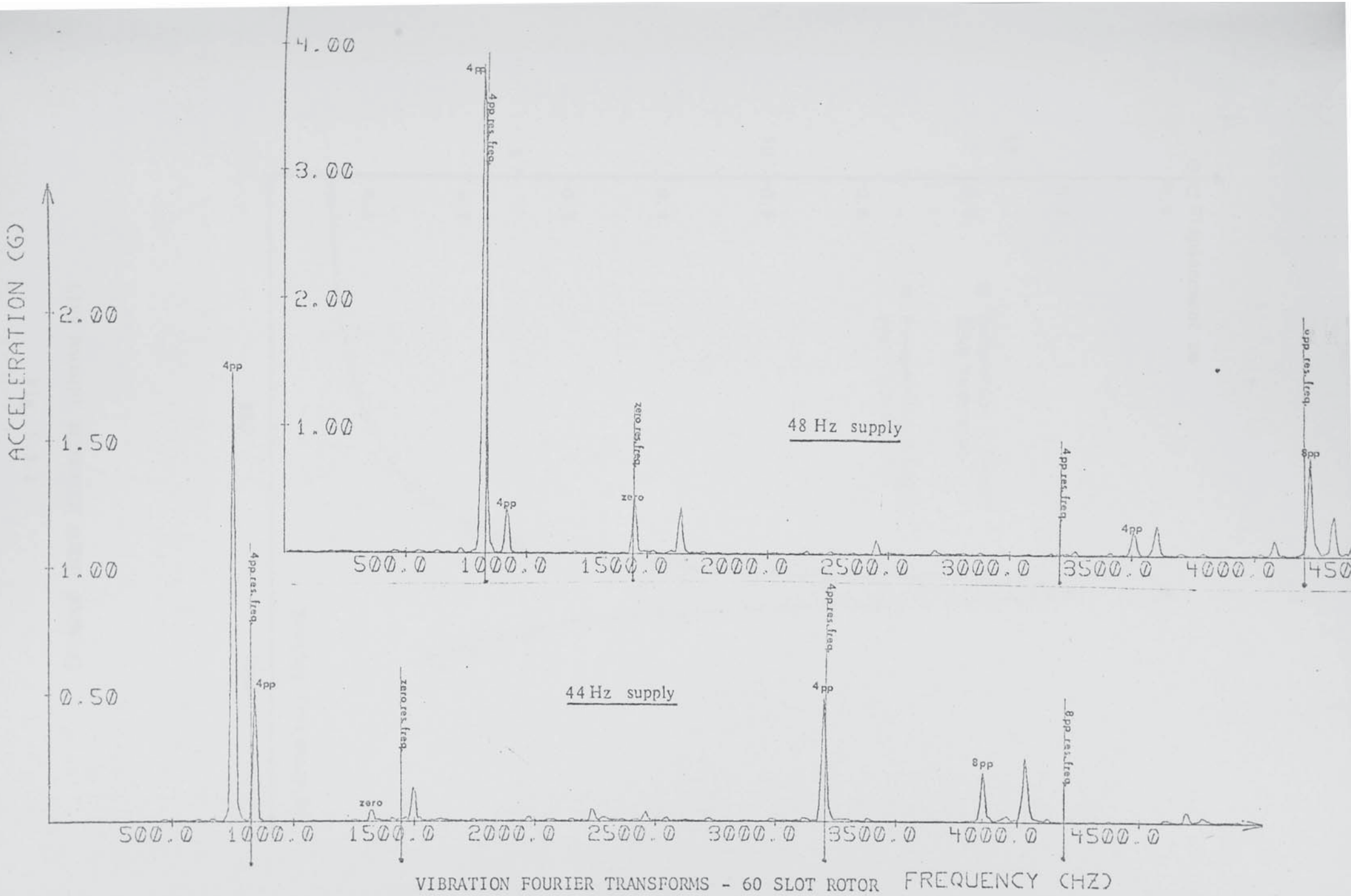
ACCELERATION (G)
4.00
3.00
2.00
1.50
1.00
0.50
4pp
4pp res. freq.
zero
zero res. freq.
8pp
8pp res. freq.
48 Hz supply
44 Hz supply
500.0
1000.0
1500.0
2000.0
2500.0
3000.0
3500.0
4000.0
4500.0
VIBRATION FOURIER TRANSFORMS - 60 SLOT ROTOR
FREQUENCY (HZ)

Fig. 6.3.1

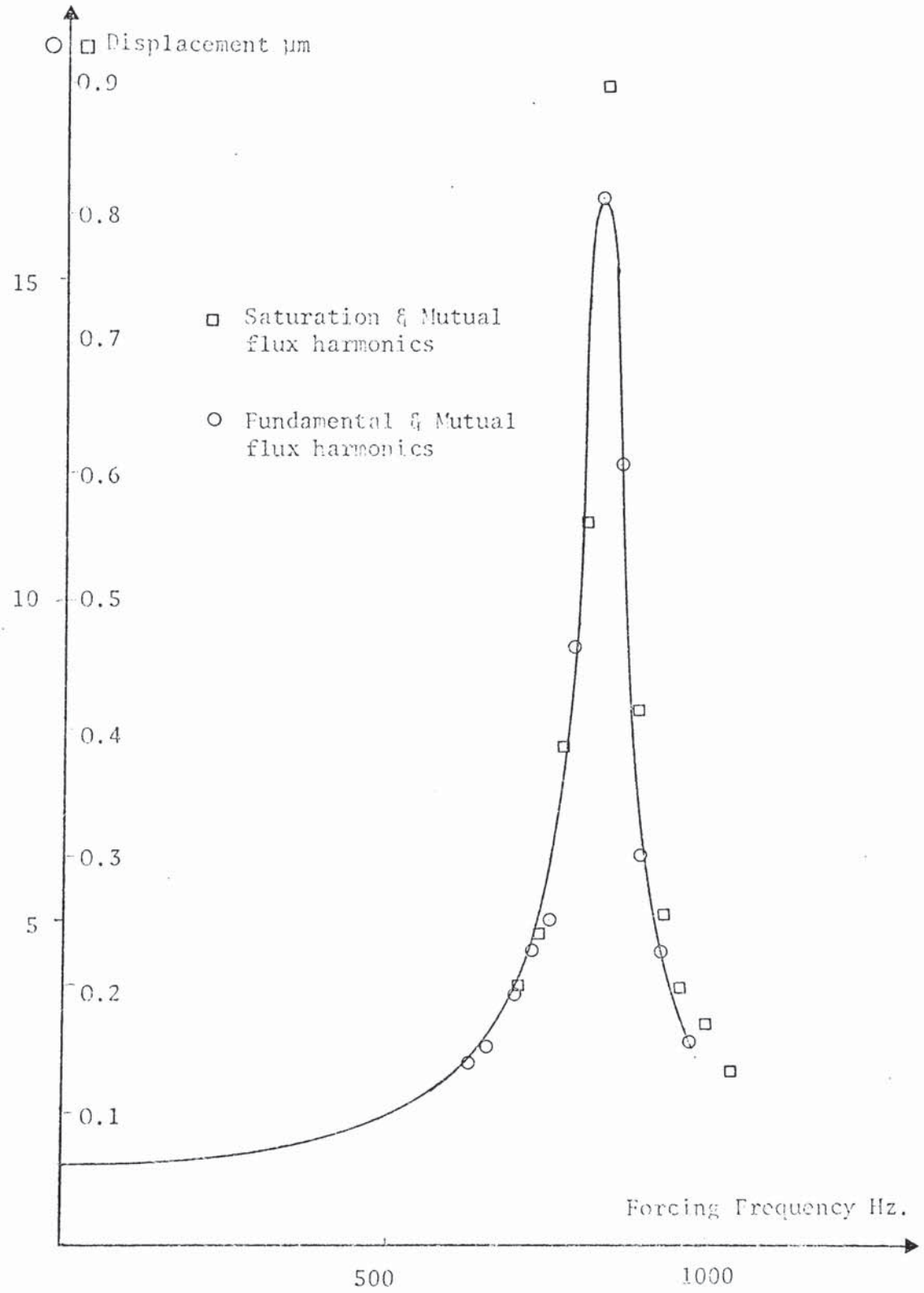

LIVE MACHINE RESONANCE CURVE (MODE 4)

Fig. 6.3.2

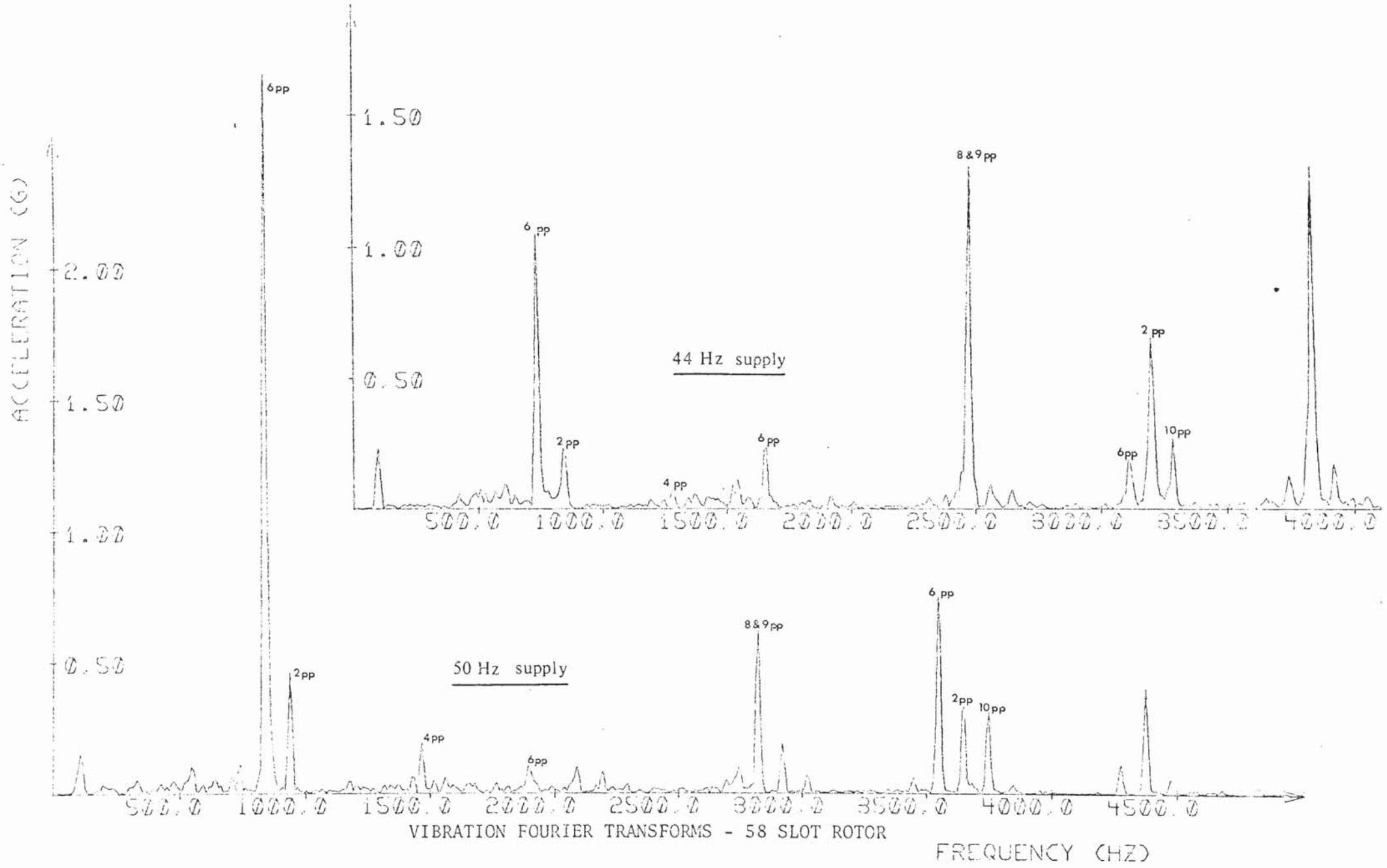
ACCELERATION (G)
2.00
1.50
1.00
0.50
6pp
2pp
4pp
6pp
8&9pp
10pp
50 Hz supply
1.50
1.00
0.50
6pp
2pp
4pp
6pp
8&9pp
2pp
6pp
10pp
44 Hz supply
500.0
1000.0
1500.0
2000.0
2500.0
3000.0
3500.0
4000.0
4500.0
VIBRATION FOURIER TRANSFORMS - 58 SLOT ROTOR
FREQUENCY (HZ)

Fig. 6.3.3

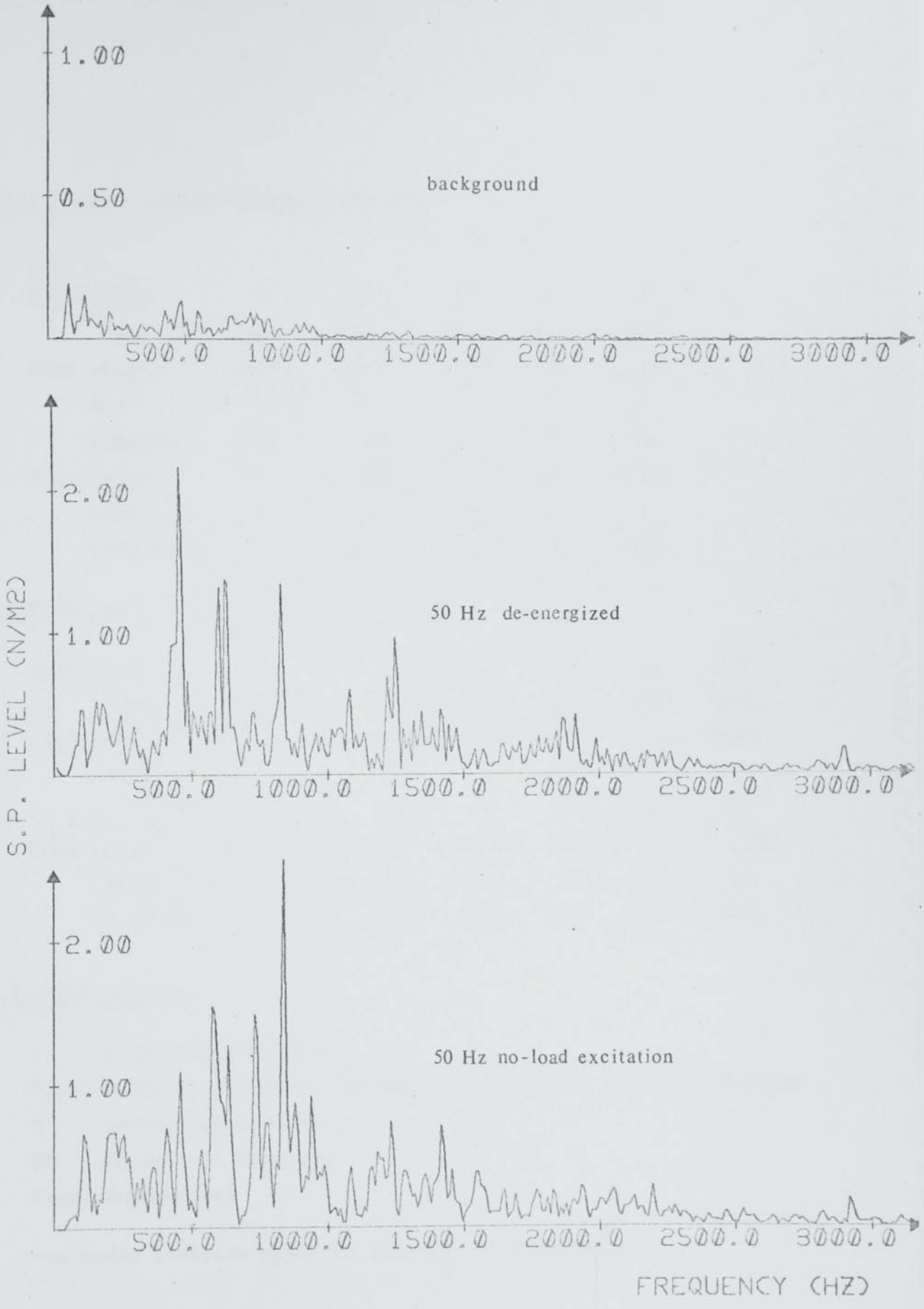

SOUND PRESSURE LEVELS - 58 SLOT ROTOR

Fig. 6.3.4

60 SLOT DESIGN - 50 Hz supply, zero slip

Force mode	0	4	4	4	8
freq. Hz	1500	850	950	3650	4400
Flux origin	R/2SS	Fund.	R/1SS	Funf.	R/1SS
mode	-20	4	-8	4	-16
freq.Hz	1550	50	800	50	700
Flux origin	PB	R/1SS	S	R/4SS	R/4SS
mode	-20	-8	12	8	8
freq.Hz	50	800	150	3700	3700

58 SLOT DESIGN - 50 Hz supply, zero slip

Force mode	2	6	6	6	8	9	10
freq.Hz	3625	825	1875	3525	2800	2800	3725
Flux origin	Fund	Fund	R/2SS	Fund	Fund	R/2SS	Fund
mode	4	4	26	4	4	12	4
freq.Hz	50	50	2125	50	50	2850	50
Flux origin	R/4SS	R/1SS	S	R/4SS	R/3SS	E	R/4SS
mode	6	-10	20	-2	12	3	6
freq.Hz	3675	775	250	3575	2850	50	3675

Key to flux origins

E Eccentricity harmonic

R/4SS Rotor slot harmonic produced by 4th order stator slot harm.

S Saturation harmonic

PB Phase belt harmonic

Fund. Fundamental

-ve modes indicate opposite rotation to fundamental

ORIGINS OF THE VARIOUS VIBRATIONS

Fig. 6.3.5

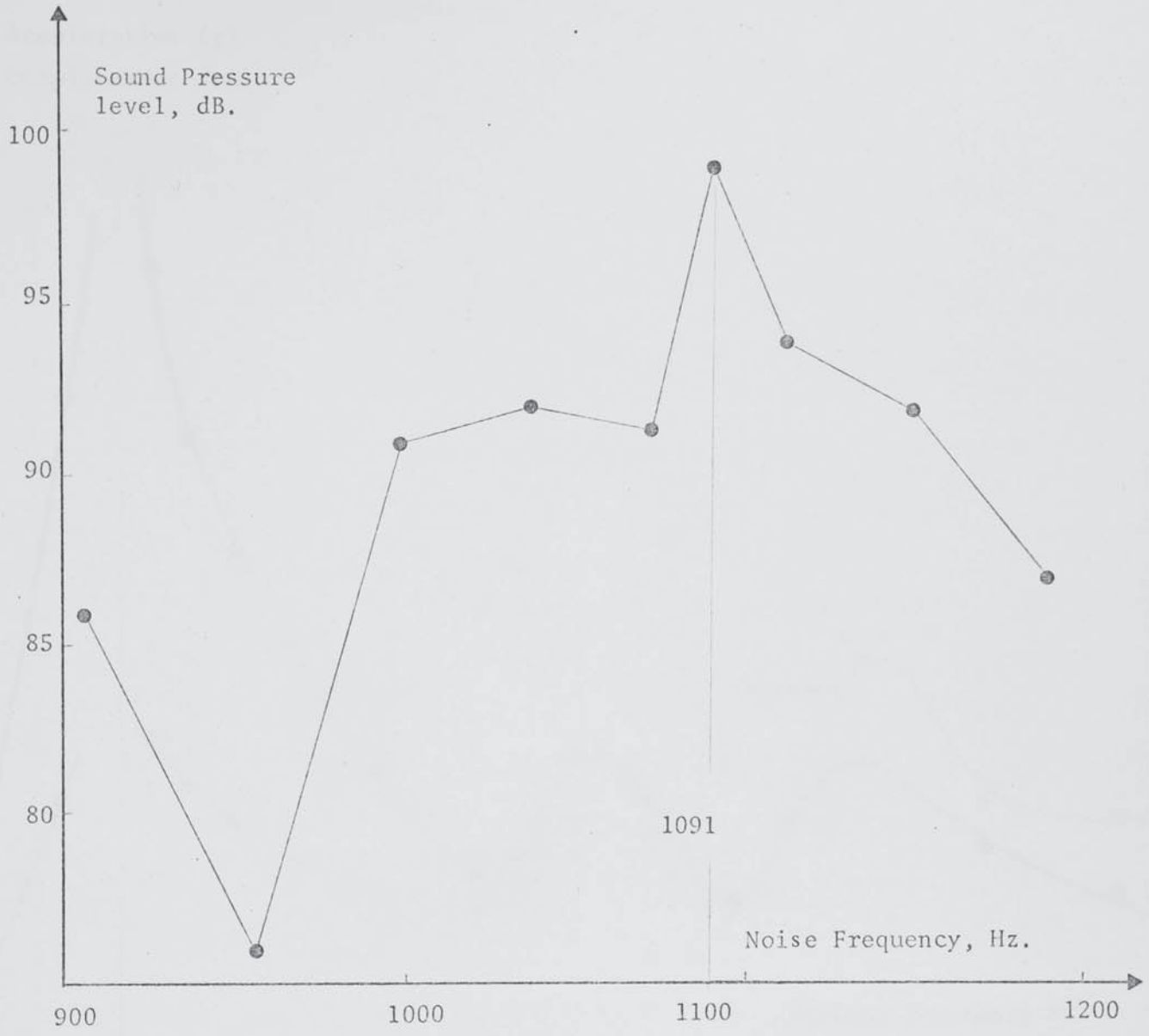

Outside dia 1066.8 mm Slots 126 x 9.84 mm

Inside dia 965.5 mm Wedges 2mm deep, fit = 0.1

Airgap dia 849.9 mm Winding etc. 210 kg
(laminations not segmental)

NOISE PEAK OF 12 POLE SYNCHRONOUS MOTOR

Fig. 6.4.1

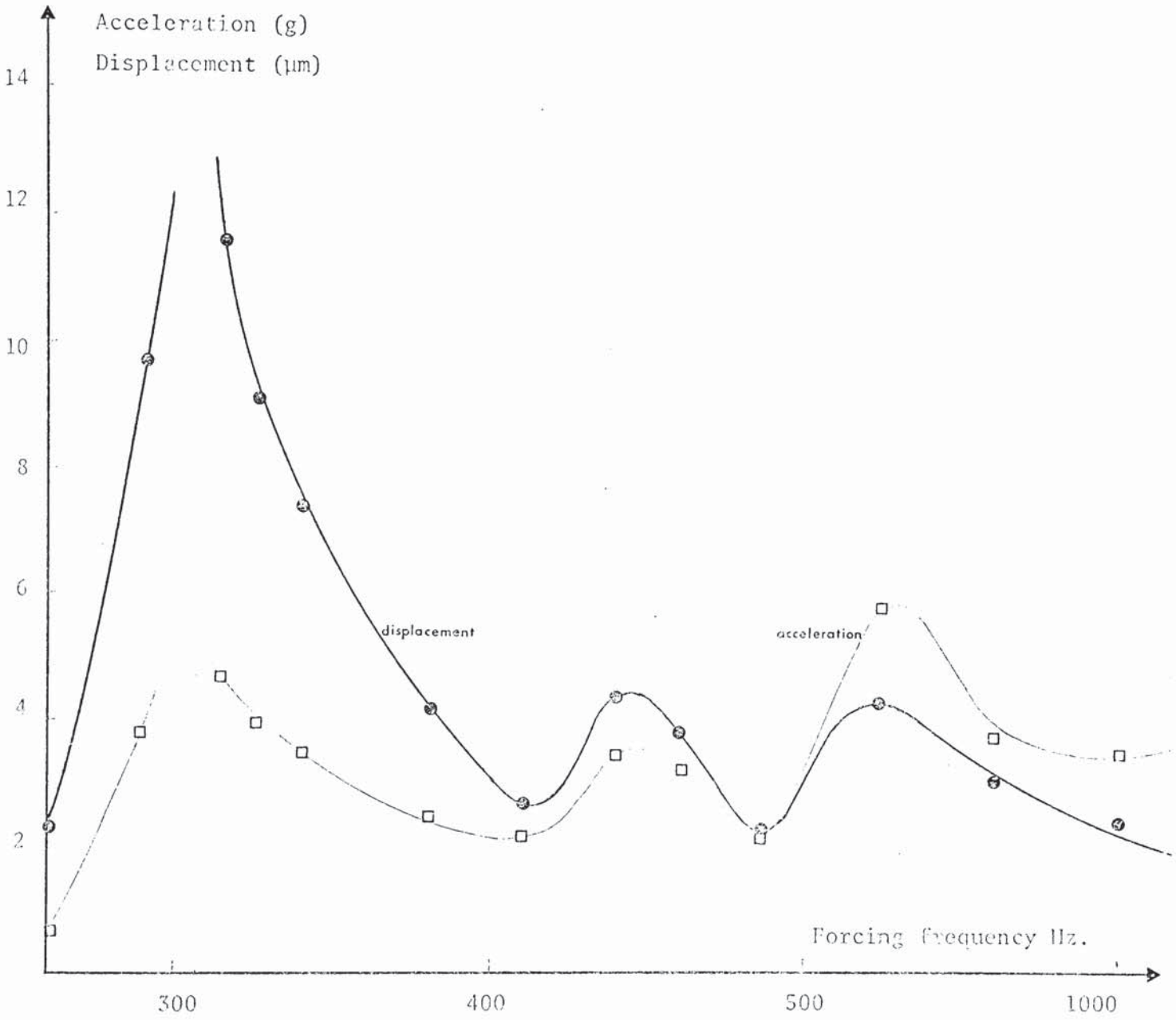

Outside dia. 3302 mm Slots 288 x 14.4 mm
Inside dia. 3180 mm Winding 1418 kg
Airgap dia. 2990 mm

VIBRATION LEVELS OF A 48 POLE SYNCHRONOUS MOTOR

Fig. 6.4.2

Outside dia. 2959.1 mm (2934.1 mm)

Inside dia. 2758.5 mm

Airgap dia. 2600.0 mm Slots 216 x 15.8 mm

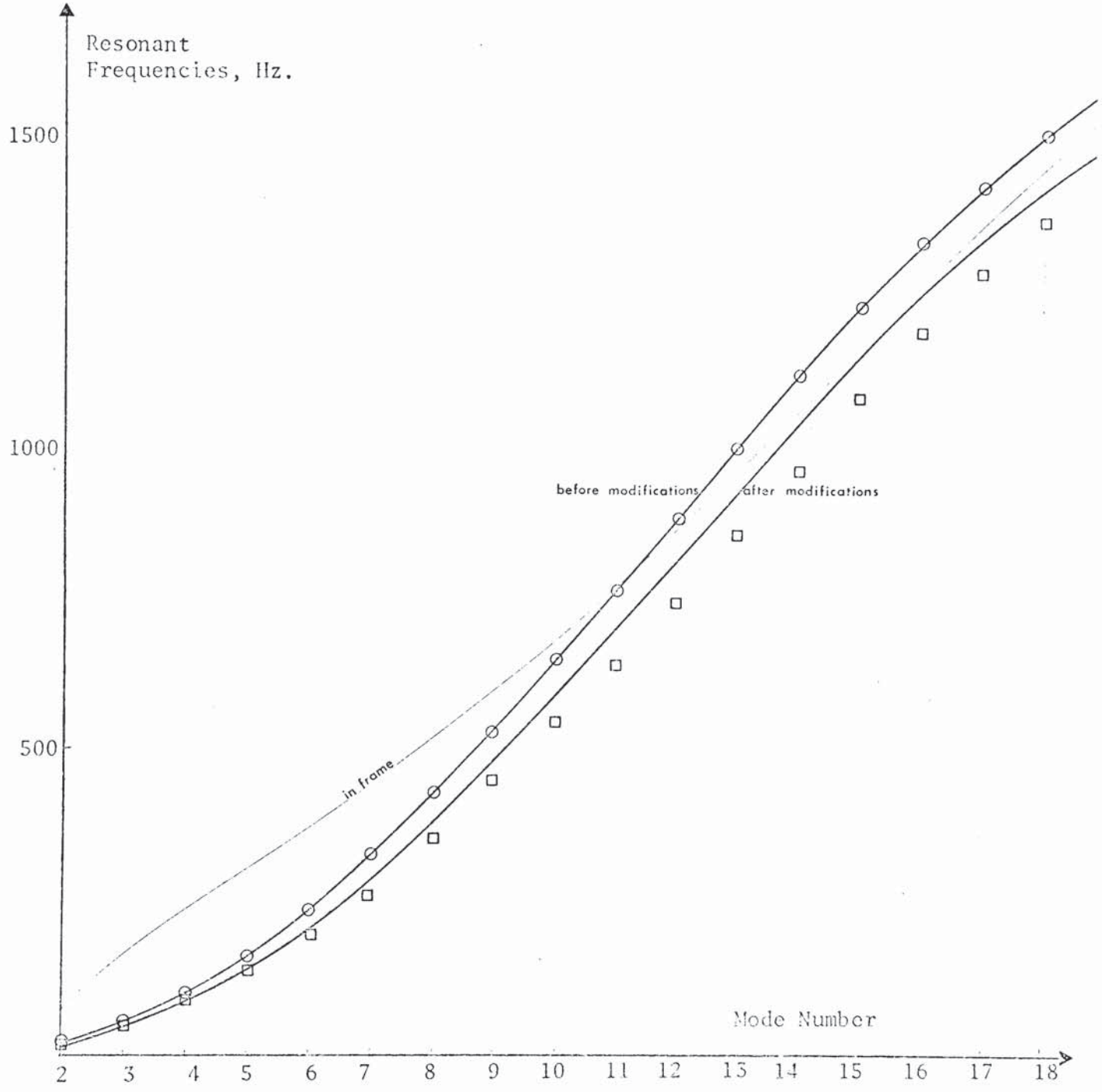

CORE RESONANT FREQUENCIES

Fig. 6.5.1

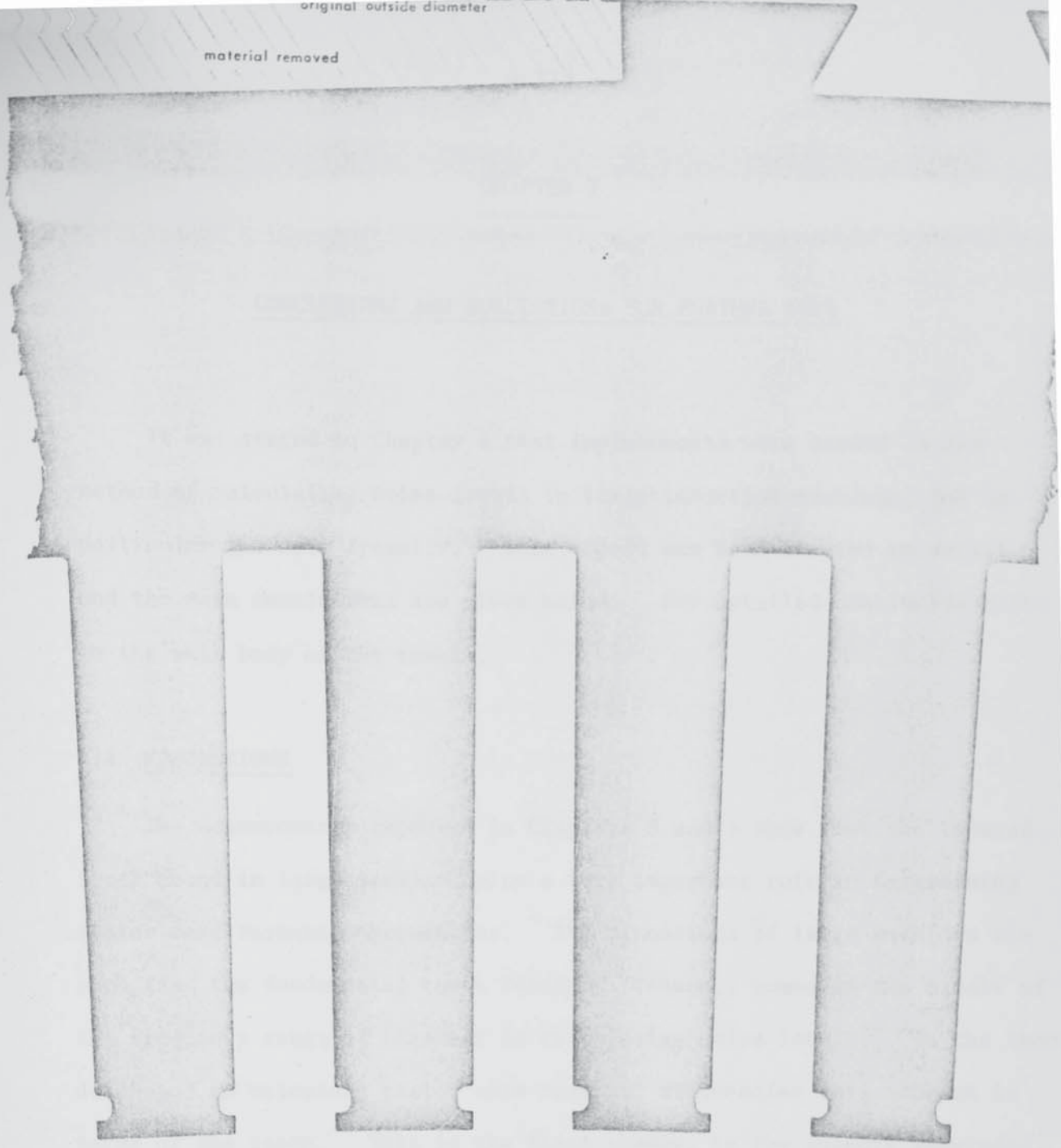

	Original Design		Modified Design		
Mode	Meas.	Calc.	Meas.	Calc.	Meas.in frame
2	19.0	19.2	20.7	16.0	77.5
3	48.6	54	42.8	45	164.6
4	91.2	102.7	81.1	85.7	236.2
5	199.2	164.5	128	138	300
6	264.4	238.6	199	200	378
7	322.1	324	302	272	450
8	431.2	420	408	353	514
9	538	524	480	442	597
10	643.8	637	646	539	671
11	757	756	702	641	741
12	865.2	877	784	748	823
13	997.3	999	926	858	952
14	1117	1119	1042	968	1053
15	1215	1234	1149	1077	1151
16	1328	1338	1249	1181	1261
17	1423	1430	1342	1278	1355
18	1506	1508	1421	1366	1462
19	1581	1572	1490	1443	1544

DETAILS OF THE MODIFIED LAMINATIONS

Fig. 6.5.2

CHAPTER 7

CONCLUSIONS AND SUGGESTIONS FOR FURTHER WORK

It was stated in Chapter 1 that improvements were needed in the method of calculating noise levels in large induction machines, and in particular the core dynamics. This aspect has been studied in detail and the main conclusions are given below. For detailed conclusion refer to the main body of the thesis.

7.1 CONCLUSIONS

The measurements reported in Chapters 5 and 6 show that the tapered teeth found in large machines play a very important role in determining stator core resonant frequencies. The dimensions of large machines are such that the fundamental tooth resonant frequency comes in the middle of the frequency range of interest in calculating noise levels. In the theory developed to calculate stator core resonant frequencies full account is taken of the teeth. This is the first theory, to the authors knowledge, which considered the teeth as an integral part of the core. Flexing of the teeth is accounted for, together with secondary tooth effects such as root flexibility and shear. The resulting equations are basically simple.

The experimental investigations revealed that the winding retention wedges in large machines can play a major role in determining core resonant frequencies. This is particularly true with bonded wedges which are increas ingly being used by some manufacturers. Wedges add stiffness to the core and also increase the tooth resonant frequency. In one example of bonded wedges

the stiffness was increased by 55% and the tooth resonant frequency by 100%. These two effects of wedges are included in the theory and examples are given showing good correlation between measurements and calculations. The importance of wedges has been completely overlooked by previous authors.

It has always been assumed that the winding mass, or some proportion of it, should be included in the equations of motion of stator cores. Measurements on a number of live machines show that the winding does not move with the core except for the zero order mode. This means that calculations of radial bending mode resonant frequencies should be made ignoring the winding mass. This conclusion applies to large machines with consolidated windings. It may not apply to small machines.

Frames of large machines are very varied. However, in all of the machines tested the frames increased the core stiffness and thereby the core resonant frequencies. Measurements of cores within and without frames have shown clearly that this increase applies only at low frequencies. In the examples given the framesbecame completely uncoupled above approximately 600 Hz. These are the first reported measurements showing the influence of frames on resonant frequencies. The uncoupling is attributed to the method of connecting the core to the frame. In large machines the main contact between the two is through the core clamping rings i.e. in a plane perpendicular to the direction of motion. The mechanism of the uncoupling is not understood. Calculations with the frame (or endrings) coupled and completely uncoupled show excellent agreement with measurements. Further experimental and theoretical work is needed to predict accurately the core resonant frequencies with intermediate frame coupling.

The non-uniformity of frames is shown to produce a number of resonant frequencies close together for each mode. A live-machine measurement is given where this phenomenon resulted in a standing wave vibration excited by a rotating force wave.

In all of the resonant frequency measurements damping factors were observed. These showed that the damping was generally very light and unpredictable. The use of high damping wedges is explored theoretically and experimentally. It is shown that present day damping materials are unable to impart sufficient damping to produce a critically damped system.

A new live-machine test technique was adopted for measuring core resonant frequencies of production machines. This may be incorporated into the normal test routine so that the testing time is not increased. Other noise based methods for measuring core resonant frequencies are shown to be inefficient and potentially misleading.

Experimental evidence is given of the effects of various secondary factors such as axial ventilation holes, segmentation, duct spacers, over-hung teeth and set back wedge grooves. Each of these effects are accounted for theoretically or empirically. Excellent agreement is obtained between calculated and measured resonant frequencies throughout the research. Over 600 different core resonant frequencies were measured. The factors that influence large machine dynamics have been investigated and quantified and the calculation methods produced for obtaining resonant frequencies are considerably more accurate than previous methods (± 6% for 95% confidence limit).

7.2 SUGGESTIONS FOR FURTHER WORK

Further experimental work is required to understand the mechanism of frame uncoupling. The theoretical analysis of coupled frames is given in Chapter 4, but more work is needed to be able to predict the way in which resonant frequencies progressively transfer from the coupled to the uncoupled calculations. For skeleton frames the coupled resonant frequency calculations are made by considering the frame as equivalent to two large endrings - see Fig.4.2.3.

The effects of wedges on tooth resonant frequencies are discussed in Sections 5.3.1 and 4.4.2. The calculated increases in resonant frequencies show reasonable agreement with the measurements. However, there are only three measurements and these were made on only one design of tooth, with different wedges. More measurements of tooth resonant frequencies with wedges would enable a more critical appraisal of the theory developed.

The live-machine test described in Section 6.3 is suitable for the routine factory measurement of core resonant frequencies. It is hoped that its further use will give rise to extra information with which to measure the accuracy - or otherwise - of the calculation methods. The conclusions drawn about the effects of windings may also apply to small machines. Live-machine measurements on small machines are necessary to test these conclusions.

The theory for calculating the zero order resonant frequency for machines with axial ventilation holes was found to be inaccurate. The deformations in this mode of vibration are similar to those in a perforated bar in tension. The holes reduce the stiffness of the core and the zero order resonant frequency. This effect is not accounted for in the theory presented. Further work is needed to refine this particular calculation.

In accounting for the flexing of teeth the Euler equations of motion were used. With very tapered teeth or bonded wedges this simplification can lead to appreciable errors. Improved calculations may be obtained with an alternative system of equations for the vibration of teeth. For large machines the improvement would be evident only at high mode numbers in cores with bonded wedges.

APPENDIX I

Mode h/2a	2	3	4	5	6	7	8	9	10
.01	.9998	.9995	.9991	.9986	.9979	.9972	.9963	.9953	.9941
.02	.9993	.9981	.9965	.9943	.9918	.9888	.9853	.9815	.9772
.03	.9984	.9958	.9921	.9874	.9818	.9752	.9678	.9597	.9508
.04	.9972	.9925	.9861	.9779	.9683	.9572	.9449	.9315	.9172
.05	.9956	.9884	.9785	.9662	.9517	.9355	.9177	.8988	.8789
.06	.9937	.9834	.9695	.9524	.9327	.9109	.8875	.8631	.8381
.07	.9914	.9776	.9591	.9368	.9116	.8842	.8555	.8261	.7965
.08	.9888	.9711	.9477	.9199	.8890	.8562	.8225	.7888	.7556
.09	.9860	.9639	.9352	.9017	.8654	.8275	.7895	.7522	.7161
.10	.9828	.9560	.9218	.8828	.8411	.7988	.7570	.7168	.6786
.11	.9793	.9476	.9077	.8632	.8166	.7703	.7255	.6830	.6434
.12	.9756	.9386	.8931	.8432	.7922	.7424	.6952	.6511	.6106
.13	.9715	.9292	.8780	.8231	.7681	.7154	.6662	.6212	.5802
.14	.9673	.9194	.8626	.8029	.7444	.6894	.6388	.5931	.5520
.15	.9628	.9092	.8470	.7830	.7214	.6644	.6129	.5669	.5260
.16	.9581	.8987	.8313	.7632	.6990	.6407	.5886	.5425	.5020
.17	.9531	.8880	.8155	.7439	.6775	.6180	.5656	.5198	.4798
.18	.9480	.8771	.7998	.7250	.6568	.5966	.5441	.4987	.4593
.19	.9427	.8661	.7843	.7065	.6369	.5762	.5239	.4790	.4403
.20	.9372	.8550	.7689	.6887	.6179	.5570	.5050	.4607	.4227
.21	.9316	.8438	.7537	.6713	.5997	.5388	.4872	.4436	.4064
.22	.9259	.8326	.7388	.6546	.5824	.5216	.4706	.4276	.3912
.23	.9200	.8214	.7243	.6384	.5658	.5053	.4549	.4127	.3771
.24	.9140	.8102	.7100	.6228	.5500	.4899	.4402	.3988	.3640
.25	.9080	.7991	.6961	.6078	.5350	.4754	.4264	.3857	.3517
.26	.9018	.7881	.6825	.5934	.5207	.4616	.4133	.3735	.3402
.27	.8956	.7772	.6693	.5796	.5070	.4486	.4011	.3620	
.28	.8894	.7665	.6564	.5662	.4940	.4362	.3895	.3512	
.29	.8830	.7558	.6440	.5534	.4817	.4246	.3786		
.30	.8767	.7454	.6319	.5412	.4699	.4135	.3683		
.31	.8703	.7351	.6201	.5294	.4586	.4030			
.32	.8640	.7250	.6088	.5181	.4479	.3930			
.33	.8576	.7150	.5978	.5072	.4377				
.34	.8512	.7053	.5871	.4968	.4279				
.35	.8449	.6958	.5768	.4868	.4186				
.36	.8385	.6864	.5668	.4772	.4097				
.37	.8323	.6773	.5572	.4680					
.38	.8260	.6684	.5479	.4591					
.39	.8198	.6597	.5389	.4506					
.40	.8136	.6512	.5302	.4425					
.41	.8075	.6429	.5217						
.42	.8015	.6348	.5136						
.43	.7955	.6269	.5058						
.44	.7896	.6192	.4982						
.45	.7837	.6117	.4908						
.46	.7780	.6044	.4838						
.47	.7723	.5974							
.48	.7667	.5905							
.49	.7613	.5838							
.50	.7559	.5772							
.51	.7506	.5709							
.52	.7453	.5648							
.53	.7402	.5588							
.54	.7353	.5530							
.55	.7304	.5474							

THICK RING RESONANT FREQUENCY CORRECTION FACTORS

The above correction factors are to be used to multiply resonant frequencies calculated by the classical theory (Hope) to obtain the results of the theory elaborated in Chapter 4. Applies to steel rings of rectangular cross section only.

Mode h/2a	11	12	13	14	15	16	17	18	19	20
.01	.9929	.9916	.9901	.9886	.9869	9851	.9833	.9813	.9792	.9770
.02	.9726	.9675	.9622	.9565	.9505	.9442	.9377	.9309	.9238	.9166
.03	.9413	.9311	.9205	.9094	.8979	.8861	.8740	.8618	.8493	.8368
.04	.9022	.8865	.8703	.8538	.8371	.8203	.8035	.7867	.7701	.7536
.05	.8584	.8376	.8165	.7955	.7746	.7540	.7338	.7140	.6948	.6761
.06	.8128	.7876	.7626	.7382	.7144	.6914	.6691	.6477	.6272	.6076
.07	.7673	.7387	.7110	.6843	.6587	.6343	.6111	.5891	.5682	.5485
.08	.7233	.6924	.6628	.6348	.6084	.5834	.5600	.5380	.5173	.4979
.09	.6817	.6492	.6186	.5900	.5633	.5384	.5152	.4936	.4735	.4548
.10	.6428	.6094	.5784	.5497	.5232	.4987	.4761	.4551	.4358	.4178
.11	.6068	.5730	.5420	.5136	.4876	.4637	.4418	.4216	.4031	.3859
.12	.5736	.5399	.5092	.4813	.4560	.4328	.4117	.3923	.3746	.3583
.13	.5432	.5098	.4796	.4524	.4278	.4054	.3851	.3666	.3497	.3341
.14	.5153	.4824	.4529	.4264	.4026	.3811	.3616	.3439	.3277	
.15	.4897	.4574	.4287	.4030	.3800	.3593	.3406	.3237		
.16	.4663	.4347	.4068	.3819	.3597	.3398	.3219			
.17	.4448	.4140	.3869	.3628	.3414	.3222				
.18	.4250	.3950	.3687	.3454	.3248					
.19	.4068	.3776	.3521	.3296						
.20	.3900	.3616	.3369							
.21	.3745	.3469								
.22	.3601	.3333								
.23	.3468									
.24	.3344									

Ring resonant frequency for the k^{th} mode ($k \geq 2$)

$$f_k = \frac{hk(k^2-1)^2}{2\pi a^2 \sqrt{k^2+1}} \sqrt{\frac{E}{12\rho}} \times \text{correction factor}$$

REFERENCES

1. WAKELY, K. "Noise problems on large rotating machines" GEC Journal of Science and Technology, Vol.41, No.4, 1974, pp125-134.

2. ACTON, W.I.
BULL, T.W.
HORE, R.A.
SCHWARZ, K.K. "Noise reduction in the circulating water pumphouse at Blythe B Power Station" Symposium on Noise from Power Plant Equipment, Southampton 21-23 Sept. 1966. I.Mech.E.

3. GLEW, C.N. "Noise problems associated with Induction Motors" Americal Oil Society, The Hague, October 4th,1972.

4. ERDELYI, E. "Predetermination of sound-pressure levels of magnetic noise of polyphase-induction machines". Trans AIEE, 1955, No.74, part III, pp1269-1280.

5. CARTER, F.W. "Magnetic Noise in Dynamo-Electric Machines" Engineering. Nov 4th and 11th, 1932, pp548-579.

6. JORDAN, H. "Der Geräuscharme Elektromotor" - Book (Giradet, Essen. 1950)

7. ALGER, P.L. "Magnetic noise in polyphase-induction motors" Trans AIEE, 1954, No.73, part IIIA, pp118-125.

8. ELLISON, A.J.
YANG, A.J. "Calculation of Acoustic Power Radiated by an Electric Machine" Acustica, Vol.25(1971),pp28-34

9. ELLISON, A.J.
YANG, S.J. "National frequencies of stators of small electric machines". Proc.IEE, Vol.118, Jan.1974, pp185-190.

10. FREEMAN, E.M. "The calculation of harmonics due to slotting in the flux density wave form of a dynamo electric machine". Proc. I.E.E. Monograph No. 523 U.

11. HOLZMANN, F. "Eigenfrequenzen des Blechpaketes von Drehstrommaschinen unter Berücksichtigung des Schwingungsverhaltens der Zähne". ETZ-A,Bd 93(1972), pp82-85.

12. BUCKENS, F. "Influence of the Relative Radial Thickness of a Ring on its Natural Frequencies". Journal Acoustical Soc. of America, Vol.22, No.4, 1950, pp437-443.

13. ALGER, P.L. "The Nature of Induction Machines" - Book Gordan and Branch, 1965, pages 376-377.

14. JORDAN, H.
FROHNE, H. "Ermittlung der Eigen frequenzen des Ständers von Drehstrommotoren". Lärmbekämpfung N., 1957, No.1, pp137-140.

15. UNER, Z.
JORDAN, H. "Berechnung der Eigenfrequenzen der Blechpakete von Drehstrommaschinen" Konstruktion, No.16(1964), Heft 3, pp108-111.

16. JORDAN, H.
NOWACK, S.
WEIS, M. Uber den magnetischen Lärm von Synchronmaschinen" E.und M., 1967, No.84, pp1-8.

17. BOLDERL, P.
JORDAN, H.
RODER, G. "Ermittlung der Biegeeigenfrequenz fur die 4-Knoten-Schwinging des Ständerblechpakete von Turbogeneratoren" AEG - Mitt. Vol.57, No.1(1967), pp35-39.

18. VERMA, S.P.
GIRGIS, R.S. "Resonant Frequencies of Electrical Machine Stators having encased construction. Part II: Numerical Results and Experimental verification" Trans IEEE,PAS(1973), pp1586-1593.

19. PAVLOVSKY, H. "Die Eigenfrequenzen der Standerblechpakete umlaufender elektrischer Maschinen" E.und M.,1971, Vol.88, Heft 11, pp479-486.

20. POON, P.L. "Frequency response of toothed beams (with application of the Timoshenko beam theory)". M.Sc. Thesis, Oct.1974, The University of Aston in Birmingham.

21. VERMA, S.P.
GIRGIS, R.S.
"Resonant Frequencies of Electrical Machine Stators having encased construction. Part I: Derivation of the General Frequency equation." Trans IEEE,PAS(1973), pp1577-1585.

22. VERMA, S.P.
GIRGIS, R.S.
As reference 18. Equations relating to teeth obtained in correspondence with these authors.

23. FROHNE,H.
"Uber die primären Bestimmungsgrössen der Lautstärke bei Asynchronmaschinen" Thesis, Hanover Technical High School, 1959.

24. JORDAN, H.
NOWACK, S.
WEIS, M.
"Der Einfluss des Gehäuses auf den magnetischen Lärm von Wasserkraftgeneratoren." Konstruktion, No.18(1966), Heft 9, pp374-378.

25. JORDAN, H.
PURKERMANI, M.
RAUBE, W.
RÖDER, G.
The effect of a thin frame on the magnetic noise of polyphase machines (in German), Lärmbekampfung, August 1970, pp81-87

26. STAIGER, A.
JORDAN, H.
"Der Einfluss des Gehäuses auf das schwingingstechnisch Verhaltens des Ständers von Drehstrommaschinen. AEG-Mitt. 52(1962), pp194-197.

27. KUHL, W.
"Messungen zu den Theorien der Eigenschwinggungen von Kreisringen beliebiger Wandstärke" Akustische Zeitschrift, July 1942, pp125-152.

28. SEIDEL, B.S.
ERDELYI, E.A.
"On the vibration of a Thick Ring in its own plane" Trans ASME, Journal of Engineering for Industry. August 1964, pp240-244.

29. COWPER,
"The shear coefficient in Timoshenko's beam theory" Trans ASME, Journal of Applied Mechanics, 1966, pp335-3

30. AALAMI, B.
ATZORI, B.
"Flexural vibrations and Timoshenko's beam theory" Journal AIAA, Vol.12(5), May 1974, pp679-685.

31. CRANCH, E. ADLER, A. "Bending vibrations of variable section beams". Journal of App.Mech.,No.78(1956), pp103-108.

32. PENNY,J.E. REED, J.R. "An integral equation approach to the fundamental frequency of vibrating beams" Journal of Sound and Vibration (1971), No.19(4), pp393-400.

33. GAINES, J.H. VOLTERRA, E. "Transverse Vibrations of Cantilever Bars of Variable cross-section" Journal of Acoustical Society of America Vol.39(4), 1966, pp674-679

34. MACBAIN,J.C. GENIN, J. "Natural Frequencies of a Beam considering support characteristics" Journal of Sound and Vibration, 1973, 27(2), pp197-206.

35. MACBAIN, J.C. GENIN, J. "Effect of support flexibility on the Fundamental Frequency of vibrating beams" Journal of the Franklin Institute, Vol.296,No.4, Oct.1973, pp259-273.

36. O'DONNELL, W.J. "The Additional deflection of a Cantilever due to the Elasticity of the Support". Trans ASME Journal of App.Mech.,Sept.1960, pp461-464.

37. DAHLQUIST, C.A. "A family of Viscoelastic Materials for Diverse Damping Applications" ASME Conference publication, 71-Vibr-47, pp1-8.

38. TIMOSHENKO, S. "Vibration problems in Engineering" - Book D.Van Nostrand Co.Ltd., 3rd Edition 1955.

39. SUBBA RAO,V. BUTLER,O. "Stray losses of polyphase cage-induction motors with particular reference to the condition of imperfect rotor-bar-iron insulation" Proc IEE,Vol.116,No.5, May 1969, pp737-751.

40. CHRISTOFIDES,N. "The origins of load losses in squirrel cage induction motors with cast aluminium rotors". Ph.D.Thesis,1966, Imperial College, London.

41. NEUHAUS, W.
WEPPLER, R.
"Der Einfluss der Nutöffnungen auf den Drehmomentverlauf von Drehstrom - Asynchronmotoren mit Kafigläufer". ETZ-A, Bd 90(1969), Heft 8, pp186-191.

42. BEAMA
"BEAMA Recommendations for the measurement and Classification of Acoustic Noise from Rotating Electrical Machines" Publication 125, 1967 .

NOMENCLATURE

a	radius of core section centroid
$a(x,x)$	particular flexibility influence coefficient
$a(x,\eta)$	generalised flexibility influence coefficient
A	core section area; integration constant
A_o	tooth tip section area
A_1, A_2, A_3, A_4 $A_1^*, A_2^*, A_3^*, A_4^*$	coefficients of tooth displacement function
B	integration constant
b	core section width
b_1	tooth section width
b_2	frame section width
b_3	cooling fin section width
b_4	endring section width
b_5	modified endring section width
b_6	modified frame section width
c	core depth as fraction of tooth length
C	constant in root flexibility formula; integration constant
C_r	tooth res.freq. correction factor accounting for root flexibility
C_s	tooth res.freq. correction factor accounting for shear etc.
C_w	tooth res.freq. correction factor accounting for wedge support
d	half width of elipse
D	Integration constant
dB	decibel
e	half height of elipse

E	modulus of elasticity, $E = E_1 + jE_2$
E_1	storage modulus
E_2	loss modulus
F	force
f_t	tooth resonant frequency, Hz
fit	factor denoting quality of fit of wedge in the groove
G	shear modulus
h	radial thickness of ring
alternatively	depth of tooth; depth of tooth base
h_o	depth of tooth at tip
I	denotes integral
I_c	equivalent second moment of area of a curved beam
I_x	second moment of area of a tooth as a function of x
I_o	second moment of area at tooth tip
$I_1 \rightarrow I_8$	integrals in calculation of rotary inertia factor
j	complex operator
J_r	moment of inertia
k	mode number
alternatively	slot opening factor; length constant
k_b	base spring stiffness
k_c	tooth pitch factor
k_r	core taper factor
k_w	wedge spring stiffness
$K(x,x)$	mass-flexibility product
k_o	tooth taper factor
k_1, k_2, k_3, k_4	section width correction factors
k_5, k_6, k_7	

ℓ	length of tooth
ℓn	natural logarithm
ℓ_c	nett core section length
m	mass per unit length; mass
M	bending moment
M_c	core moment
M_t	tooth moment
n	Timoshenko shear coefficient
N	normal stress resultant
p	machine pole pairs
alternatively	pivot point as a fraction of the tooth length
p.c.r.	pitch circle radius of ventilation holes
Q	shear stress resultant
alternatively	damping factor, E_1/E_2
r	radius of core section neutral layer
R	radius of core section centre of gravity (C. of G.)
alternatively	number of rotor slots
r_a	outside radius of ring
R_n	normalised response function
R_p	radius of core section centre of percussion
r_o	gap radius
r_1	inside wedge radius
r_2	outside wedge radius
r_3	slot bottom radius
r_4	core outside radius and frame inside radius
r_5	frame outside radius
r_6	fin outside radius
r_7	endring inside radius
r_8	endring outside radius

s	shear constant
SPL	sound pressure level(s)
T	time interval
t	time
t_2	rotor slot pitch
u	wedge displacement
U_o	end of wedge displacement amplitude
v	tangential displacement of core
V	tooth displacement
$V(x,\Omega)$	tooth displacement as a function of x and Ω
V_k	peak tangential displacement amplitude, mode k
V_o	tooth base displacement amplitude
w	radial displacement of core
alternatively	work done in displacing wedges
W_k	peak radial displacement, mode k
$W_{k,o}$	peak radial displacement at zero frequency, mode k
$W_{k,\Omega}$	peak radial displacement at frequency Ω, mode k
W_s	slot width
W_w	effective wedge width
x	length variable
X	intermediate integral
y	length variable
alternatively	tooth displacement
Y	intermediate integral
z	radius variable
alternatively	normalised resonant frequency squared
Z	intermediate integral

α	length constant
β	damping ratio E_2/E_1
γ	strain ratio
δ	radius ratio
ε	radius ratio
alternatively	wedge strain
η	force position variable
θ	rotation
θ_m	rotation due to a moment
μ	harmonic order (rotor)
ν	Poisson's ratio
alternatively	harmonic order (stator)
ξ	rotational inertia moment factor
ξ_t	rotation inertia moment factor of teeth alone
ρ	density
σ	radius ratio
alternatively	wedge stress
ψ	tangential displacement mass factor
ψ_t	tangential displacement mass factor of teeth alone
Ω	frequency, rad/sec.
Ω_k	core resonant frequency, mode k
Ω_t	tooth resonant frequency, rad/sec
Ω_o	core resonant frequency, zero order mode.

SUBSCRIPTS AND SUPERSCRIPTS

c	core
er	endring
f	frame
k	mode number
s	slot
t	tooth
w	wedge
μ	μ^{th} harmonic order
ν	ν^{th} harmonic order
Ω	at frequency, Ω
$\cdot$	differential with respect to time
$'$	differential with respect to length or rotation (x or θ)